


On-shell versus curvature mass parameter fixing schemes in the three flavor quark-meson model with vacuum fluctuations

Vivek Kumar Tiwari^{*}

Department of Physics, University of Allahabad, Prayagraj, India-211002

 (Received 24 November 2022; revised 1 August 2023; accepted 23 August 2023; published 3 October 2023)

The tree-level parameters of the $2 + 1$ flavor quark-meson model become inconsistent when the quark one-loop vacuum fluctuation is included in its effective potential. Relating the counterterms in the $\overline{\text{MS}}$ scheme to those in the on-shell scheme, the relations between the renormalized parameters of both the schemes have been determined, and the consistent effective potential for the renormalized quark-meson (RQM) model has been calculated using the modified minimal subtraction method where the relations between the physical quantities (i.e. pole masses of the pseudoscalar π , K , η , and η' and the scalar σ mesons, the pion and kaon decay constants f_π and f_K) and the running couplings have been used as input. The effective potentials, order parameters, and phase diagrams have been computed for the RQM model and compared respectively with the corresponding calculations in the quark-meson model without the vacuum term and the quark-meson model with the vacuum term where the curvature meson masses have been used for fixing the model parameters. The f_π , f_K , the Yukawa coupling g , and the minimum of the effective potential do not change but the explicit symmetry breaking strength h_x gets a small reduction equal to the two flavor RQM model correction while the strength h_y becomes weaker by a relatively large amount in the $2 + 1$ flavor RQM model because the pion curvature mass $m_{\pi,c} = 135.95$ MeV is 2.05 MeV smaller than its pole mass $m_\pi = 138.0$ MeV and the kaon curvature mass $m_{K,c} = 467.99$ MeV is 28.01 MeV smaller than its pole mass $m_K = 496.0$ MeV after the renormalization. Therefore the $2 + 1$ flavor RQM model phase diagrams and the critical end point location differ noticeably from the existing two flavor RQM model results [S. K. Rai and V. K. Tiwari, *Phys. Rev. D* **105**, 094010 (2022)]. The enhanced coefficient of the 't Hooft determinant term in the RQM model modifies the $T(\mu)$ dependence of the $U_A(1)$ axial symmetry restoration pattern.

DOI: [10.1103/PhysRevD.108.074002](https://doi.org/10.1103/PhysRevD.108.074002)

I. INTRODUCTION

The study of a quantum chromodynamics (QCD) phase diagram and all of its details has been a very active research area of strong interaction physics since the 1970s when the first QCD schematic phase diagram appeared [1]. It depicted a confined phase of hadrons at a low temperature (low baryonic density) and a deconfined phase of quarks and gluons [2–5] at a high temperature (zero baryonic density) or high baryonic density (zero temperature). One gets important and valuable information for the QCD phase transition from the lattice QCD simulations [6–14] at zero chemical potential, but for the nonzero baryon densities/chemical potentials, the lattice QCD calculations get seriously compromised as the QCD action becomes complex on account of

the fermion sign problem [8]. For mapping out the phase diagram regions where the lattice simulations do not work, one gets much help from the investigations carried out in the ambit of phenomenological models developed using the effective degrees of freedom [15,16].

The QCD Lagrangian for the three flavors of massless quarks has the $SU_{L+R}(3) \times SU_{L-R}(3)$ symmetry. The chiral symmetry (axial $A = L - R$ symmetry) gets spontaneously broken in the low energy QCD vacuum of the hadron degrees of freedom. Due to this, the chiral condensate forms in the nonstrange and strange directions and one gets eight massless Goldstone bosons which are pseudoscalars. The chiral symmetry gets explicitly broken as well due to the small mass of the light quarks u , d and a relatively heavy s quark. We find the light pions in nature, while the kaons and the eta are heavier on account of the large strange quark mass. Furthermore 't Hooft [17] showed that the $U_A(1)$ axial symmetry is explicitly broken to $Z_A(N_f)$ at the quantum level by the instanton effects. The η' meson is not a massless Goldstone boson even in the chiral limit of the massless quarks, as it acquires a mass of about 1 GeV due to the $U_A(1)$ axial anomaly. The three

^{*}vivekkrt@gmail.com

Published by the American Physical Society under the terms of the Creative Commons Attribution 4.0 International license. Further distribution of this work must maintain attribution to the author(s) and the published article's title, journal citation, and DOI. Funded by SCOAP³.

(2 + 1) flavor linear sigma model [18,19] is a very conducive framework for investigating the interplay of the $SU_A(3)$ chiral and the $U_A(1)$ axial symmetry breaking and restoration. One can construct the chiral invariant combinations using the chiral partners from the respective octet and the singlet of the scalar and pseudoscalar mesons. One gets the richer framework of the quark-meson (QM) model for exploring the QCD phase structure when the nine scalar and nine pseudoscalar mesons are coupled to the three flavors of quarks. Furthermore, the QCD confinement of the quarks inside the hadrons is implemented by the introduction of the Polyakov loop when the chiral models are coupled to a constant background $SU(N_c)$ gauge field A_μ^a [20–24]. Adding the free energy density from the gluons in the form of the Polyakov loop potential [25,26] to the QM model, one gets the framework of the PQM model. Several QCD phase structure studies, have already been performed in the chiral models [27–41], the two and the three flavor QM model [42–44] as well as the PQM model [45–48].

Several QM model studies [19,27,36,42–48] in the standard mean field approximation (s-MFA) neglected the quark one-loop vacuum fluctuations assuming that the redefinition of the meson effective potential parameters would account for their effects. The QM model in the s-MFA gives a first-order chiral phase transition at the zero baryon density which looks inconsistent in the light of the general theoretical arguments [49,50] that the chiral phase transition at $\mu = 0$ is of second order. The proper treatment of the Dirac sea was first done in the Ref. [51] to remove this inconsistency. Afterwards, the quark one-loop vacuum corrections were included in the two and three flavor QM/PQM models and its detailed impact on the QCD phase structure and the thermodynamics were investigated in several research papers [52–65]. These publications used the curvature masses of the mesons for the model parameter fixing while the pion decay constant is identified with the vacuum expectation value of the nonstrange condensate, and the kaon decay constant needed for the three flavor QM/PQM model studies [54,55,58,59,65] is fixed by the combination of the vacuum expectation values of the strange and the nonstrange condensate. The minimal subtraction scheme has been used in the above-mentioned works to regularize the quark one-loop vacuum divergence. The above parameter fixing procedure becomes inconsistent when one notes that the curvature masses are defined by the evaluation of the self-energies at zero momentum because the effective potential is the generator of the n -point functions of the theory at vanishing external momenta [66–70]. This model setting has been termed the quark-meson model with vacuum term (QMVT).

The use of the tree-level parameters for calculating the effective potential becomes inconsistent because the radiative corrections to the physical quantities change their tree-level relations to the parameters of the Lagrangian.

The parameters in the $\overline{\text{MS}}$ scheme are running and renormalization scale Λ dependent while the on-shell (OS) parameters have their tree-level values. Following the correct renormalization prescription, one calculates the counter-terms both in the $\overline{\text{MS}}$ scheme and in the on-shell scheme and then connects the renormalized parameters of the two schemes. Afterwards the effective potential is calculated using the modified minimal subtraction procedure where the relations between the on-shell parameters (physical quantities) and the running parameters are used as the input [67]. In a series of papers, Adhikari and collaborators [67,71–73] used this renormalization prescription for including the quark one-loop fluctuation in the two flavor QM model which uses the $O(4)$ sigma model with the scalar σ and the pseudoscalar $\vec{\pi}$ meson. In our recent work, we also applied [74] the on-shell renormalization method for fixing the model parameters to that version of the quark-meson (QM) model in which the two flavors of quarks is coupled to the eight mesons of the $SU_L(2) \times SU_R(2)$ linear sigma model, and we made a comparative study of the effective potential and the phase diagram.

In the present work, we will be calculating the consistent effective potential and the on-shell renormalized parameters for the 2 + 1 flavor quark-meson (QM) model where the quark one-loop vacuum fluctuation is properly renormalized. The application of the exact on-shell renormalization prescription to the 2 + 1 flavor QM model becomes quite involved and complicated because (i) one does not have the direct relations between the parameters and the masses where the mixed states are involved and (ii) in addition to the self-energy corrections for the pion and the kaon, one needs to calculate the self-energy corrections also for the scalar σ and the pseudoscalar η and η' mesons which are the mixed states of the 00 and 88 components in the respective scalar and pseudoscalar directions. The seven parameters are to be fixed after the renormalization in the present 2 + 1 flavor renormalized quark-meson (RQM) model. The two flavor RQM model results [74] together with the results obtained in the 2 + 1 flavor QM and QMVT model provide the benchmark against which, the consistency, correctness, similarities, and differences of the 2 + 1 flavor RQM model results can be compared and checked. Since the $U_A(1)$ axial anomaly coefficient has a condensate-dependent component [75–79], it becomes interesting to know how the coefficient of the 't Hooft determinant term gets affected (renormalized) by the on-shell renormalization of the quark one-loop vacuum fluctuation. Calculating the temperature (chemical potential) dependence of the curvature masses of the mesons a_0 , σ , π , η , and η' , the modification of the $U_A(1)$ axial symmetry restoration pattern will also be investigated in the present work. The exact on-shell parameter fixed 2 + 1 flavor RQM model provides us the framework in which the consistent physics of the chiral symmetry restoration can be integrated with the deconfinement transition physics.

The paper is arranged as follows. The $SU_L(3) \times SU_R(3)$ QM model is presented in Sec. II. Section III presents the effective potential calculation for the quark-meson model with vacuum term together with its parameter fixing procedure. The on-shell scheme counterterms and self-energy calculations are presented in the Sec. IV A. The relations between the physical quantities and the running parameters are derived in Sec. IV B, and the derivation of the effective potential in the RQM model is presented in Sec. IV C. Section V presents the calculation of the curvature masses of the mesons. The result and discussion are presented in Sec. VI. Section VI A presents the comparison of the effective potentials, the order parameters, and the phase diagrams while Sec. VI B discusses the differences between the results of the present 2 + 1 flavor work and the existing results of the two flavor RQM model. Section VI C presents the results for the modification of the $U_A(1)$ axial symmetry restoration pattern. Finally the summary and conclusion are presented in Sec. VII.

II. MODEL FORMULATION

We present the formulation of the $SU_L(3) \times SU_R(3)$ quark-meson model in this section. Three flavors of quarks in this model are coupled to the $SU_V(3) \times SU_A(3)$ symmetric meson fields. The model Lagrangian is written in terms of quarks, mesons, and couplings as

$$\mathcal{L}_{\mathcal{QM}} = \bar{\psi}[i\gamma^\mu \partial_\mu - gT_a(\sigma_a + i\gamma_5\pi_a)]\psi + \mathcal{L}(\mathcal{M}), \quad (1)$$

where ψ is a color N_c -plet, a four-component Dirac spinor, as well as a flavor triplet

$$\psi = \begin{pmatrix} u \\ d \\ s \end{pmatrix}. \quad (2)$$

The flavor blind Yukawa coupling g couples the three flavors of quarks with the nine scalar ($\sigma_a, J^P = 0^+$) and nine pseudoscalar ($\pi_a, J^P = 0^-$) mesons.

The massless quarks become massive due to the spontaneous breaking of the chiral symmetry as the chiral condensate assumes nonzero vacuum expectation value. The Lagrangian for the meson fields has the following form [19,28,48]:

$$\begin{aligned} \mathcal{L}(\mathcal{M}) = & \text{Tr}(\partial_\mu \mathcal{M}^\dagger \partial^\mu \mathcal{M} - m^2(\mathcal{M}^\dagger \mathcal{M})) \\ & - \lambda_1 [\text{Tr}(\mathcal{M}^\dagger \mathcal{M})]^2 - \lambda_2 \text{Tr}(\mathcal{M}^\dagger \mathcal{M})^2 \\ & + c[\det \mathcal{M} + \det \mathcal{M}^\dagger] + \text{Tr}[H(\mathcal{M} + \mathcal{M}^\dagger)]. \end{aligned} \quad (3)$$

Here the field \mathcal{M} is a complex 3×3 matrix which contains the nine scalars σ_a and the nine pseudoscalar π_a mesons,

$$\mathcal{M} = T_a \xi_a = T_a(\sigma_a + i\pi_a). \quad (4)$$

Here the T_a represent nine generators of $U(3)$ with $T_a = \frac{\lambda_a}{2}$ where $a = 0, 1, \dots, 8$. The λ_a are standard Gell-Mann matrices with $\lambda_0 = \sqrt{\frac{2}{3}}\mathbb{1}_{3 \times 3}$. The generators follow the $U(3)$ algebra $[T_a, T_b] = if_{abc}T_c$ and $\{T_a, T_b\} = d_{abc}T_c$ where f_{abc} and d_{abc} are the standard antisymmetric and symmetric structure constants respectively with $f_{ab0} = 0$ and $d_{ab0} = \sqrt{\frac{2}{3}}\delta_{ab}$ and matrices are normalized as $\text{Tr}(T_a T_b) = \frac{\delta_{ab}}{2}$. The following term breaks the $SU_L(3) \times SU_R(3)$ chiral symmetry explicitly:

$$H = T_a h_a. \quad (5)$$

Here H is a 3×3 matrix with nine external parameters. On account of the spontaneous breaking of the chiral symmetry, the field ξ picks up the nonzero vacuum expectation value, $\bar{\xi}$. Only three possible nonzero parameters $h_0, h_3,$ and h_8 might cause the explicit breakdown of the chiral symmetry because $\bar{\xi}$ must have the quantum numbers of the vacuum. We are choosing $h_0, h_8 \neq 0$ and isospin symmetry breaking is neglected. Thus having the nonzero condensates $\bar{\sigma}_0$ and $\bar{\sigma}_8$, one gets the 2 + 1 flavor symmetry breaking scenario. The model has five other parameters in addition to the h_0 and h_8 . These are the tree-level mass parameter squared m^2 , quartic coupling constants λ_1 and λ_2 , a Yukawa coupling g , and a cubic coupling constant c which models the $U_A(1)$ axial anomaly of the QCD vacuum.

A. Grand potential in the mean field approach

The considered system is spatially uniform and it is in thermal equilibrium at temperature T and quark chemical potential μ_f ($f = u, d, s$). The partition function is obtained by the path integral over the quark/antiquark and meson fields [19,48]

$$\begin{aligned} \mathcal{Z} = & \text{Tr} \exp \left[-\beta \left(\hat{\mathcal{H}} - \sum_{f=u,d,s} \mu_f \hat{\mathcal{N}}_f \right) \right] \\ = & \int \prod_a \mathcal{D}\sigma_a \mathcal{D}\pi_a \int \mathcal{D}\psi \mathcal{D}\bar{\psi} \exp \left[-\int_0^\beta d\tau \int_V d^3x \right. \\ & \left. \times \left(\mathcal{L}_{\mathcal{QM}}^E + \sum_{f=u,d,s} \mu_f \bar{\psi}_f \gamma^0 \psi_f \right) \right], \end{aligned} \quad (6)$$

where $\beta = \frac{1}{T}$ and the three-dimensional volume of the system is V . In general, the three quark chemical potentials will be different for the three quark flavors. It is assumed that the $SU_V(2)$ symmetry is preserved in this work. Hence the small difference in the mass of u and d quark is neglected. Thus the quark chemical potential for the u and d quarks is equal $\mu_u = \mu_d$ and the strange quark chemical potential is μ_s .

In the standard mean-field approximation [19,27,48], the partition function is calculated by replacing the meson fields with their vacuum expectation values $\langle M \rangle = T_0 \bar{\sigma}_0 + T_8 \bar{\sigma}_8$ and neglecting the thermal as well as quantum fluctuations of the meson fields while retaining the quarks and antiquarks as quantum fields. Using the standard method given in Refs. [21,45,80], one can find the expression of the grand potential as the sum of meson and quark/antiquark contribution,

$$\Omega_{\text{MF}}(T, \mu) = -\frac{T \ln Z}{V} = U(\sigma_0, \sigma_8) + \Omega_{q\bar{q}}(T, \mu). \quad (7)$$

The 2 + 1 flavor case is studied by performing the following basis transformation of condensates and external fields from the original singlet octet (0, 8) basis to the nonstrange strange basis (x, y):

$$\sigma_x = x = \sqrt{\frac{2}{3}} \bar{\sigma}_0 + \frac{1}{\sqrt{3}} \bar{\sigma}_8, \quad (8)$$

$$\sigma_y = y = \frac{1}{\sqrt{3}} \bar{\sigma}_0 - \sqrt{\frac{2}{3}} \bar{\sigma}_8. \quad (9)$$

The grand potential is written in x, y basis as

$$\Omega_{\text{MF}}(T, \mu) = U(x, y) + \Omega_{q\bar{q}}(T, \mu). \quad (10)$$

The external fields (h_x, h_y) are written in terms of the (h_0, h_8) by similar expressions. Since the nonstrange and strange quark/antiquark decouple, the quark masses are written as

$$m_u = g \frac{x}{2}, \quad m_s = g \frac{y}{\sqrt{2}}. \quad (11)$$

The tree-level effective potential in the nonstrange-strange basis is written as

$$\begin{aligned} U(x, y) &= \frac{m^2}{2} (x^2 + y^2) - h_x x - h_y y - \frac{c}{2\sqrt{2}} x^2 y \\ &\quad + \frac{\lambda_1}{2} x^2 y^2 + \frac{1}{8} (2\lambda_1 + \lambda_2) x^4 \\ &\quad + \frac{1}{8} (2\lambda_1 + 2\lambda_2) y^4. \end{aligned} \quad (12)$$

The stationarity conditions $\frac{\partial U(x, y)}{\partial x} \Big|_{x=\bar{x}, y=\bar{y}} = 0 = \frac{\partial U(x, y)}{\partial y} \Big|_{x=\bar{x}, y=\bar{y}}$ for the effective potential (12) give

$$h_x = \bar{x} m_\pi^2 \quad \text{and} \quad h_y = \left\{ \frac{\sqrt{2}}{2} (m_K^2 - m_\pi^2) \bar{x} + m_K^2 \bar{y} \right\}. \quad (13)$$

The tree-level curvature masses of the pions, kaons, and other mesons in the QM model are given by the mass matrix $(m_{\alpha, ab})^2$ evaluated in Refs. [18,19]. Here $\alpha = s, p$; ‘‘s’’ stands for the scalar and ‘‘p’’ stands for the pseudoscalar mesons and $a, b = 0, 1, 2, \dots, 8$. In the scalar sector, the a_0 meson mass is given by the 11 element (degenerate with the 22 and 33 elements) and the κ meson mass is given by the 44 element (degenerate with the 55, 66, and 77 elements). The σ and f_0 meson masses are found by diagonalizing the (00)-(88) sector of the scalar mass matrix. In exactly analogous manner for the pseudoscalar sector $m_{p,11}^2 = m_{p,22}^2 = m_{p,33}^2 \equiv m_\pi^2$ and $m_{p,44}^2 = m_{p,55}^2 = m_{p,66}^2 = m_{p,77}^2 \equiv m_K^2$. Diagonalization of the pseudoscalar (00)-(88) sector of the mass matrix gives us the masses of the physical η and η' mesons. All the meson masses are given in the Table I.

The quark/antiquark contribution is given by

$$\Omega_{q\bar{q}}(T, \mu; x, y) = \Omega_{q\bar{q}}^{\text{vac}} + \Omega_{q\bar{q}}^{T, \mu}(x, y), \quad (14)$$

$$\Omega_{q\bar{q}}^{\text{vac}} = -2N_c \sum_{u,d,s} \int \frac{d^3 p}{(2\pi)^3} E_f \theta(\Lambda_c^2 - \vec{p}^2), \quad (15)$$

TABLE I. Meson masses calculated from the second derivative of the grand potential at its minimum as given in Refs. [19,33].

Scalar meson masses		Pseudoscalar meson masses	
$(m_{a_0})^2$	$m^2 + \lambda_1(x^2 + y^2) + \frac{3\lambda_2}{2}x^2 + \frac{\sqrt{2}c}{2}y$	$(m_\pi)^2$	$m^2 + \lambda_1(x^2 + y^2) + \frac{\lambda_2}{2}x^2 - \frac{\sqrt{2}c}{2}y$
$(m_\kappa)^2$	$m^2 + \lambda_1(x^2 + y^2) + \frac{\lambda_2}{2}(x^2 + \sqrt{2}xy + 2y^2) + \frac{c}{2}x$	$(m_K)^2$	$m^2 + \lambda_1(x^2 + y^2) + \frac{\lambda_2}{2}(x^2 - \sqrt{2}xy + 2y^2) - \frac{c}{2}x$
$(m_{s,00})^2$	$m^2 + \frac{\lambda_1}{3}(7x^2 + 4\sqrt{2}xy + 5y^2) + \lambda_2(x^2 + y^2) - \frac{\sqrt{2}c}{3}(\sqrt{2}x + y)$	$(m_{p,00})^2$	$m^2 + \lambda_1(x^2 + y^2) + \frac{\lambda_2}{3}(x^2 + y^2) + \frac{c}{3}(2x + \sqrt{2}y)$
$(m_{s,88})^2$	$m^2 + \frac{\lambda_1}{3}(5x^2 - 4\sqrt{2}xy + 7y^2) + \lambda_2(\frac{x^2}{2} + 2y^2) + \frac{\sqrt{2}c}{3}(\sqrt{2}x - \frac{y}{2})$	$(m_{p,88})^2$	$m^2 + \lambda_1(x^2 + y^2) + \frac{\lambda_2}{6}(x^2 + 4y^2) - \frac{c}{6}(4x - \sqrt{2}y)$
$(m_{s,08})^2$	$\frac{2\lambda_1}{3}(\sqrt{2}x^2 - xy - \sqrt{2}y^2) + \sqrt{2}\lambda_2(\frac{x^2}{2} - y^2) + \frac{c}{3\sqrt{2}}(x - \sqrt{2}y)$	$(m_{p,08})^2$	$\frac{\sqrt{2}\lambda_2}{6}(x^2 - 2y^2) - \frac{c}{6}(\sqrt{2}x - 2y)$
$(m_{s,xx})^2$	$m^2 + 3(\lambda_1 + \frac{\lambda_2}{2})x^2 + \lambda_1 y^2 - \frac{c}{\sqrt{2}}y$	$(m_{p,xx})^2$	$m^2 + (\lambda_1 + \frac{\lambda_2}{2})x^2 + \lambda_1 y^2 + \frac{c}{\sqrt{2}}y$
$(m_{s,yy})^2$	$m^2 + \lambda_1 x^2 + 3(\lambda_1 + \lambda_2)y^2$	$(m_{p,yy})^2$	$m^2 + \lambda_1 x^2 + (\lambda_1 + \lambda_2)y^2$
$(m_{s,xy})^2$	$2\lambda_1 xy - \frac{c}{\sqrt{2}}x$	$(m_{p,xy})^2$	$\frac{c}{\sqrt{2}}x$
m_σ^2	$\frac{1}{2}(m_{s,00}^2 + m_{s,88}^2) - \frac{1}{2}\sqrt{(m_{s,00}^2 - m_{s,88}^2)^2 + 4m_{s,00}^4}$	m_η^2	$\frac{1}{2}(m_{p,00}^2 + m_{p,88}^2) - \frac{1}{2}\sqrt{(m_{p,00}^2 - m_{p,88}^2)^2 + 4m_{p,00}^4}$
$m_{f_0}^2$	$\frac{1}{2}(m_{s,00}^2 + m_{s,88}^2) + \frac{1}{2}\sqrt{(m_{s,00}^2 - m_{s,88}^2)^2 + 4m_{s,00}^4}$	$m_{\eta'}^2$	$\frac{1}{2}(m_{p,00}^2 + m_{p,88}^2) + \frac{1}{2}\sqrt{(m_{p,00}^2 - m_{p,88}^2)^2 + 4m_{p,00}^4}$

$$\Omega_{q\bar{q}}^{T,\mu}(x,y) = -2N_c \sum_{u,d,s} \int \frac{d^3p}{(2\pi)^3} T [\ln(1 + e^{-E_f^\pm/T}) + \ln(1 + e^{-E_{\bar{f}}^\pm/T})]. \quad (16)$$

The fermion vacuum contribution is given by the first term of Eq. (14), where Λ_c is the ultraviolet cutoff. $E_f^\pm = E_f \mp \mu_f$ and $E_f = \sqrt{p^2 + m_f^2}$ is the flavor-dependent single particle energy of the quark/antiquark, $m_u = m_d = \frac{m_s}{2}$ is the mass of the light quarks u, d , and the strange quark mass is $m_s = \frac{m_s}{\sqrt{2}}$. For the present work, it is assumed that $\mu_u = \mu_d = \mu_s = \mu$.

In the standard mean-field approximation, the quark one-loop vacuum term of the Eq. (14) is neglected and the QM model grand potential is written as

$$\Omega_{\text{QM}}(T, \mu, x, y) = U(x, y) + \Omega_{q\bar{q}}^{T,\mu}(x, y). \quad (17)$$

The chiral order parameters x for the nonstrange and y for the strange sector are obtained by minimizing the thermodynamic potential the Eq. (17) in the nonstrange and strange directions

$$\left. \frac{\partial \Omega_{\text{QM}}(T, \mu, x, y)}{\partial x} \right|_{x,y} = \left. \frac{\partial \Omega_{\text{QM}}(T, \mu, x, y)}{\partial y} \right|_{x,y} = 0. \quad (18)$$

B. Parameter fixing

The six model parameters m^2 , λ_1 , λ_2 , c , h_x , and h_y are obtained using six experimentally known quantities in the vacuum. The pion, kaon mass, the average squared mass of the η and η' mesons ($m_\eta^2 + m_{\eta'}^2$) from the pseudoscalar side, and the mass m_σ of the scalar meson σ together with the pion and kaon decay constants f_π and f_K are used as the input [18,19] for determining the six model parameters.

In accordance of the partially conserved axial-vector current (PCAC) relation, the vacuum condensates values are $\bar{x} = f_\pi$ and $\bar{y} = (2f_K - f_\pi)/\sqrt{2}$. The minimum of the effective potential in Eq. (18) for $T = 0$, $\mu = 0$ is located at the above values. The parameters λ_2 and c in the vacuum are obtained as

$$\lambda_2 = \frac{2}{(x^2 + 4y^2)(\sqrt{2}y - x)} \left[(3\sqrt{2}y)m_K^2 - (\sqrt{2}y + 2x)m_\pi^2 - (\sqrt{2}y - x)(m_\eta^2 + m_{\eta'}^2) \right], \quad (19)$$

$$c = \frac{2(m_K^2 - m_\pi^2)}{(\sqrt{2}y - x)} - \sqrt{2}y\lambda_2. \quad (20)$$

The difference of the σ and π mass squares ($m_\sigma^2 - m_\pi^2$) does not have any mass parameter m^2 dependence. It depends on the parameters λ_1 , λ_2 , and c . When the λ_2 and c as obtained

from the above two equations are put into the expression of ($m_\sigma^2 - m_\pi^2$) and $x = \bar{x} = f_\pi$ and $y = \bar{y} = (2f_K - f_\pi)/\sqrt{2}$, one gets the vacuum value of the parameter λ_1 . Using the expression of m_π^2 , the mass parameter m^2 can be written as

$$m^2 = m_\pi^2 - \lambda_1(x^2 + y^2) - \frac{\lambda_2}{2}x^2 + \frac{c}{\sqrt{2}}y. \quad (21)$$

Putting the vacuum values of m_π^2 , λ_1 , λ_2 , c , x , and y in Eq. (21), one gets the value of the mass parameter m^2 . Putting the \bar{x} and \bar{y} values in Eq. (13), one gets

$$h_x = f_\pi m_\pi^2 \quad \text{and} \quad h_y = \sqrt{2}f_K m_K^2 - \frac{1}{\sqrt{2}}f_\pi m_\pi^2. \quad (22)$$

Finally, the Yukawa coupling is fixed from the nonstrange constituent quark mass $g = \frac{2m_u}{f_\pi}$. For the $f_\pi = 92.4$ MeV and $m_u \sim 300.3$ MeV, the $g \sim 6.5$ and strange quark mass are predicted to be $m_s \sim 334.34$ MeV. The experimental value $m_\eta = 547.5$ MeV and $m_{\eta'} = 957.78$ MeV. In Ref. [19], the parameter λ_2 is determined by taking the $m_\eta = 539.0$ MeV and $m_{\eta'} = 963.0$ MeV as inputs because the sum of the squared masses $m_\eta^2 + m_{\eta'}^2 = (539.0)^2 + (963.0)^2$ is almost equal to the $(547.5)^2 + (957.78)^2$ and the calculated parameters reproduce $m_\eta = 539.0$ MeV and $m_{\eta'} = 963.0$ MeV in the output.

III. QM MODEL WITH VACUUM TERM

This section contains a brief description of the effective potential calculation when the scalar and pseudoscalar mesons curvature masses are used for the parameter fixing and the vacuum value of the nonstrange condensate is put equal to the pion decay constant while the strange condensate vacuum value is a combination of the pion and kaon decay constant. The quark one-loop vacuum divergence given by the first term of Eq. (14) is regularized under the minimal subtraction scheme using the dimensional regularization as done for the two flavor case in Refs. [51,53,57] and the three flavor case in Refs. [54,55,58,59]. The quark one-loop vacuum term is written as

$$\Omega_{q\bar{q}}^{\text{vac}} = -2N_c \sum_{f=u,d,s} \int \frac{d^3p}{(2\pi)^3} E_f. \quad (23)$$

The dimensional regularization of Eq. (23) near three dimensions $d = 3 - 2\epsilon$ yields the ϵ zeroth order potential as

$$\Omega_{q\bar{q}}^{\text{vac}} = \sum_{f=u,d,s} \frac{N_c m_f^4}{16\pi^2} \left[\frac{1}{\epsilon} - \frac{\{-3 + 2\gamma_E + 4 \ln(\frac{m_f}{2\sqrt{\pi}\Lambda})\}}{2} \right], \quad (24)$$

Here Λ is the arbitrary renormalization scale. When the following counterterm $\delta\mathcal{L}$ is added to the QM model Lagrangian,

$$\delta\mathcal{L} = \sum_{f=u,d,s} \frac{N_c}{16\pi^2} m_f^4 \left[\frac{1}{\epsilon} - \frac{1}{2} \{-3 + 2\gamma_E - 4\ln(2\sqrt{\pi})\} \right], \quad (25)$$

one gets the renormalized fermion vacuum loop contribution as

$$\Omega_{q\bar{q}}^{\text{vac}} = - \sum_{f=u,d,s} \frac{N_c}{8\pi^2} m_f^4 \ln\left(\frac{m_f}{\Lambda}\right), \quad (26)$$

The vacuum grand potential becomes the renormalization scale Λ dependent when the quark one-loop contribution in the first term of Eq. (14) is replaced by Eq. (26) and one writes

$$\Omega^\Lambda(x, y) = U(x, y) + \Omega_{q\bar{q}}^{\text{vac}}. \quad (27)$$

Here the six unknown parameters m^2 , λ_1 , λ_2 , h_x , h_y , and c of the meson potential $U(x, y)$, are obtained from the x - and y -dependent curvature masses of the mesons. The procedural details of finding the different parameters are presented in the Appendix A. When the parameter λ_2 is determined, the logarithmic Λ dependence in the term $\Omega_{q\bar{q}}^{\text{vac}}$ generates a renormalization scale Λ -dependent part $\lambda_{2\Lambda}$ and one gets $\lambda_2 = \lambda_{2s} + n + \lambda_{2+} + \lambda_{2\Lambda}$. λ_{2s} is the same old λ_2 parameter of the QM/PQM model in Refs. [18,19,48]. Here, $n = \frac{N_c g^4}{32\pi^2}$, $\lambda_{2+} = \frac{n f_\pi^2}{f_K(f_K - f_\pi)} \ln\left\{\frac{2f_K - f_\pi}{f_\pi}\right\}$ and $\lambda_{2\Lambda} = 4n \ln\left\{\frac{g(2f_K - f_\pi)}{2\Lambda}\right\}$. When this value of the λ_2 is substituted in the expression of $U(x, y)$ and all the terms of the summation in $\Omega_{q\bar{q}}^{\text{vac}}$ expression are written explicitly, Eq. (27) takes the form

$$\begin{aligned} \Omega^\Lambda(x, y) = & \frac{m^2}{2} (x^2 + y^2) - h_x x - h_y y - \frac{c}{2\sqrt{2}} x^2 y \\ & + \frac{\lambda_1}{4} (x^4 + y^4 + 2x^2 y^2) \\ & + \frac{(\lambda_{2v} + n + \lambda_{2\Lambda})}{8} (x^4 + 2y^4) \\ & - \frac{nx^4}{2} \ln\left(\frac{gx}{2\Lambda}\right) - ny^4 \ln\left(\frac{gy}{\sqrt{2}\Lambda}\right). \end{aligned} \quad (28)$$

Then $\lambda_{2v} = \lambda_{2s} + \lambda_{2+}$. When the terms are rearranged, one finds that the scale dependence of all the terms in $\Omega_{q\bar{q}}^{\text{vac}}$ gets completely cancelled by the logarithmic Λ dependence of the λ_2 contained in $\lambda_{2\Lambda}$. The scale-independent vacuum effective potential expression is

$$\begin{aligned} \Omega(x, y) = & \frac{m^2}{2} (x^2 + y^2) - h_x x - h_y y - \frac{c}{2\sqrt{2}} x^2 y \\ & + \frac{\lambda_1}{4} (x^4 + y^4 + 2x^2 y^2) + \frac{(\lambda_{2v} + n)}{8} (x^4 + 2y^4) \\ & - \frac{nx^4}{2} \ln\left(\frac{x}{(2f_K - f_\pi)}\right) - ny^4 \ln\left(\frac{\sqrt{2}y}{(2f_K - f_\pi)}\right). \end{aligned} \quad (29)$$

One notes that the parameters m^2 , λ_1 , and λ_2 are modified by the fermionic vacuum correction in this parameter fixing scheme while the parameters h_x , h_y , and c are not affected.

The thermodynamic grand potential with the renormalized fermionic vacuum correction in the quark meson model with vacuum term is written as

$$\Omega_{\text{QMVT}}(T, \mu; x, y) = \Omega(x, y) + \Omega_{q\bar{q}}^{T,\mu}(x, y). \quad (30)$$

The nonstrange and strange quark condensates x and y are found by searching the global minimum of the grand potential for a given temperature T and chemical potential μ ,

$$\left. \frac{\partial \Omega_{\text{QMVT}}(T, \mu; x, y)}{\partial x} \right|_{x,y} = \left. \frac{\partial \Omega_{\text{QMVT}}(T, \mu; x, y)}{\partial y} \right|_{x,y} = 0. \quad (31)$$

Here it is relevant to remind the reader that the dressing of the meson propagator is not considered in the curvature mass scheme of parameter fixing. Hence the pion and kaon decay constants f_π and f_K do not get renormalized. The quark one-loop vacuum correction to the effective potential modifies the parameters in such a way that the stationarity conditions in the nonstrange and strange directions for $T = 0$ give the same result for h_x and h_y as in the QM model. The modified curvature masses of the pion and kaon as presented in Appendix B of Ref. [59] remain the same as their pole masses. The minimum of the vacuum effective potential remains at $\bar{x} = f_\pi$ and $\bar{y} = \frac{(2f_K - f_\pi)}{\sqrt{2}}$.

IV. RENORMALIZED QUARK MESON MODEL

Model parameters in several of the recent research works were fixed by taking the π , K , η , η' , and σ meson masses equal to the their curvature (or screening) masses [52–65] while the nonstrange condensate is put equal to the pion decay constant and the strange condensate is related to the pion and kaon decay constant. However, we know that the poles of the meson propagators give their physical masses, and the residue of the pion propagator at its pole is related to the pion decay constant [68–70]. Furthermore, the curvature masses are akin to defining the meson masses by evaluating their self-energies at zero momentum [66,67,71,72] as it is known that the effective potential is the generator of the n -point functions of the theory at zero external momenta. It is also to be noted that the pole definition is the physical and gauge invariant one [81,82]. In the absence of the Dirac sea contributions, the pole mass prescription is equivalent to the curvature mass prescription for the parameter fixing of the model, but when the quark one-loop vacuum correction is taken into account, the pole masses of the mesons start to differ from their screening masses [68,70]. The above arguments necessitate the use of the exact on-shell parameter fixing method for the renormalized quark-meson (RQM) model where the physical (pole) masses of the mesons, the pion, and kaon decay constants are put into the relation of the

running mass parameter and couplings by using the on-shell and the minimal subtraction renormalization prescriptions [71,73,74].

A. Self-energies and counterterms

When the quark one-loop vacuum corrections are included, the tree-level parameters of Eqs. (19)–(22) become inconsistent unless one uses the on-shell renormalization scheme. The divergent loop integrals in the on-shell scheme are also regularized by the dimensional regularization but the counterterm choices are different from the minimal subtraction scheme. The suitable choice of counterterms in the on-shell scheme leads to the exact cancellation of the loop corrections to the self-energies. Since the couplings are evaluated on-shell, the renormalized parameters become renormalization scale independent. The parameters and wave functions/fields of Eq. (1) are bare quantities. The counterterms δm^2 , $\delta\lambda_1$, $\delta\lambda_2$, δc , δh_x , δh_y , and δg^2 for the parameters and the counterterms δZ_π , δZ_K , δZ_σ , δZ_η , $\delta Z_\eta'$, δZ_ψ , δZ_x , and δZ_y for the wave functions/fields are introduced in the Lagrangian (1) where the couplings and renormalized fields are defined as

$$\pi_b^i = \sqrt{Z_\pi}\pi^i, \quad K_b = \sqrt{Z_K}K, \quad \eta_b = \sqrt{Z_\eta}\eta, \quad (32)$$

$$\eta_b' = \sqrt{Z_\eta'}\eta', \quad \sigma_b = \sqrt{Z_\sigma}\sigma, \quad m_b^2 = Z_m m^2 \quad (33)$$

$$\psi_b = \sqrt{Z_\psi}\psi, \quad \lambda_{1b} = Z_{\lambda_1}\lambda_1, \quad \lambda_{2b} = Z_{\lambda_2}\lambda_2, \quad (34)$$

$$g_b = \sqrt{Z_g}g, \quad h_{xb} = Z_{h_x}h_x, \quad h_{yb} = Z_{h_y}h_y, \quad (35)$$

$$c_b = Z_c c, \quad x_b = \sqrt{Z_x}x, \quad y_b = \sqrt{Z_y}y. \quad (36)$$

Here the $Z_{(\pi,K,\eta,\eta',\sigma,\psi,x,y)} = 1 + \delta Z_{(\pi,K,\eta,\eta',\psi,x,y)}$ denote the field strength renormalization constants while $Z_{(m,\lambda_1,\lambda_2,g,h_x,h_y,c)} = 1 + \delta Z_{(m,\lambda_1,\lambda_2,g,h_x,h_y,c)}$ denote the mass and coupling renormalization constants. One-loop correction to the quark fields and the quark masses is zero because in the large N_c limit, the π and σ loops that may renormalize the quark propagators are of the order N_c^0 . Hence the $Z_\psi = 1$ and the respective quark self-energy corrections for the nonstrange quarks and the strange quarks are

$$\begin{aligned} \delta\lambda_{\text{1NUMI}} = & \sqrt{(m_{s,00}^2 - m_{s,88}^2)^2 + 4m_{s,08}^4} (\delta m_\sigma^2 - \delta m_\pi^2) - \left\{ \delta\lambda_2 \frac{(x^2 + 6y^2)}{4} + \delta c \frac{\sqrt{2}y}{4} \right\} \sqrt{(m_{s,00}^2 - m_{s,88}^2)^2 + 4m_{s,08}^4} \\ & + \left\{ \delta\lambda_2 \frac{(x^2 - 2y^2)}{4} - \delta c \frac{\sqrt{2}(4\sqrt{2}x + y)}{12} \right\} (m_{s,00}^2 - m_{s,88}^2) + \left\{ \delta\lambda_2 \sqrt{2}(x^2 - 2y^2) + \delta c \frac{\sqrt{2}(x - \sqrt{2}y)}{3} \right\} m_{s,08}^2 \\ & - \lambda_2 \delta Z_\pi \left\{ \frac{(x^2 + 6y^2)}{4} \sqrt{(m_{s,00}^2 - m_{s,88}^2)^2 + 4m_{s,08}^4} - \frac{(x^2 - 2y^2)}{4} (m_{s,00}^2 - m_{s,88}^2) - \sqrt{2}(x^2 - 2y^2)m_{s,08}^2 \right\} \\ & - c \frac{\delta Z_\pi}{2} \left\{ \frac{\sqrt{2}y}{4} \sqrt{(m_{s,00}^2 - m_{s,88}^2)^2 + 4m_{s,08}^4} + \frac{\sqrt{2}(4\sqrt{2}x + y)}{12} (m_{s,00}^2 - m_{s,88}^2) + \frac{\sqrt{2}(\sqrt{2}y - x)}{3} m_{s,08}^2 \right\}. \quad (42) \end{aligned}$$

$\delta m_u = 0$ and $\delta m_s = 0$. Also, the one-loop correction at the pion-quark $\pi\bar{\psi}\psi$ vertex is of order N_c^0 , and hence gets neglected. As a consequence, we get $Z_\psi \sqrt{Z_g g^2} \sqrt{Z_\pi} \approx g(1 + \frac{1}{2}\frac{\delta g^2}{g^2} + \frac{1}{2}\delta Z_\pi) = g$. Thus $\frac{\delta g^2}{g^2} + \delta Z_\pi = 0$. Furthermore the $\delta m_u = 0$ and $\delta m_s = 0$ implies that $\delta g x/2 + g \delta x/2 = 0$ and $\delta g y/\sqrt{2} + g \delta y/\sqrt{2} = 0$. This gives $\delta x/x = \delta y/y = -\delta g/g$ which is written as

$$\frac{\delta x^2}{x^2} = \frac{\delta y^2}{y^2} = -\frac{\delta g^2}{g^2} = \delta Z_\pi. \quad (37)$$

Following Refs. [67,71–74] and using Eqs. (32)–(36) together with Eqs. (19) and (20), the counterterm $\delta\lambda_2$ can be expressed in terms of the counterterms δm_π^2 , δm_K^2 , δm_η^2 , $\delta m_\eta'^2$ and δZ_π while the δc is expressed in terms of the δm_π^2 , δm_K^2 , δZ_π and the preceding $\delta\lambda_2$. The resulting expressions of the $\delta\lambda_2$ and δc are the following:

$$\delta\lambda_2 = \frac{2}{(x^2 + 4y^2)(\sqrt{2}y - x)} \left[(3\sqrt{2}y)\delta m_K^2 - (\sqrt{2}y + 2x)\delta m_\pi^2 - (\sqrt{2}y - x)(\delta m_\eta^2 + \delta m_\eta'^2) \right] - \lambda_2 \delta Z_\pi, \quad (38)$$

$$\delta c = \frac{2(\delta m_K^2 - \delta m_\pi^2)}{(\sqrt{2}y - x)} - \sqrt{2}y\delta\lambda_2 - (2\sqrt{2}y\lambda_2 + c)\frac{\delta Z_\pi}{2}. \quad (39)$$

Once the $\delta\lambda_2$ and δc are written, using the expression of $(\delta m_\sigma^2 - \delta m_\pi^2)$ and doing some algebraic manipulations, one can write the counterterm $\delta\lambda_1$ as follows:

$$\delta\lambda_1 = \frac{\delta\lambda_{\text{1NUMI}}}{\lambda_{\text{1DENOM}}} - \lambda_1 \delta Z_\pi, \quad (40)$$

$$\begin{aligned} \lambda_{\text{1DENOM}} = & \left(\sqrt{(m_{s,00}^2 - m_{s,88}^2)^2 + 4m_{s,08}^4} \right) (x^2 + y^2) \\ & - \frac{(m_{s,00}^2 - m_{s,88}^2)}{3} (x^2 + 4\sqrt{2}xy - y^2) \\ & - \frac{4m_{s,08}^2}{3} (\sqrt{2}x^2 - xy - \sqrt{2}y^2), \quad (41) \end{aligned}$$

Finally the counterterm δm^2 is written in terms of δm_π^2 , $\delta\lambda_1$, $\delta\lambda_2$, δc , and δZ_π ,

$$\delta m^2 = \delta m_\pi^2 - \delta\lambda_1(x^2 + y^2) - \frac{(\delta\lambda_2)x^2}{2} + \frac{\delta cy}{\sqrt{2}} - \delta Z_\pi \left\{ \lambda_1(x^2 + y^2) + \frac{\lambda_2 x^2}{2} - \frac{cy}{2\sqrt{2}} \right\}. \quad (43)$$

Figure 1(a) depicts the Feynman diagrams of the self-energy and tadpole contributions for the scalar particles while Fig. 1(b) depicts the corresponding counterterm diagrams. The Feynman diagrams of the self-energy and tadpole contributions for the pseudoscalar particles are given in Fig. 2(a) and the corresponding diagrams for the counterterms are presented in the Fig. 2(b). The self-energies of the scalar sigma σ , pseudoscalar eta (η), eta-prime (η'), pion (π), and kaon (K) are required for the on-shell parameter fixing. The scalar σ self-energy correction is obtained in terms of the self-energy corrections $\Sigma_{s,00}(p^2)$, $\Sigma_{s,88}(p^2)$, and $\Sigma_{s,08}(p^2)$ while pseudoscalar η and η' self-energy corrections are obtained in terms of self-energy corrections $\Sigma_{p,00}(p^2)$, $\Sigma_{p,88}(p^2)$, and $\Sigma_{p,08}(p^2)$. The expressions of scalar and pseudoscalar self-energies are written below:

$$\Sigma_{s,00}(p^2) = -\frac{2}{3}N_c g^2 [2\mathcal{A}(m_u^2) - (p^2 - 4m_u^2)\mathcal{B}(p^2, m_u)] - \frac{1}{3}N_c g^2 [2\mathcal{A}(m_s^2) - (p^2 - 4m_s^2)\mathcal{B}(p^2, m_s)] + \Sigma_{s,00}^{\text{tad}}, \quad (44)$$

$$\Sigma_{s,11}(p^2) = -N_c g^2 [2\mathcal{A}(m_u^2) - (p^2 - 4m_u^2)\mathcal{B}(p^2, m_u)] + \Sigma_{s,11}^{\text{tad}}, \quad (45)$$

$$\Sigma_{s,44}(p^2) = -N_c g^2 [\mathcal{A}(m_u^2) + \mathcal{A}(m_s^2) - (p^2 - (m_u + m_s)^2)\mathcal{B}(p^2, m_u, m_s)] + \Sigma_{s,44}^{\text{tad}}, \quad (46)$$

$$\Sigma_{s,88}(p^2) = -\frac{1}{3}N_c g^2 [2\mathcal{A}(m_u^2) - (p^2 - 4m_u^2)\mathcal{B}(p^2, m_u)] - \frac{2}{3}N_c g^2 [2\mathcal{A}(m_s^2) - (p^2 - 4m_s^2)\mathcal{B}(p^2, m_s)] + \Sigma_{s,88}^{\text{tad}}, \quad (47)$$

$$\Sigma_{s,08}(p^2) = -\frac{\sqrt{2}}{3}N_c g^2 [2\mathcal{A}(m_u^2) - (p^2 - 4m_u^2)\mathcal{B}(p^2, m_u)] + \frac{\sqrt{2}}{3}N_c g^2 [2\mathcal{A}(m_s^2) - (p^2 - 4m_s^2)\mathcal{B}(p^2, m_s)] + \Sigma_{s,08}^{\text{tad}}, \quad (48)$$

$$\Sigma_{p,00}(p^2) = -\frac{2}{3}N_c g^2 [2\mathcal{A}(m_u^2) - p^2\mathcal{B}(p^2, m_u)] - \frac{1}{3}N_c g^2 [2\mathcal{A}(m_s^2) - p^2\mathcal{B}(p^2, m_s)] + \Sigma_{p,00}^{\text{tad}}, \quad (49)$$

$$\Sigma_{p,11}(p^2) = \Sigma_\pi(p^2) = -N_c g^2 [2\mathcal{A}(m_u^2) - p^2\mathcal{B}(p^2, m_u)] + \Sigma_{p,11}^{\text{tad}}, \quad (50)$$

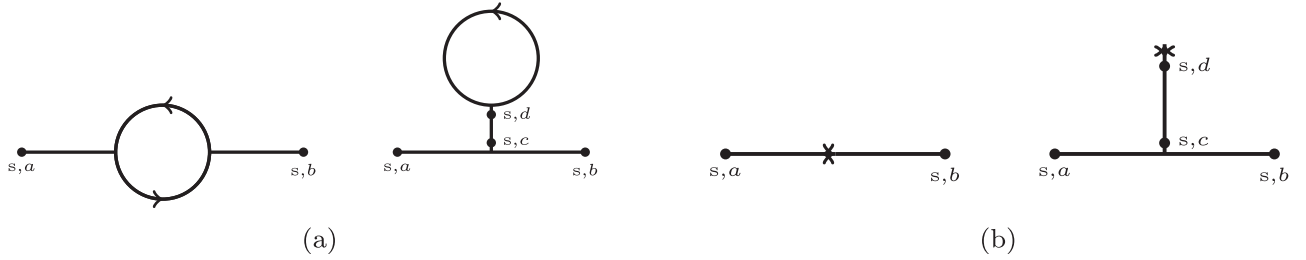


FIG. 1. The solid line represents scalar particles and an arrow on the solid line denotes a quark. (a) One-loop self-energy and tadpole diagrams. (b) One-loop self-energy and tadpole counterterm diagrams.

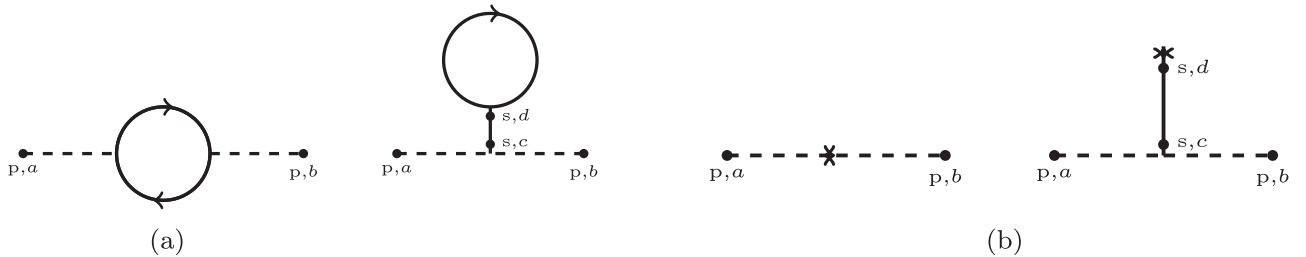


FIG. 2. The dashed line represents pseudoscalar particles and an arrow on the solid line denotes a quark. (a) One-loop self-energy and tadpole diagrams. (b) One-loop self-energy and tadpole counterterm diagrams.

$$\begin{aligned}\Sigma_{p,44}(p^2) &= \Sigma_K(p^2) \\ &= -N_c g^2 [\mathcal{A}(m_u^2) + \mathcal{A}(m_s^2) - \{p^2 - (m_u - m_s)^2\}] \\ &\quad \times \mathcal{B}(p^2, m_u, m_s) + \Sigma_{p,44}^{\text{tad}},\end{aligned}\quad (51)$$

$$\begin{aligned}\Sigma_{p,88}(p^2) &= -\frac{1}{3} N_c g^2 [2\mathcal{A}(m_u^2) - p^2 \mathcal{B}(p^2, m_u)] \\ &\quad - \frac{2}{3} N_c g^2 [2\mathcal{A}(m_s^2) - p^2 \mathcal{B}(p^2, m_s)] \\ &\quad + \Sigma_{p,88}^{\text{tad}},\end{aligned}\quad (52)$$

$$\begin{aligned}\Sigma_{p,08}(p^2) &= -\frac{\sqrt{2}}{3} N_c g^2 [2\mathcal{A}(m_u^2) - p^2 \mathcal{B}(p^2, m_u)] \\ &\quad + \frac{\sqrt{2}}{3} N_c g^2 [2\mathcal{A}(m_s^2) - p^2 \mathcal{B}(p^2, m_s)] \\ &\quad + \Sigma_{p,08}^{\text{tad}}.\end{aligned}\quad (53)$$

The one-point function diagram for the quark one-loop correction to the nonstrange component of the scalar σ and its counterterm is shown in the Fig. 3. It is written as

$$\delta\Gamma_x^{(1)} = -4N_c g m_u \mathcal{A}(m_u^2) + i\delta t_x. \quad (54)$$

Figure 4 presents the one-point function diagram for the quark one-loop correction to the strange component of the scalar σ and its counterterm. It can be written as

$$\delta\Gamma_y^{(1)} = -2\sqrt{2}N_c g m_s \mathcal{A}(m_s^2) + i\delta t_y. \quad (55)$$

B. Parameters with renormalization

The one-point functions $\Gamma_x^{(1)} = it_x = i(h_x - m_\pi^2 x)$ for the nonstrange and $\Gamma_y^{(1)} = it_y = i\{h_y - \frac{\sqrt{2}}{2}(m_K^2 - m_\pi^2)x - m_K^2 y\}$ for the strange degree of freedom become zero and we get two tree-level equations of motion $t_x = 0$ and $t_y = 0$. Thus the classical minimum of the effective potential gets fixed.



FIG. 3. One point diagram for the nonstrange scalar and its counterterm.



FIG. 4. One point diagram for the strange scalar and its counterterm.

The first renormalization condition for the nonstrange $\langle\sigma_x\rangle = 0$ and the strange degree of freedom $\langle\sigma_y\rangle = 0$ requires that the respective one-loop corrections $\delta\Gamma_x^{(1)}$ and $\delta\Gamma_y^{(1)}$ to the one-point functions are put to zero such that the minimum of the effective potential does not change. Thus the $\delta\Gamma_x^{(1)} = 0$ and $\delta\Gamma_y^{(1)} = 0$ give us

$$\delta t_x = -4iN_c g m_u \mathcal{A}(m_u^2), \quad (56)$$

$$\delta t_y = -2\sqrt{2}iN_c g m_s \mathcal{A}(m_s^2). \quad (57)$$

Using the equation $h_x = t_x + m_\pi^2 x$ and $h_y = t_y + \{\frac{\sqrt{2}}{2}(m_K^2 - m_\pi^2)x + m_K^2 y\}$, one can write the counterterms δh_x and δh_y in terms of the corresponding tadpole counterterms δt_x and δt_y as the following:

$$\delta h_x = m_\pi^2 \delta x + \delta m_\pi^2 x + \delta t_x, \quad (58)$$

$$\begin{aligned}\delta h_y &= \left\{ \frac{\sqrt{2}}{2} (m_K^2 - m_\pi^2) \delta x + \frac{\sqrt{2}}{2} (\delta m_K^2 - \delta m_\pi^2) x \right\} \\ &\quad + m_K^2 \delta y + \delta m_K^2 y + \delta t_y.\end{aligned}\quad (59)$$

Using Eq. (37), one can write

$$\delta h_x = \frac{1}{2} m_\pi^2 x \delta Z_\pi + \delta m_\pi^2 x + \delta t_x, \quad (60)$$

$$\begin{aligned}\delta h_y &= \left\{ \frac{\sqrt{2}}{2} (m_K^2 - m_\pi^2) x \frac{\delta Z_\pi}{2} + \frac{\sqrt{2}}{2} (\delta m_K^2 - \delta m_\pi^2) x \right\} \\ &\quad + m_K^2 y \frac{\delta Z_\pi}{2} + \delta m_K^2 y + \delta t_y.\end{aligned}\quad (61)$$

The inverse propagator for the pseudoscalar π , K mesons can be written as

$$p^2 - m_{\pi,K}^2 - i\Sigma_{\pi,K}(p^2) + \text{counterterms}. \quad (62)$$

The mixing in the 00 and 88 components for the scalar (s) and pseudoscalar (p) particles gives us the physical states of the σ and f_0 as the scalar particles and the η and η' as the pseudoscalar particles. The inverse propagator is given by the 2×2 matrix showing the mixing of the 00 and 88 components. When the determinant of this matrix is put to zero, the negative root of the resulting equation gives the inverse propagator of the physical σ in the scalar and η in the pseudoscalar channel. The positive root gives the inverse propagator of the physically observed particles f_0 and η' in the respective scalar and pseudoscalar channels,

$$\text{Det} \begin{pmatrix} p^2 - m_{s(p),00}^2 - i\Sigma_{s(p),00}(p^2) & -m_{s(p),08}^2 - i\Sigma_{s(p),08}(p^2) \\ -m_{s(p),08}^2 - i\Sigma_{s(p),08}(p^2) & p^2 - m_{s(p),88}^2 - i\Sigma_{s(p),88}(p^2) \end{pmatrix} = 0. \quad (63)$$

We obtain two solutions for p^2 :

$$p^2 = \frac{1}{2} \left[\{m_{s(p),00}^2 + i\Sigma_{s(p),00}(p^2)\} + \{m_{s(p),88}^2 + i\Sigma_{s(p),88}(p^2)\} \right. \\ \left. \mp \sqrt{(\{m_{s(p),00}^2 + i\Sigma_{s(p),00}(p^2)\} - \{m_{s(p),88}^2 + i\Sigma_{s(p),88}(p^2)\})^2 + 4(m_{s(p),08}^2 + i\Sigma_{s(p),08}(p^2))^2} \right]. \quad (64)$$

Neglecting the higher order (N_c^2) terms like $\{\Sigma_{s(p),00}(p^2) - \Sigma_{s(p),88}(p^2)\}^2$ and $\Sigma_{s(p),08}^2(p^2)$ in self-energy corrections, the above expression is written as

$$p^2 = \frac{1}{2} \left[(m_{s(p),00}^2 + m_{s(p),88}^2) \mp \sqrt{(m_{s(p),00}^2 - m_{s(p),88}^2)^2 + 4(m_{s(p),08}^2)^2} \right] + \frac{1}{2} \left[(i\Sigma_{s(p),00}(p^2) + i\Sigma_{s(p),88}(p^2)) \right. \\ \left. \mp \frac{1}{\sqrt{(m_{s(p),00}^2 - m_{s(p),88}^2)^2 + 4m_{s(p),08}^4}} \{ (i\Sigma_{s(p),00}(p^2) - i\Sigma_{s(p),88}(p^2))(m_{s(p),00}^2 - m_{s(p),88}^2) + 4i\Sigma_{s(p),08}(p^2)m_{s(p),08}^2 \} \right]. \quad (65)$$

The negative root of Eq. (65) gives the sum of the mass and self-energy correction for the scalar σ (pseudoscalar η):

$$p^2 = m_{\sigma(\eta)}^2 + i\Sigma_{\sigma(\eta)}(p^2) \quad \text{where } m_{\sigma(\eta)}^2 = \frac{1}{2} \left[(m_{s(p),00}^2 + m_{s(p),88}^2) - \sqrt{(m_{s(p),00}^2 - m_{s(p),88}^2)^2 + 4(m_{s(p),08}^2)^2} \right] \quad \text{and} \\ \Sigma_{\sigma(\eta)}(p^2) = \frac{1}{2} \left[\Sigma_{s(p),00}(p^2) + \Sigma_{s(p),88}(p^2) - \frac{1}{\sqrt{(m_{s(p),00}^2 - m_{s(p),88}^2)^2 + 4m_{s(p),08}^4}} \right. \\ \left. \times \{ (\Sigma_{s(p),00}(p^2) - \Sigma_{s(p),88}(p^2))(m_{s(p),00}^2 - m_{s(p),88}^2) + 4\Sigma_{s(p),08}(p^2)m_{s(p),08}^2 \} \right]. \quad (66)$$

The positive root of Eq. (65) gives the sum of the mass and self-energy correction for the scalar f_0 (pseudoscalar η'):

$$p^2 = m_{f_0(\eta')}^2 + i\Sigma_{f_0(\eta')}(p^2) \quad \text{where } m_{f_0(\eta')}^2 = \frac{1}{2} \left[(m_{s(p),00}^2 + m_{s(p),88}^2) + \sqrt{(m_{s(p),00}^2 - m_{s(p),88}^2)^2 + 4(m_{s(p),08}^2)^2} \right] \quad \text{and} \\ \Sigma_{f_0(\eta')}(p^2) = \frac{1}{2} \left[\Sigma_{s(p),00}(p^2) + \Sigma_{s(p),88}(p^2) + \frac{1}{\sqrt{(m_{s(p),00}^2 - m_{s(p),88}^2)^2 + 4m_{s(p),08}^4}} \right. \\ \left. \times \{ (\Sigma_{s(p),00}(p^2) - \Sigma_{s(p),88}(p^2))(m_{s(p),00}^2 - m_{s(p),88}^2) + 4\Sigma_{s(p),08}(p^2)m_{s(p),08}^2 \} \right]. \quad (67)$$

Thus the inverse propagator for the scalar σ and the pseudoscalar η, η' mesons can be written as

$$p^2 - m_{\sigma,\eta,\eta'}^2 - i\Sigma_{\sigma,\eta,\eta'}(p^2) + \text{counterterms}. \quad (68)$$

The renormalized mass in the Lagrangian is put equal to the physical mass, i.e. $m = m_{\text{pole}}$ ¹ when the on-shell scheme gets implemented and one can write

¹The contributions of the imaginary parts of the self-energies for defining the mass are neglected.

$$\Sigma(p^2 = m_{\sigma,\eta,\eta',\pi,K}^2) + \text{counterterms} = 0. \quad (69)$$

Since the propagator residue is put to unity in the on-shell scheme, one gets

$$\frac{\partial}{\partial p^2} \Sigma_{\sigma,\eta,\eta',\pi,K}(p^2) \Big|_{p^2 = m_{\sigma,\eta,\eta',\pi,K}^2} + \text{counterterms} = 0. \quad (70)$$

Using the diagrams of Figs. 1(b) and 2(b), the counterterms of the two-point functions of the scalar and pseudoscalar mesons can be written as

$$\Sigma_\sigma^{\text{ct1}}(p^2) = i[\delta Z_\sigma(p^2 - m_\sigma^2) - \delta m_\sigma^2], \quad (71)$$

$$\Sigma_\pi^{\text{ct1}}(p^2) = i[\delta Z_\pi(p^2 - m_\pi^2) - \delta m_\pi^2], \quad (72)$$

$$\Sigma_K^{\text{ct1}}(p^2) = i[\delta Z_K(p^2 - m_K^2) - \delta m_K^2], \quad (73)$$

$$\Sigma_\eta^{\text{ct1}}(p^2) = i[\delta Z_\eta(p^2 - m_\eta^2) - \delta m_\eta^2], \quad (74)$$

$$\Sigma_{\eta'}^{\text{ct1}}(p^2) = i[\delta Z_{\eta'}(p^2 - m_{\eta'}^2) - \delta m_{\eta'}^2]. \quad (75)$$

The tadpole contributions to the scalar and pseudoscalar self-energies contain two independent terms proportional to $N_c g m_u \mathcal{A}(m_u^2)$ and $N_c g m_s \mathcal{A}(m_s^2)$ respectively as presented in the Appendix B. The tadpole counterterms Σ^{ct2} for the scalar and pseudoscalar particles are chosen (negative of the respective tadpole contributions to the scalar and pseudoscalar self-energies) such that they completely cancel the respective tadpole contributions to the self-energies. The evaluation of the self-energies and their derivatives in the on-shell conditions give all the

renormalization constants. When Eqs. (69)–(75) are combined, we obtain the following set of equations:

$$\delta m_\pi^2 = -i\Sigma_\pi(m_\pi^2); \quad \delta Z_\pi = i \frac{\partial}{\partial p^2} \Sigma_\pi(p^2) \Big|_{p^2=m_\pi^2}, \quad (76)$$

$$\delta m_K^2 = -i\Sigma_K(m_K^2); \quad \delta Z_K = i \frac{\partial}{\partial p^2} \Sigma_K(p^2) \Big|_{p^2=m_K^2}, \quad (77)$$

$$\delta m_\eta^2 = -i\Sigma_\eta(m_\eta^2); \quad \delta Z_\eta = i \frac{\partial}{\partial p^2} \Sigma_\eta(p^2) \Big|_{p^2=m_\eta^2}, \quad (78)$$

$$\delta m_{\eta'}^2 = -i\Sigma_{\eta'}(m_{\eta'}^2); \quad \delta Z_{\eta'} = i \frac{\partial}{\partial p^2} \Sigma_{\eta'}(p^2) \Big|_{p^2=m_{\eta'}^2}, \quad (79)$$

$$\delta m_\sigma^2 = -i\Sigma_\sigma(m_\sigma^2); \quad \delta Z_\sigma = i \frac{\partial}{\partial p^2} \Sigma_\sigma(p^2) \Big|_{p^2=m_\sigma^2}. \quad (80)$$

When the self-energy (neglecting the tadpole contributions) expressions from Eqs. (49)–(51), and (67) are used, we get the following set of equations:

$$\delta m_\pi^2 = 2ig^2 N_c \left[\mathcal{A}(m_u^2) - \frac{1}{2} m_\pi^2 \mathcal{B}(m_\pi^2, m_u) \right], \quad (81)$$

$$\delta m_K^2 = ig^2 N_c [\mathcal{A}(m_u^2) + \mathcal{A}(m_s^2) - \{m_K^2 - (m_u - m_s)^2\} \mathcal{B}(m_K^2, m_u, m_s)], \quad (82)$$

$$\begin{aligned} \delta m_\eta^2 = & \frac{-i}{2} \left[\Sigma_{p,00}(m_\eta^2) + \Sigma_{p,88}(m_\eta^2) - \frac{1}{\sqrt{(m_{p,00}^2 - m_{p,88}^2)^2 + 4m_{p,08}^4}} \right. \\ & \left. \times \{(\Sigma_{p,00}(m_\eta^2) - \Sigma_{p,88}(m_\eta^2))(m_{p,00}^2 - m_{p,88}^2) + 4\Sigma_{p,08}(m_\eta^2)m_{p,08}^2\} \right], \quad (83) \end{aligned}$$

$$\begin{aligned} \delta m_{\eta'}^2 = & ig^2 N_c \left[\left\{ \mathcal{A}(m_u^2) + \mathcal{A}(m_s^2) - \frac{1}{2} m_{\eta'}^2 \mathcal{B}(m_{\eta'}^2, m_u) - \frac{1}{2} m_{\eta'}^2 \mathcal{B}(m_{\eta'}^2, m_s) \right\} \right. \\ & \left. - \frac{\{(m_{p,00}^2 - m_{p,88}^2) + 4\sqrt{2}m_{p,08}^2\}}{3\sqrt{(m_{p,00}^2 - m_{p,88}^2)^2 + 4m_{p,08}^4}} \left\{ \mathcal{A}(m_u^2) - \mathcal{A}(m_s^2) - \frac{1}{2} m_{\eta'}^2 \mathcal{B}(m_{\eta'}^2, m_u) + \frac{1}{2} m_{\eta'}^2 \mathcal{B}(m_{\eta'}^2, m_s) \right\} \right], \quad (84) \end{aligned}$$

$$\begin{aligned} \delta m_{\eta'}^2 = & \frac{-i}{2} \left[\Sigma_{p,00}(m_{\eta'}^2) + \Sigma_{p,88}(m_{\eta'}^2) + \frac{1}{\sqrt{(m_{p,00}^2 - m_{p,88}^2)^2 + 4m_{p,08}^4}} \right. \\ & \left. \times \{(\Sigma_{p,00}(m_{\eta'}^2) - \Sigma_{p,88}(m_{\eta'}^2))(m_{p,00}^2 - m_{p,88}^2) + 4\Sigma_{p,08}(m_{\eta'}^2)m_{p,08}^2\} \right], \quad (85) \end{aligned}$$

$$\begin{aligned} \delta m_{\eta'}^2 = & ig^2 N_c \left[\left\{ \mathcal{A}(m_u^2) + \mathcal{A}(m_s^2) - \frac{1}{2} m_{\eta'}^2 \mathcal{B}(m_{\eta'}^2, m_u) - \frac{1}{2} m_{\eta'}^2 \mathcal{B}(m_{\eta'}^2, m_s) \right\} \right. \\ & \left. + \frac{\{(m_{p,00}^2 - m_{p,88}^2) + 4\sqrt{2}m_{p,08}^2\}}{3\sqrt{(m_{p,00}^2 - m_{p,88}^2)^2 + 4m_{p,08}^4}} \left\{ \mathcal{A}(m_u^2) - \mathcal{A}(m_s^2) - \frac{1}{2} m_{\eta'}^2 \mathcal{B}(m_{\eta'}^2, m_u) + \frac{1}{2} m_{\eta'}^2 \mathcal{B}(m_{\eta'}^2, m_s) \right\} \right], \quad (86) \end{aligned}$$

$$\delta m_\sigma^2 = \frac{-i}{2} \left[\Sigma_{s,00}(m_\sigma^2) + \Sigma_{s,88}(m_\sigma^2) - \frac{1}{\sqrt{(m_{s,00}^2 - m_{s,88}^2)^2 + 4m_{s,08}^4}} \right. \\ \left. \times \{(\Sigma_{s,00}(m_\sigma^2) - \Sigma_{s,88}(m_\sigma^2))(m_{s,00}^2 - m_{s,88}^2) + 4\Sigma_{s,08}(m_\sigma^2)m_{s,08}^2\} \right], \quad (87)$$

$$\delta m_\sigma^2 = ig^2 N_c \left[\left\{ \mathcal{A}(m_u^2) + \mathcal{A}(m_s^2) - \frac{1}{2}(m_\sigma^2 - 4m_u^2)\mathcal{B}(m_\sigma^2, m_u) - \frac{1}{2}(m_\sigma^2 - 4m_s^2)\mathcal{B}(m_\sigma^2, m_s) \right\} \right. \\ \left. - \frac{\{(m_{s,00}^2 - m_{s,88}^2) + 4\sqrt{2}m_{s,08}^2\}}{3\sqrt{(m_{s,00}^2 - m_{s,88}^2)^2 + 4m_{s,08}^4}} \left\{ \mathcal{A}(m_u^2) - \mathcal{A}(m_s^2) - \frac{(m_\sigma^2 - 4m_u^2)}{2}\mathcal{B}(m_\sigma^2, m_u) + \frac{(m_\sigma^2 - 4m_s^2)}{2}\mathcal{B}(m_\sigma^2, m_s) \right\} \right], \quad (88)$$

$$\delta Z_\pi = ig^2 N_c [\mathcal{B}(m_\pi^2, m_u) + m_\pi^2 \mathcal{B}'(m_\pi^2, m_u)], \quad (89)$$

$$\delta Z_K = ig^2 N_c [\mathcal{B}(m_K^2, m_u, m_s) + (m_K^2 - (m_u - m_s)^2)\mathcal{B}'(m_K^2, m_u, m_s)], \quad (90)$$

$$\delta Z_\eta = \frac{ig^2 N_c}{2} \left[\{\mathcal{B}(m_\eta^2, m_u) + \mathcal{B}(m_\eta^2, m_s) + m_\eta^2 \mathcal{B}'(m_\eta^2, m_u) + m_\eta^2 \mathcal{B}'(m_\eta^2, m_s)\} \right. \\ \left. + \frac{\{(m_{p,00}^2 - m_{p,88}^2) + 4\sqrt{2}m_{p,08}^2\}}{3\sqrt{(m_{p,00}^2 - m_{p,88}^2)^2 + 4m_{p,08}^4}} \{-\mathcal{B}(m_\eta^2, m_u) + \mathcal{B}(m_\eta^2, m_s) - m_\eta^2 \mathcal{B}'(m_\eta^2, m_u) + m_\eta^2 \mathcal{B}'(m_\eta^2, m_s)\} \right], \quad (91)$$

$$\delta Z_{\eta'} = \frac{ig^2 N_c}{2} \left[\{\mathcal{B}(m_{\eta'}^2, m_u) + \mathcal{B}(m_{\eta'}^2, m_s) + m_{\eta'}^2 \mathcal{B}'(m_{\eta'}^2, m_u) + m_{\eta'}^2 \mathcal{B}'(m_{\eta'}^2, m_s)\} \right. \\ \left. - \frac{\{(m_{p,00}^2 - m_{p,88}^2) + 4\sqrt{2}m_{p,08}^2\}}{3\sqrt{(m_{p,00}^2 - m_{p,88}^2)^2 + 4m_{p,08}^4}} \{-\mathcal{B}(m_{\eta'}^2, m_u) + \mathcal{B}(m_{\eta'}^2, m_s) - m_{\eta'}^2 \mathcal{B}'(m_{\eta'}^2, m_u) + m_{\eta'}^2 \mathcal{B}'(m_{\eta'}^2, m_s)\} \right], \quad (92)$$

$$\delta Z_\sigma = \frac{ig^2 N_c}{2} \left[\{\mathcal{B}(m_\sigma^2, m_u) + \mathcal{B}(m_\sigma^2, m_s) + (m_\sigma^2 - 4m_u^2)\mathcal{B}'(m_\sigma^2, m_u) + (m_\sigma^2 - 4m_s^2)\mathcal{B}'(m_\sigma^2, m_s)\} \right. \\ \left. + \frac{\{(m_{s,00}^2 - m_{s,88}^2) + 4\sqrt{2}m_{s,08}^2\}}{3\sqrt{(m_{s,00}^2 - m_{s,88}^2)^2 + 4m_{s,08}^4}} \{\mathcal{B}(m_\sigma^2, m_s) - \mathcal{B}(m_\sigma^2, m_u) - (m_\sigma^2 - 4m_u^2)\mathcal{B}'(m_\sigma^2, m_u) + (m_\sigma^2 - 4m_s^2)\mathcal{B}'(m_\sigma^2, m_s)\} \right]. \quad (93)$$

The expressions of δZ_K , δZ_η , $\delta Z_{\eta'}$, and δZ_σ are given above. However, in the calculations below, only the simplified expression of the δZ_π is needed. Substituting the expressions of δZ_π , δm_K^2 , δm_π^2 , $\delta m_{\eta'}^2$, and $\delta m_{\eta'}^2$ from the above in Eq. (38), $\delta\lambda_2$ is written as

$$\delta\lambda_{2OS} = \frac{2iN_c g^2}{(x^2 + 4y^2)(\sqrt{2}y - x)} \left[(3\sqrt{2}y) \left\{ \mathcal{A}(m_u^2) + \mathcal{A}(m_s^2) - \left(m_K^2 - (m_s - m_u)^2 \right) \mathcal{B}(m_K^2, m_u, m_s) \right\} \right. \\ - (\sqrt{2}y + 2x) \left\{ 2\mathcal{A}(m_u^2) - m_\pi^2 \mathcal{B}(m_\pi^2, m_u) \right\} - (\sqrt{2}y - x) \left\{ 2\mathcal{A}(m_u^2) + 2\mathcal{A}(m_s^2) - \frac{m_\eta^2}{2} \left\{ \mathcal{B}(m_\eta^2, m_u) + \mathcal{B}(m_\eta^2, m_s) \right\} \right. \\ \left. - \frac{m_{\eta'}^2}{2} \left\{ \mathcal{B}(m_{\eta'}^2, m_u) + \mathcal{B}(m_{\eta'}^2, m_s) \right\} \right\} - \frac{(m_{p,00}^2 - m_{p,88}^2 + 4\sqrt{2}m_{p,08}^2)}{6 \left(\sqrt{(m_{p,00}^2 - m_{p,88}^2)^2 + 4m_{p,08}^4} \right)} \\ \left. \times \left\{ m_\eta^2 \left\{ -\mathcal{B}(m_\eta^2, m_u) + \mathcal{B}(m_\eta^2, m_s) \right\} - m_{\eta'}^2 \left\{ -\mathcal{B}(m_{\eta'}^2, m_u) + \mathcal{B}(m_{\eta'}^2, m_s) \right\} \right\} \right], \quad (94)$$

We defined a common factor that occurs in several of the equations below as:

$$\text{SCF} = \left[\ln\left(\frac{\Lambda^2}{m_u^2}\right) + \mathcal{C}(m_\pi^2, m_u) + m_\pi^2 \mathcal{C}'(m_\pi^2, m_u) \right]. \quad (95)$$

$$\delta\lambda_{2\text{OS}} = \delta\lambda_{2\text{div}} + \lambda_{2\text{FIN}} + \lambda_{2\text{SCF}}; \lambda_{2\text{SCF}} = \frac{(N_c g^2) \lambda_2}{(4\pi)^2} \text{SCF}. \quad (96)$$

$$\begin{aligned} \lambda_{2\text{FIN}} = & \frac{N_c g^2}{(4\pi)^2} (\lambda_2 - g^2) \ln\left(\frac{\Lambda^2}{m_u^2}\right) + \frac{N_c g^2}{(4\pi)^2} \frac{2}{(x^2 + 4y^2)} \left[\frac{(\sqrt{2}y + 2x)}{(\sqrt{2}y - x)} \left\{ m_u^2 - m_s^2 \left\{ 1 - 2 \ln\left(\frac{m_s}{m_u}\right) \right\} \right. \right. \\ & \left. \left. - m_\pi^2 \mathcal{C}(m_\pi^2, m_u) \right\} + \frac{3\sqrt{2}y}{(\sqrt{2}y - x)} \left\{ m_K^2 - (m_s - m_u)^2 \right\} \mathcal{C}(m_K^2, m_u, m_s) - \frac{m_\eta^2}{2} \left\{ \mathcal{C}(m_\eta^2, m_u) + \mathcal{C}(m_\eta^2, m_s) \right. \right. \\ & \left. \left. - 2 \ln\left(\frac{m_s}{m_u}\right) \right\} - \frac{m_{\eta'}^2}{2} \left\{ \mathcal{C}(m_{\eta'}^2, m_u) + \mathcal{C}(m_{\eta'}^2, m_s) - 2 \ln\left(\frac{m_s}{m_u}\right) \right\} + \frac{(m_{p,00}^2 - m_{p,88}^2 + 4\sqrt{2}m_{p,08}^2)}{6\left(\sqrt{(m_{p,00}^2 - m_{p,88}^2)^2 + 4m_{p,08}^4}\right)} \right. \\ & \left. \times \left\{ m_\eta^2 \left\{ \mathcal{C}(m_\eta^2, m_u) - \mathcal{C}(m_\eta^2, m_s) + 2 \ln\left(\frac{m_s}{m_u}\right) \right\} - m_{\eta'}^2 \left\{ \mathcal{C}(m_{\eta'}^2, m_u) - \mathcal{C}(m_{\eta'}^2, m_s) + 2 \ln\left(\frac{m_s}{m_u}\right) \right\} \right\} \right]. \quad (97) \end{aligned}$$

Substituting the expressions of δZ_π , δm_K^2 , δm_π^2 , $\delta\lambda_2$ in Eq. (39), δc is written as

$$\begin{aligned} \delta c_{\text{OS}} = & \frac{2iN_c g^2}{(\sqrt{2}y - x)} \left\{ A(m_u^2) + A(m_s^2) - (m_K^2 - (m_s - m_u)^2) \mathcal{B}(m_K^2, m_u, m_s) - 2A(m_u^2) + m_\pi^2 \mathcal{B}(m_\pi^2, m_u) \right\} \\ & - \sqrt{2}y \delta\lambda_{2\text{OS}} - (2\sqrt{2}y \lambda_2 + c) \frac{\delta Z_\pi}{2}; \quad \delta c_{\text{OS}} = \delta c_{\text{div}} + c_{\text{FINTOT}} + c_{\text{SCF}}; \quad c_{\text{FINTOT}} = -\sqrt{2}y \lambda_{2\text{FIN}} + c_{\text{FIN}}, \quad (98) \end{aligned}$$

$$\begin{aligned} c_{\text{FIN}} = & \frac{N_c g^2}{(4\pi)^2} \left[\left\{ c + \sqrt{2}y(\lambda_2 - g^2) \right\} \ln\left(\frac{\Lambda^2}{m_u^2}\right) + \frac{2}{(\sqrt{2}y - x)} \left\{ \left\{ m_K^2 - (m_s - m_u)^2 \right\} \mathcal{C}(m_K^2, m_u, m_s) - m_\pi^2 \mathcal{C}(m_\pi^2, m_u) \right\} \right. \\ & \left. - \frac{g^2}{2} (\sqrt{2}y + x) + \frac{2g^2 y^2}{(\sqrt{2}y - x)} \ln\left(\frac{m_s}{m_u}\right) \right]; \quad c_{\text{SCF}} = \frac{(N_c g^2) c}{2(4\pi)^2} \text{SCF}. \quad (99) \end{aligned}$$

Using Eq. (40) and substituting the expressions of δZ_π , δm_σ^2 , δm_π^2 , $\delta\lambda_2$, and δc in Eq. (42), $\delta\lambda_1$ is written as

$$\delta\lambda_{1\text{OS}} = \frac{\lambda_{1\text{NUMOS}}}{\lambda_{1\text{DENOM}}} - \lambda_1 \delta Z_\pi, \quad (100)$$

$$\begin{aligned} \lambda_{1\text{NUMOS}} = & iN_c g^2 \left[\left(\sqrt{(m_{s,00}^2 - m_{s,88}^2)^2 + 4m_{s,08}^4} \right) \left\{ A(m_u^2) + A(m_s^2) - \left(\frac{m_\sigma^2 - 4m_u^2}{2} \right) \mathcal{B}(m_\sigma^2, m_u) \right. \right. \\ & \left. \left. - \left(\frac{m_\sigma^2 - 4m_s^2}{2} \right) \mathcal{B}(m_\sigma^2, m_s) - 2A(m_u^2) + m_\pi^2 \mathcal{B}(m_\pi^2, m_u) \right\} \right. \\ & \left. - \left(\frac{m_{s,00}^2 - m_{s,88}^2 + 4\sqrt{2}m_{s,08}^2}{3} \right) \left\{ A(m_u^2) - A(m_s^2) - \left(\frac{m_\sigma^2 - 4m_u^2}{2} \right) \mathcal{B}(m_\sigma^2, m_u) + \left(\frac{m_\sigma^2 - 4m_s^2}{2} \right) \mathcal{B}(m_\sigma^2, m_s) \right\} \right] \\ & + \frac{(m_{s,00}^2 - m_{s,88}^2)}{12} \left\{ (3x^2 - 6y^2) \delta\lambda_{2\text{OS}} - \sqrt{2}(4\sqrt{2}x + y) \delta c_{\text{OS}} \right\} \\ & - \frac{\sqrt{2}m_{s,08}^2}{3} \left\{ (2y^2 - x^2) \delta\lambda_{2\text{OS}} + (\sqrt{2}y - x) \delta c_{\text{OS}} \right\} - \frac{1}{4} \sqrt{(m_{s,00}^2 - m_{s,88}^2)^2 + 4m_{s,08}^4} \left\{ (x^2 + 6y^2) \delta\lambda_{2\text{OS}} + \sqrt{2}y \delta c_{\text{OS}} \right\} \\ & + \delta Z_\pi \left[\frac{(m_{\sigma,00}^2 - m_{s,88}^2)}{12} \left\{ (3x^2 - 6y^2) \lambda_2 - \sqrt{2}(4\sqrt{2}x + y) \frac{c}{2} \right\} - \frac{\sqrt{2}m_{s,08}^2}{3} \left\{ (2y^2 - x^2) \lambda_2 + (\sqrt{2}y - x) \frac{c}{2} \right\} \right. \\ & \left. - \frac{1}{4} \left(\sqrt{(m_{s,00}^2 - m_{s,88}^2)^2 + 4m_{s,08}^4} \right) \left\{ (x^2 + 6y^2) \lambda_2 + \sqrt{2}y \frac{c}{2} \right\} \right], \quad (101) \end{aligned}$$

$$\delta\lambda_{1\text{OS}} = \delta\lambda_{1\text{div}} + \lambda_{1\text{FIN}} + \lambda_{1\text{SCF}}; \quad \lambda_{1\text{FIN}} = \frac{\lambda_{1\text{NUMF}}}{\lambda_{1\text{DENOM}}}; \quad \lambda_{1\text{NUMF}} = \lambda_{1\text{NUMF-I}} + \lambda_{1\text{NUMF-II}}; \quad \lambda_{1\text{SCF}} = \frac{N_c g^2 \lambda_1}{(4\pi)^2} \text{SCF}. \quad (102)$$

The expression of $\lambda_{1\text{DENOM}}$ is given in Eq. (41),

$$\begin{aligned} \lambda_{1\text{NUMF-I}} = & \frac{(m_{s,00}^2 - m_{s,88}^2)}{12} \left\{ (3x^2 + 8\sqrt{2}xy - 4y^2)\lambda_{2\text{FIN}} - \sqrt{2}(4\sqrt{2}x + y)c_{\text{FIN}} \right\} \\ & - \frac{\sqrt{2}m_{s,08}^2}{3} \left\{ (\sqrt{2}y - x)c_{\text{FIN}} + (4y^2 + \sqrt{2}xy - 3x^2)\lambda_{2\text{FIN}} \right\} \\ & - \left(\frac{1}{4} \sqrt{(m_{s,00}^2 - m_{s,88}^2)^2 + 4m_{s,08}^4} \right) \left\{ (x^2 + 4y^2)\lambda_{2\text{FIN}} + \sqrt{2}yc_{\text{FIN}} \right\}, \end{aligned} \quad (103)$$

$$\begin{aligned} \lambda_{1\text{NUMF-II}} = & \frac{N_c g^2}{(4\pi)^2} \left[\left(\sqrt{(m_{s,00}^2 - m_{s,88}^2)^2 + 4m_{s,08}^4} \right) \left\{ \frac{g^2}{4} (x^2 - 2y^2) + (m_\sigma^2 - m_\pi^2 - m_u^2 - 3m_s^2) \ln \left(\frac{\Lambda^2}{m_u^2} \right) \right. \right. \\ & + 2m_s^2 \ln \left(\frac{m_s}{m_u} \right) + \frac{(m_\sigma^2 - 4m_u^2)}{2} \mathcal{C}(m_\sigma^2, m_u) + \frac{(m_\sigma^2 - 4m_s^2)}{2} \left(\mathcal{C}(m_\sigma^2, m_s) - 2 \ln \left(\frac{m_s}{m_u} \right) \right) - m_\pi^2 \mathcal{C}(m_\pi^2, m_u) \left. \right\} \\ & - \left(\frac{(m_{s,00}^2 - m_{s,88}^2) + 4\sqrt{2}m_{s,08}^2}{3} \right) \left\{ \frac{g^2}{4} (2y^2 - x^2) \left(1 + 3 \ln \left(\frac{\Lambda^2}{m_u^2} \right) \right) + (m_\sigma^2 - 6m_s^2) \ln \left(\frac{m_s}{m_u} \right) \right. \\ & \left. \left. + \frac{(m_\sigma^2 - 4m_u^2)}{2} \mathcal{C}(m_\sigma^2, m_u) - \frac{(m_\sigma^2 - 4m_s^2)}{2} \mathcal{C}(m_\sigma^2, m_s) \right\} \right], \end{aligned} \quad (104)$$

Using Eq. (43) the δm^2 is written as:

$$\begin{aligned} \delta m_{\text{OS}}^2 = & iN_c g^2 \{ 2A(m_u^2) - m_\pi^2 \mathcal{B}(m_\pi^2, m_u) \} - \delta\lambda_{1\text{OS}}(x^2 + y^2) - \delta\lambda_{2\text{OS}} \frac{x^2}{2} + \frac{\delta c_{\text{OS}y}}{\sqrt{2}} - \delta Z_\pi \left\{ \lambda_1(x^2 + y^2) + \lambda_2 \frac{x^2}{2} - \frac{cy}{2\sqrt{2}} \right\}, \\ \delta m_{\text{OS}}^2 = & \delta m_{\text{div}}^2 + m_{\text{FIN}}^2, \end{aligned} \quad (105)$$

$$m_{\text{FIN}}^2 = \frac{N_c g^2}{(4\pi)^2} \left[-2m_u^2 + (m_\pi^2 - 2m_u^2) \ln \left(\frac{\Lambda^2}{m_u^2} \right) + m_\pi^2 \mathcal{C}(m_\pi^2, m_u) \right] - \left[\lambda_{1\text{FIN}}(x^2 + y^2) + \lambda_{2\text{FIN}} \frac{x^2}{2} - c_{\text{FINTOT}} \frac{y}{\sqrt{2}} \right], \quad (106)$$

Using Eqs. (60) and (61), the δh_x and δh_y can be written as: $\delta h_{y\text{OS}} = \delta h_{y\text{div}} + h_{y\text{FIN}}$, (111)

$$\delta h_{x\text{OS}} = -\frac{i}{2} N_c g^2 m_\pi^2 x [\mathcal{B}(m_\pi^2, m_u) - m_\pi^2 \mathcal{B}'(m_\pi^2, m_u)], \quad (107) \quad h_{y\text{FIN}} = \frac{N_c g^2}{(4\pi)^2} \left[\frac{h_y}{2} \left\{ \ln \left(\frac{\Lambda^2}{m_u^2} \right) - \mathcal{C}(m_\pi^2, m_u) - m_\pi^2 \mathcal{C}'(m_\pi^2, m_u) \right\} \right.$$

$$\delta h_{x\text{OS}} = \delta h_{x\text{div}} + h_{x\text{FIN}}, \quad (108) \quad \left. - \frac{\sqrt{2}h_x}{2} \mathcal{C}(m_\pi^2, m_u) \right.$$

$$\begin{aligned} h_{x\text{FIN}} = & \frac{N_c g^2}{2(4\pi)^2} h_x \left[\ln \left(\frac{\Lambda^2}{m_u^2} \right) + \mathcal{C}(m_\pi^2, m_u) - m_\pi^2 \mathcal{C}'(m_\pi^2, m_u) \right], \\ & + \left(\frac{\sqrt{2}x}{2} - y \right) \left\{ m_u^2 - m_s^2 + 2m_s^2 \ln \left(\frac{m_s}{m_u} \right) \right\} \\ & + \left(\frac{\sqrt{2}x}{2} + y \right) \left\{ m_K^2 - (m_s - m_u)^2 \right\} \mathcal{C}(m_K^2, m_u, m_s) \left. \right], \end{aligned} \quad (109)$$

$$\delta h_{y\text{OS}} = iN_c g^2 \left[\left(\frac{\sqrt{2}}{2} x - y \right) \{ \mathcal{A}(m_s^2) - \mathcal{A}(m_u^2) \} \right. \quad (112)$$

$$\left. - \left(\frac{\sqrt{2}}{2} x + y \right) \{ m_K^2 - (m_u - m_s)^2 \} \mathcal{B}(m_K^2, m_u, m_s) \right.$$

$$\left. + \left(\frac{\sqrt{2}}{2} x + y \right) \frac{m_K^2}{2} [\mathcal{B}(m_\pi^2, m_u) + m_\pi^2 \mathcal{B}'(m_\pi^2, m_u)] \right.$$

$$\left. + \frac{\sqrt{2}}{4} x m_\pi^2 [\mathcal{B}(m_\pi^2, m_u) - m_\pi^2 \mathcal{B}'(m_\pi^2, m_u)] \right], \quad (110)$$

Using Eqs. (37) and (89), the δZ_π , δx^2 and δy^2 can be written as:

$$\begin{aligned} \delta Z_\pi^{\text{OS}} = & \delta Z_{\pi,\text{div}} - \frac{N_c g^2}{(4\pi)^2} \left[\ln \left(\frac{\Lambda^2}{m_u^2} \right) + \mathcal{C}(m_\pi^2, m_u) \right. \\ & \left. + m_\pi^2 \mathcal{C}'(m_\pi^2, m_u) \right], \end{aligned} \quad (113)$$

$$\begin{aligned} \delta g_{\text{OS}}^2 &= -iN_c g^4 [m_\pi^2 \mathcal{B}'(m_\pi^2, m_u) + \mathcal{B}(m_\pi^2, m_u)] \\ &= \delta g_{\text{div}}^2 + \frac{N_c g^4}{(4\pi)^2} \left[\ln \left(\frac{\Lambda^2}{m_u^2} \right) + \mathcal{C}(m_\pi^2, m_u) \right. \\ &\quad \left. + m_\pi^2 \mathcal{C}'(m_\pi^2, m_u) \right], \end{aligned} \quad (114)$$

$$\begin{aligned} \delta x_{\text{OS}}^2 &= iN_c g^2 x^2 [m_\pi^2 \mathcal{B}'(m_\pi^2, m_u) + \mathcal{B}(m_\pi^2, m_u)] \\ &= \delta x_{\text{div}}^2 - \frac{N_c g^2 x^2}{(4\pi)^2} \left[\ln \left(\frac{\Lambda^2}{m_u^2} \right) + \mathcal{C}(m_\pi^2, m_u) \right. \\ &\quad \left. + m_\pi^2 \mathcal{C}'(m_\pi^2, m_u) \right], \end{aligned} \quad (115)$$

$$\begin{aligned} \delta y_{\text{OS}}^2 &= iN_c g^2 y^2 [m_\pi^2 \mathcal{B}'(m_\pi^2, m_u) + \mathcal{B}(m_\pi^2, m_u)] \\ &= \delta y_{\text{div}}^2 - \frac{N_c g^2 y^2}{(4\pi)^2} \left[\ln \left(\frac{\Lambda^2}{m_u^2} \right) + \mathcal{C}(m_\pi^2, m_u) \right. \\ &\quad \left. + m_\pi^2 \mathcal{C}'(m_\pi^2, m_u) \right]. \end{aligned} \quad (116)$$

$\mathcal{A}(m_f^2)$, $\mathcal{B}(m^2, m_f)$, $\mathcal{B}(m^2, m_u, m_s)$, $\mathcal{B}'(m^2, m_f)$, $\mathcal{C}(m^2, m_f)$, $\mathcal{C}(m^2, m_u, m_s)$, $\mathcal{C}'(m^2, m_f)$, and $\mathcal{C}'(m^2, m_u, m_s)$ are defined in the Appendix C. The divergent parts of the counterterms are $\delta\lambda_{2\text{div}} = \frac{N_c g^2}{(4\pi)^2 \epsilon} (2\lambda_2 - g^2)$, $\delta c_{\text{div}} = \frac{3N_c g^2 c}{2(4\pi)^2 \epsilon}$, $\delta\lambda_{1\text{div}} = \frac{N_c g^2 2\lambda_1}{(4\pi)^2 \epsilon}$, $\delta m_{\text{div}}^2 = \frac{N_c g^2 m^2}{(4\pi)^2 \epsilon}$, $\delta h_{x\text{div}} = \frac{N_c g^2 h_x}{2(4\pi)^2 \epsilon}$, $\delta h_{y\text{div}} = \frac{N_c g^2 h_y}{2(4\pi)^2 \epsilon}$, $\delta g_{\text{div}}^2 = \frac{N_c g^4}{(4\pi)^2 \epsilon}$, $\delta x_{\text{div}}^2 = -\frac{N_c g^2 x^2}{(4\pi)^2 \epsilon}$, $\delta y_{\text{div}}^2 = -\frac{N_c g^2 y^2}{(4\pi)^2 \epsilon}$, $\delta Z_{\pi,\text{div}} = -\frac{N_c g^2}{(4\pi)^2 \epsilon}$. For both, the on-shell and the $\overline{\text{MS}}$ schemes, the divergent parts of the counterterms are the same, i.e. $\delta\lambda_{1\text{div}} = \delta\lambda_{1\overline{\text{MS}}}$, $\delta\lambda_{2\text{div}} = \delta\lambda_{2\overline{\text{MS}}}$ etc.

Since the bare parameters are independent of the renormalization scheme, we can immediately write down the relations between the renormalized parameters in the on-shell and $\overline{\text{MS}}$ schemes as the following:

$$\lambda_{2\overline{\text{MS}}} = \lambda_2 + \delta\lambda_{2\text{OS}} - \delta\lambda_{2\overline{\text{MS}}}, \quad (117)$$

$$c_{\overline{\text{MS}}} = c + \delta c_{\text{OS}} - \delta c_{\overline{\text{MS}}}, \quad (118)$$

$$\lambda_{1\overline{\text{MS}}} = \lambda_1 + \delta\lambda_{1\text{OS}} - \delta\lambda_{1\overline{\text{MS}}}, \quad (119)$$

$$m_{\overline{\text{MS}}}^2 = m^2 + \delta m_{\text{OS}}^2 - \delta m_{\overline{\text{MS}}}^2, \quad (120)$$

$$h_{x\overline{\text{MS}}} = h_x + \delta h_{x\text{OS}} - \delta h_{x\overline{\text{MS}}}, \quad (121)$$

$$h_{y\overline{\text{MS}}} = h_y + \delta h_{y\text{OS}} - \delta h_{y\overline{\text{MS}}}, \quad (122)$$

$$g_{\overline{\text{MS}}}^2 = g^2 + \delta g_{\text{OS}}^2 - \delta g_{\overline{\text{MS}}}^2, \quad (123)$$

$$x_{\overline{\text{MS}}}^2 = x^2 + \delta x_{\text{OS}}^2 - \delta x_{\overline{\text{MS}}}^2, \quad (124)$$

$$y_{\overline{\text{MS}}}^2 = y^2 + \delta y_{\text{OS}}^2 - \delta y_{\overline{\text{MS}}}^2. \quad (125)$$

The minimum of the vacuum effective potential is at $\bar{x} = f_\pi$ and $\bar{y} = \frac{(2f_K - f_\pi)}{\sqrt{2}}$. Using the above set of equations together with Eqs. (96), (98), (102), (105), (108), (111), and (113)–(116), one can write the scale Λ -dependent running parameters in the $\overline{\text{MS}}$ scheme as the following:

$$\lambda_{2\overline{\text{MS}}}(\Lambda) = \lambda_2 + \lambda_{2\text{FIN}} + \lambda_{2\text{SCF}}, \quad (126)$$

$$c_{\overline{\text{MS}}}(\Lambda) = c + c_{\text{FINTOT}} + c_{\text{SCF}}, \quad (127)$$

$$\lambda_{1\overline{\text{MS}}}(\Lambda) = \lambda_1 + \lambda_{1\text{FIN}} + \lambda_{1\text{SCF}}, \quad (128)$$

$$m_{\overline{\text{MS}}}^2(\Lambda) = m^2 + m_{\text{FIN}}^2, \quad (129)$$

$$h_{x\overline{\text{MS}}}(\Lambda) = h_x + h_{x\text{FIN}}, \quad (130)$$

$$h_{y\overline{\text{MS}}}(\Lambda) = h_y + h_{y\text{FIN}}, \quad (131)$$

$$g_{\overline{\text{MS}}}^2(\Lambda) = g^2 + \frac{N_c g^4}{(4\pi)^2} \text{SCF}, \quad (132)$$

$$x_{\overline{\text{MS}}}^2(\Lambda) = f_\pi^2 - \frac{4N_c m_u^2}{(4\pi)^2} \text{SCF}, \quad (133)$$

$$y_{\overline{\text{MS}}}^2(\Lambda) = \left(\frac{2f_K - f_\pi}{\sqrt{2}} \right)^2 - \frac{2N_c m_s^2}{(4\pi)^2} \text{SCF}. \quad (134)$$

The parameters λ_2 , c , λ_1 , m^2 , h_x , h_y , and g^2 in Eqs. (126)–(132), and also in the earlier expressions, have the same tree-level values of the QM model that one obtains after putting $x = f_\pi$ and $y = \frac{(2f_K - f_\pi)}{\sqrt{2}}$ in the expressions of the parameters described in Sec. II B.

In the large- N_c limit the parameters $\lambda_{2\overline{\text{MS}}}$, $c_{\overline{\text{MS}}}$, $\lambda_{1\overline{\text{MS}}}$, $m_{\overline{\text{MS}}}^2$, $h_{x\overline{\text{MS}}}$, $h_{y\overline{\text{MS}}}$, and $g_{\overline{\text{MS}}}^2$ are running with the scale Λ and satisfy a set of the following simultaneous renormalization group equations:

$$\frac{d\lambda_{2\overline{\text{MS}}}(\Lambda)}{d\ln(\Lambda)} = \frac{2N_c}{(4\pi)^2} [2\lambda_{2\overline{\text{MS}}} g_{\overline{\text{MS}}}^2 - g_{\overline{\text{MS}}}^4], \quad (135)$$

$$\frac{dc_{\overline{\text{MS}}}(\Lambda)}{d\ln(\Lambda)} = \frac{3N_c}{(4\pi)^2} g_{\overline{\text{MS}}}^2 c_{\overline{\text{MS}}}, \quad (136)$$

$$\frac{d\lambda_{1\overline{\text{MS}}}(\Lambda)}{d\ln(\Lambda)} = \frac{4N_c}{(4\pi)^2} g_{\overline{\text{MS}}}^2 \lambda_{1\overline{\text{MS}}}, \quad (137)$$

$$\frac{dm_{\overline{\text{MS}}}^2(\Lambda)}{d\ln(\Lambda)} = \frac{2N_c}{(4\pi)^2} g_{\overline{\text{MS}}}^2 m_{\overline{\text{MS}}}^2, \quad (138)$$

$$\frac{dh_{x\overline{\text{MS}}}(\Lambda)}{d\ln(\Lambda)} = \frac{N_c}{(4\pi)^2} g_{\overline{\text{MS}}}^2 h_{x\overline{\text{MS}}}, \quad (139)$$

$$\frac{dh_{y\overline{\text{MS}}}(\Lambda)}{d\ln(\Lambda)} = \frac{N_c}{(4\pi)^2} g_{\overline{\text{MS}}}^2 h_{y\overline{\text{MS}}}, \quad (140)$$

$$\frac{dg_{\overline{\text{MS}}}^2}{d\ln(\Lambda)} = \frac{2N_c}{(4\pi)^2} g_{\overline{\text{MS}}}^4, \quad (141)$$

$$\frac{dx_{\overline{\text{MS}}}^2}{d\ln(\Lambda)} = -\frac{2N_c}{(4\pi)^2} g_{\overline{\text{MS}}}^2 x_{\overline{\text{MS}}}^2, \quad (142)$$

$$\frac{dy_{\overline{\text{MS}}}^2}{d\ln(\Lambda)} = -\frac{2N_c}{(4\pi)^2} g_{\overline{\text{MS}}}^2 y_{\overline{\text{MS}}}^2. \quad (143)$$

Solving the differential Eqs. (135)–(143), we get the following solutions:

$$\lambda_{2\overline{\text{MS}}}(\Lambda) = \frac{\lambda_{20} - \frac{N_c g_0^4}{(4\pi)^2} \ln\left(\frac{\Lambda^2}{\Lambda_0^2}\right)}{\left(1 - \frac{N_c g_0^2}{(4\pi)^2} \ln\left(\frac{\Lambda^2}{\Lambda_0^2}\right)\right)^2}, \quad (144)$$

$$c_{\overline{\text{MS}}}(\Lambda) = \frac{c_0}{\sqrt{\left[1 - \frac{N_c g_0^2}{(4\pi)^2} \ln\left(\frac{\Lambda^2}{\Lambda_0^2}\right)\right]^3}}, \quad (145)$$

$$\lambda_{1\overline{\text{MS}}}(\Lambda) = \frac{\lambda_{10}}{\left(1 - \frac{N_c g_0^2}{(4\pi)^2} \ln\left(\frac{\Lambda^2}{\Lambda_0^2}\right)\right)^2}, \quad (146)$$

$$m_{\overline{\text{MS}}}^2(\Lambda) = \frac{m_0^2}{1 - \frac{N_c g_0^2}{(4\pi)^2} \ln\left(\frac{\Lambda^2}{\Lambda_0^2}\right)}, \quad (147)$$

$$h_{x\overline{\text{MS}}}(\Lambda) = \frac{h_{x0}}{\sqrt{1 - \frac{N_c g_0^2}{(4\pi)^2} \ln\left(\frac{\Lambda^2}{\Lambda_0^2}\right)}}, \quad (148)$$

$$h_{y\overline{\text{MS}}}(\Lambda) = \frac{h_{y0}}{\sqrt{1 - \frac{N_c g_0^2}{(4\pi)^2} \ln\left(\frac{\Lambda^2}{\Lambda_0^2}\right)}}, \quad (149)$$

$$g_{\overline{\text{MS}}}^2(\Lambda) = \frac{g_0^2}{1 - \frac{N_c g_0^2}{(4\pi)^2} \ln\left(\frac{\Lambda^2}{\Lambda_0^2}\right)}, \quad (150)$$

$$x^2 = f_\pi^2 \left[1 - \frac{N_c g_0^2}{(4\pi)^2} \ln\left(\frac{\Lambda^2}{\Lambda_0^2}\right)\right], \quad (151)$$

$$y^2 = \frac{(2f_K - f_\pi)^2}{2} \left[1 - \frac{N_c g_0^2}{(4\pi)^2} \ln\left(\frac{\Lambda^2}{\Lambda_0^2}\right)\right], \quad (152)$$

where the parameters λ_{10} , λ_{20} , g_0^2 , m_0^2 , c_0 , h_{x0} , and h_{y0} are the running parameter values at the scale Λ_0 . We can choose Λ_0 to satisfy the following relation:

$$\ln\left(\frac{\Lambda_0^2}{m_u^2}\right) + \mathcal{C}(m_\pi^2) + m_\pi^2 \mathcal{C}'(m_\pi^2) = 0. \quad (153)$$

Now, we can calculate the parameters of Eqs. (126)–(134) at the scale $\Lambda = \Lambda_0$ and find λ_{10} , λ_{20} , g_0^2 , m_0^2 , c_0 , h_{x0} , and h_{y0} .

C. Effective potential

Using the values of the parameters from Eqs. (144)–(150), the vacuum effective potential in the $\overline{\text{MS}}$ scheme can be written as

$$\Omega_{\text{vac}} = U(x_{\overline{\text{MS}}}, y_{\overline{\text{MS}}}) + \Omega_{\overline{\text{MS}}}^{q,\text{vac}} + \delta U(x_{\overline{\text{MS}}}, y_{\overline{\text{MS}}}), \quad (154)$$

where

$$\begin{aligned} U(x_{\overline{\text{MS}}}, y_{\overline{\text{MS}}}) &= \frac{m_{\overline{\text{MS}}}^2}{2} (x_{\overline{\text{MS}}}^2 + y_{\overline{\text{MS}}}^2) - h_{x\overline{\text{MS}}} x_{\overline{\text{MS}}} \\ &\quad - h_{y\overline{\text{MS}}} y_{\overline{\text{MS}}} - \frac{c_{\overline{\text{MS}}}}{2\sqrt{2}} x_{\overline{\text{MS}}}^2 y_{\overline{\text{MS}}} + \frac{\lambda_{1\overline{\text{MS}}}}{2} x_{\overline{\text{MS}}}^2 y_{\overline{\text{MS}}}^2 \\ &\quad + \frac{2\lambda_{1\overline{\text{MS}}} + \lambda_{2\overline{\text{MS}}}}{8} x_{\overline{\text{MS}}}^4 + \frac{2\lambda_{1\overline{\text{MS}}} + 2\lambda_{2\overline{\text{MS}}}}{8} y_{\overline{\text{MS}}}^4, \end{aligned} \quad (155)$$

$$\begin{aligned} \delta U(x_{\overline{\text{MS}}}, y_{\overline{\text{MS}}}) &= \frac{\delta m_{\overline{\text{MS}}}^2}{2} (x_{\overline{\text{MS}}}^2 + y_{\overline{\text{MS}}}^2) + \frac{m_{\overline{\text{MS}}}^2}{2} (\delta x_{\overline{\text{MS}}}^2 + \delta y_{\overline{\text{MS}}}^2) - \delta h_{x\overline{\text{MS}}} x_{\overline{\text{MS}}} - h_{x\overline{\text{MS}}} \delta x_{\overline{\text{MS}}} - \delta h_{y\overline{\text{MS}}} y_{\overline{\text{MS}}} - h_{y\overline{\text{MS}}} \delta y_{\overline{\text{MS}}} \\ &\quad - \frac{\delta c_{\overline{\text{MS}}}}{2\sqrt{2}} x_{\overline{\text{MS}}}^2 y_{\overline{\text{MS}}} - \frac{c_{\overline{\text{MS}}}}{2\sqrt{2}} (\delta x_{\overline{\text{MS}}}^2 y_{\overline{\text{MS}}} + x_{\overline{\text{MS}}}^2 \delta y_{\overline{\text{MS}}}) + \frac{\delta \lambda_{1\overline{\text{MS}}}}{2} x_{\overline{\text{MS}}}^2 y_{\overline{\text{MS}}}^2 + \frac{\lambda_{1\overline{\text{MS}}}}{2} (\delta x_{\overline{\text{MS}}}^2 y_{\overline{\text{MS}}}^2 + x_{\overline{\text{MS}}}^2 \delta y_{\overline{\text{MS}}}^2) \\ &\quad + \left(\frac{2\delta \lambda_{1\overline{\text{MS}}} + \delta \lambda_{2\overline{\text{MS}}}}{8}\right) x_{\overline{\text{MS}}}^4 + \left(\frac{2\lambda_{1\overline{\text{MS}}} + \lambda_{2\overline{\text{MS}}}}{8}\right) \delta x_{\overline{\text{MS}}}^4 + \left(\frac{2\delta \lambda_{1\overline{\text{MS}}} + 2\delta \lambda_{2\overline{\text{MS}}}}{8}\right) y_{\overline{\text{MS}}}^4 + \left(\frac{2\lambda_{1\overline{\text{MS}}} + 2\lambda_{2\overline{\text{MS}}}}{8}\right) \delta y_{\overline{\text{MS}}}^4. \end{aligned} \quad (156)$$

The $\mathcal{O}(N_c^2)$ terms are dropped as these are two-loop terms and one gets

$$\begin{aligned} \delta U(x_{\overline{MS}}, y_{\overline{MS}}) &= -\frac{N_c g_{\overline{MS}}^4 (x_{\overline{MS}}^4 + 2y_{\overline{MS}}^4)}{8(4\pi)^2} \frac{1}{\epsilon} \\ &= -\frac{N_c (2\Delta_x^4 + \Delta_y^4)}{(4\pi)^2} \frac{1}{\epsilon}. \end{aligned} \quad (157)$$

The quark one-loop vacuum correction for the two non-strange and one strange flavor is written as

$$\begin{aligned} \Omega_{\overline{MS}}^{q,\text{vac}} &= \frac{N_c g_{\overline{MS}}^4 x_{\overline{MS}}^4}{8(4\pi)^2} \left[\frac{1}{\epsilon} + \frac{3}{2} + \ln \left(\frac{4\Lambda^2}{g_{\overline{MS}}^2 x_{\overline{MS}}^2} \right) \right] \\ &\quad + \frac{N_c g_{\overline{MS}}^4 2y_{\overline{MS}}^4}{8(4\pi)^2} \left[\frac{1}{\epsilon} + \frac{3}{2} + \ln \left(\frac{2\Lambda^2}{g_{\overline{MS}}^2 y_{\overline{MS}}^2} \right) \right], \\ &= \frac{N_c (2\Delta_x^4 + \Delta_y^4)}{(4\pi)^2} \frac{1}{\epsilon} + \frac{2N_c \Delta_x^4}{(4\pi)^2} \left[\frac{3}{2} + \ln \left(\frac{\Lambda^2}{\Delta_x^2} \right) \right] \\ &\quad + \frac{N_c \Delta_y^4}{(4\pi)^2} \left[\frac{3}{2} + \ln \left(\frac{\Lambda^2}{\Delta_y^2} \right) \right]. \end{aligned} \quad (158)$$

$$\Omega_{\overline{MS}}^{q,\text{vac:F}} = \frac{2N_c \Delta_x^4}{(4\pi)^2} \left[\frac{3}{2} + \ln \left(\frac{\Lambda^2}{\Delta_x^2} \right) \right] + \frac{N_c \Delta_y^4}{(4\pi)^2} \left[\frac{3}{2} + \ln \left(\frac{\Lambda^2}{\Delta_y^2} \right) \right]. \quad (159)$$

One can define the scale Λ -independent parameters $\Delta_x = \frac{g_{\overline{MS}} x_{\overline{MS}}}{2}$ and $\Delta_y = \frac{g_{\overline{MS}} y_{\overline{MS}}}{\sqrt{2}}$ using Eqs. (132)–(134). It is instructive to write Eq. (155) in terms of the scale-independent Δ_x and Δ_y as

$$\begin{aligned} U(\Delta_x, \Delta_y) &= \frac{m_{\overline{MS}}^2(\Lambda)}{g_{\overline{MS}}^2(\Lambda)} (2\Delta_x^2 + \Delta_y^2) - 2 \frac{h_{x\overline{MS}}(\Lambda)}{g_{\overline{MS}}(\Lambda)} \Delta_x \\ &\quad - \sqrt{2} \frac{h_{y\overline{MS}}(\Lambda)}{g_{\overline{MS}}(\Lambda)} \Delta_y - 2 \frac{c_{\overline{MS}}(\Lambda)}{g_{\overline{MS}}^3(\Lambda)} \Delta_x^2 \Delta_y \\ &\quad + 4 \frac{\lambda_{1\overline{MS}}(\Lambda)}{g_{\overline{MS}}^4(\Lambda)} \Delta_x^2 \Delta_y^2 + 2 \frac{(2\lambda_{1\overline{MS}} + \lambda_{2\overline{MS}})}{g_{\overline{MS}}^4(\Lambda)} \Delta_x^4 \\ &\quad + \frac{(\lambda_{1\overline{MS}} + \lambda_{2\overline{MS}})}{g_{\overline{MS}}^4(\Lambda)} \Delta_y^4, \end{aligned} \quad (160)$$

$$\begin{aligned} U(\Delta_x, \Delta_y) &= \frac{m_0^2}{g_0^2} (2\Delta_x^2 + \Delta_y^2) - 2 \frac{h_{x0}}{g_0} \Delta_x - \sqrt{2} \frac{h_{y0}}{g_0} \Delta_y \\ &\quad - 2 \frac{c_0}{g_0^3} \Delta_x^2 \Delta_y + 4 \frac{\lambda_{10}}{g_0^4} \Delta_x^2 \Delta_y^2 \\ &\quad + 2 \frac{(2\lambda_{10} + \lambda_{20})}{g_0^4} \Delta_x^4 + \frac{(\lambda_{10} + \lambda_{20})}{g_0^4} \Delta_y^4. \end{aligned} \quad (161)$$

The infinite part of $\Omega_{\overline{MS}}^{q,\text{vac}}$ gets completely cancelled by $\delta U(x_{\overline{MS}}, y_{\overline{MS}})$ in Eq. (154) and Ω_{vac} is written in terms of Δ_x and Δ_y as

$$\Omega_{\text{vac}}(\Delta_x, \Delta_y) = U(\Delta_x, \Delta_y) + \Omega_{\overline{MS}}^{q,\text{vac:F}}, \quad (162)$$

$$\begin{aligned} \Omega_{\text{vac}}(\Delta_x, \Delta_y) &= \frac{m_0^2}{g_0^2} (2\Delta_x^2 + \Delta_y^2) - 2 \frac{h_{x0}}{g_0} \Delta_x - \sqrt{2} \frac{h_{y0}}{g_0} \Delta_y \\ &\quad - 2 \frac{c_0}{g_0^3} \Delta_x^2 \Delta_y + 4 \frac{\lambda_{10}}{g_0^4} \Delta_x^2 \Delta_y^2 + 2 \frac{(2\lambda_{10} + \lambda_{20})}{g_0^4} \Delta_x^4 \\ &\quad + \frac{(\lambda_{10} + \lambda_{20})}{g_0^4} \Delta_y^4 + \frac{2N_c \Delta_x^4}{(4\pi)^2} \left[\frac{3}{2} + \ln \left(\frac{\Lambda^2}{\Delta_x^2} \right) \right] \\ &\quad + \frac{N_c \Delta_y^4}{(4\pi)^2} \left[\frac{3}{2} + \ln \left(\frac{\Lambda^2}{\Delta_y^2} \right) \right]. \end{aligned} \quad (163)$$

When the couplings and mass parameter are expressed in terms of the physical meson masses, pion decay constant, kaon decay constant, and Yukawa coupling, one can write

$$\begin{aligned} \Omega_{\text{vac}}(\Delta_x, \Delta_y) &= \frac{(m^2 + m_{\text{FIN}}^2)}{2} \left\{ f_\pi^2 \left(\frac{\Delta_x^2}{m_u^2} \right) + \frac{(2f_K - f_\pi)^2}{2} \left(\frac{\Delta_y^2}{m_s^2} \right) \right\} - (h_x + h_{x\text{FIN}}) f_\pi \left(\frac{\Delta_x}{m_u} \right) - (h_y + h_{y\text{FIN}}) \frac{(2f_K - f_\pi)}{\sqrt{2}} \left(\frac{\Delta_y}{m_s} \right) \\ &\quad - \frac{(c + c_{\text{FINTOT}})}{4} f_\pi^2 (2f_K - f_\pi) \left(\frac{\Delta_x^2}{m_u^2} \right) \left(\frac{\Delta_y}{m_s} \right) + \frac{(\lambda_1 + \lambda_{1\text{FIN}})}{4} f_\pi^2 (2f_K - f_\pi)^2 \left(\frac{\Delta_x^2}{m_u^2} \right) \left(\frac{\Delta_y^2}{m_s^2} \right) \\ &\quad + \frac{\{2(\lambda_1 + \lambda_{1\text{FIN}}) + (\lambda_2 + \lambda_{2\text{FIN}})\}}{8} f_\pi^4 \left(\frac{\Delta_x^4}{m_u^4} \right) + \frac{\{(\lambda_1 + \lambda_{1\text{FIN}}) + (\lambda_2 + \lambda_{2\text{FIN}})\}}{16} (2f_K - f_\pi)^4 \left(\frac{\Delta_y^4}{m_s^4} \right) \\ &\quad + \frac{2N_c \Delta_x^4}{(4\pi)^2} \left[\frac{3}{2} - \ln \left(\frac{\Delta_x^2}{m_u^2} \right) - \mathcal{C}(m_\pi^2) - m_\pi^2 \mathcal{C}'(m_\pi^2) \right] + \frac{N_c \Delta_y^4}{(4\pi)^2} \left[\frac{3}{2} - \ln \left(\frac{\Delta_y^2}{m_s^2} \right) - \mathcal{C}(m_\pi^2) - m_\pi^2 \mathcal{C}'(m_\pi^2) \right]. \end{aligned} \quad (164)$$

It is to be noted that the pion decay constant, the kaon decay constant, and the Yukawa coupling get renormalized in the vacuum because of the dressing of the meson propagator in the on-shell scheme of the RQM model. But Eqs. (132)–(134) at the scale Λ_0 give us $g_{\overline{\text{MS}}} = g_{\text{ren}} = g$, $x_{\overline{\text{MS}}} = f_{\pi, \text{ren}} = f_\pi$ and $y_{\overline{\text{MS}}} = \frac{2f_{K, \text{ren}} - f_{\pi, \text{ren}}}{\sqrt{2}} = \frac{2f_K - f_\pi}{\sqrt{2}}$. Applying the stationarity condition $\frac{\partial \Omega_{\text{vac}}(\Delta_x, \Delta_y)}{\partial \Delta_x} = 0$ to Eq. (164) in the nonstrange direction, one gets $h_{x0} = m_{\pi, c}^2 x_{\overline{\text{MS}}} = m_\pi^2 \left\{ 1 - \frac{N_c g^2}{(4\pi)^2} m_\pi^2 \mathcal{C}'(m_\pi^2) \right\} f_\pi$. This relation makes the curvature mass of the pion as given below in Eq. (165) different from its pole mass. The stationarity condition $\frac{\partial \Omega_{\text{vac}}(\Delta_x, \Delta_y)}{\partial \Delta_y} = 0$ in the strange direction, gives $h_{y0} = \left(\frac{x_{\overline{\text{MS}}}}{\sqrt{2}} + y_{\overline{\text{MS}}} \right) m_{K, c}^2 - \frac{x_{\overline{\text{MS}}}}{\sqrt{2}} m_{\pi, c}^2 = \sqrt{2} f_K m_{K, c}^2 - \frac{f_\pi}{\sqrt{2}} m_{\pi, c}^2$. Using the expression of $h_{y, \overline{\text{MS}}}(\Lambda_0) = h_{y0}$ in Eq. (131), one gets the expression of kaon curvature mass $m_{K, c}^2$ as written below in Eq. (166). It is pointed out that the pion curvature mass $m_{\pi, c}$ (as in Refs. [68,70]) and the kaon curvature mass are different from their pole masses m_π and m_K due to the

consistent on-shell parameter fixing. The minimum of the effective potential remains fixed at $x_{\overline{\text{MS}}} = f_\pi$ and $y_{\overline{\text{MS}}} = \frac{(2f_K - f_\pi)}{\sqrt{2}}$,

$$m_{\pi, c}^2 = m_\pi^2 \left[1 - \frac{N_c g^2}{(4\pi)^2} m_\pi^2 \mathcal{C}'(m_\pi^2) \right], \quad (165)$$

$$m_{K, c}^2 = m_K^2 \left[1 - \frac{N_c g^2}{(4\pi)^2} \left(\mathcal{C}(m_\pi^2, m_u) + m_\pi^2 \mathcal{C}'(m_\pi^2, m_u) - \left(1 - \frac{(m_s - m_u)^2}{m_K^2} \right) \mathcal{C}(m_K^2, m_u, m_s) + \left(1 - \frac{f_\pi}{f_K} \right) \frac{m_u^2 - m_s^2 + 2m_s^2 \ln\left(\frac{m_s}{m_u}\right)}{m_K^2} \right) \right]. \quad (166)$$

The grand potential of the RQM model is written as

$$\Omega_{\text{RQM}}(\Delta_x, \Delta_y, T, \mu) = \Omega_{\text{vac}}(\Delta_x, \Delta_y) + \Omega_{q\bar{q}}^{T, \mu}(x, y). \quad (167)$$

$$\begin{aligned} \Omega_{\text{RQM}}(\Delta_x, \Delta_y, T, \mu) = & \frac{(m^2 + m_{\text{FIN}}^2)}{2} \left\{ f_\pi^2 \left(\frac{\Delta_x^2}{m_u^2} \right) + \frac{(2f_K - f_\pi)^2}{2} \left(\frac{\Delta_y^2}{m_s^2} \right) \right\} - (h_x + h_{x, \text{FIN}}) f_\pi \left(\frac{\Delta_x}{m_u} \right) \\ & - (h_y + h_{y, \text{FIN}}) \frac{(2f_K - f_\pi)}{\sqrt{2}} \left(\frac{\Delta_y}{m_s} \right) - \frac{(c + c_{\text{FINTOT}})}{4} f_\pi^2 (2f_K - f_\pi) \left(\frac{\Delta_x^2}{m_u^2} \right) \left(\frac{\Delta_y}{m_s} \right) \\ & + \frac{(\lambda_1 + \lambda_{1, \text{FIN}})}{4} f_\pi^2 (2f_K - f_\pi)^2 \left(\frac{\Delta_x^2}{m_u^2} \right) \left(\frac{\Delta_y^2}{m_s^2} \right) + \frac{\{2(\lambda_1 + \lambda_{1, \text{FIN}}) + (\lambda_2 + \lambda_{2, \text{FIN}})\}}{8} f_\pi^4 \left(\frac{\Delta_x^4}{m_u^4} \right) \\ & + \frac{\{(\lambda_1 + \lambda_{1, \text{FIN}}) + (\lambda_2 + \lambda_{2, \text{FIN}})\}}{16} (2f_K - f_\pi)^4 \left(\frac{\Delta_y^4}{m_s^4} \right) + \frac{2N_c \Delta_x^4}{(4\pi)^2} \left[\frac{3}{2} - \ln \left(\frac{\Delta_x^2}{m_u^2} \right) - \mathcal{C}(m_\pi^2) - m_\pi^2 \mathcal{C}'(m_\pi^2) \right] \\ & + \frac{N_c \Delta_y^4}{(4\pi)^2} \left[\frac{3}{2} - \ln \left(\frac{\Delta_y^2}{m_s^2} \right) - \mathcal{C}(m_\pi^2) - m_\pi^2 \mathcal{C}'(m_\pi^2) \right] \\ & - 2N_c T \sum_{f=u, d, s} \int \frac{d^3 p}{(2\pi)^3} \left\{ \ln [1 + e^{-E_f^+/T}] + \ln [1 + e^{-E_f^-/T}] \right\}. \quad (168) \end{aligned}$$

One gets the nonstrange condensate Δ_x and strange condensate Δ_y in the RQM model by searching the global minimum of the grand potential in Eq. (168) for a given value of temperature T and chemical potential μ

$$\frac{\partial \Omega_{\text{RQM}}(\Delta_x, \Delta_y, T, \mu)}{\partial \Delta_x} = \frac{\partial \Omega_{\text{RQM}}(\Delta_x, \Delta_y, T, \mu)}{\partial \Delta_y} = 0. \quad (169)$$

In our calculations, we have used $m_\pi = 138.0$ MeV, and $m_K = 496$ MeV. Here in the RQM model, fixing $m_\eta^2 + m_{\eta'}^2 = (547.5)^2 + (957.78)^2$ and then taking the η mass as 527.58 MeV, one gets the η' mass equal to 968.89 MeV. The pole masses $m_\eta = 527.58$ MeV and

$m_{\eta'} = 968.89$ MeV have been used for calculating the self-energy corrections (for η, η') and fixing of the parameters in the on-shell scheme because it has been checked that when the masses are calculated with the new set of renormalized parameters and respective self-energy corrections are added, the same pole masses are reproduced.

V. CURVATURE MASSES OF THE MESONS

The respective curvature of the QM, QMVT, and RQM models' grand potential in Eqs. (17), (30), and (168) at its global minimum gives the temperature and chemical potential dependence of the scalar and pseudoscalar masses of the mesons,

$$m_{\alpha,ab}^2 \Big|_{\text{T,QM/QMVT/RQM}} = \frac{\partial^2 \Omega_{\text{QM/QMVT/RQM}}(T, \mu; x, y)}{\partial \xi_{\alpha,a} \partial \xi_{\alpha,b}} \Big|_{\text{T,QM/QMVT/RQM}}$$

The $\alpha = s$ and p respectively denote the scalar and pseudoscalar mesons,

$$m_{\alpha,ab}^2 \Big|_{\text{T,QM/QMVT/RQM}} = m_{\alpha,ab}^2 \Big|_{\text{QM/QMVT/RQM}} + (\delta m_{\alpha,ab}^{\text{T}})^2. \quad (170)$$

The meson masses get their temperature (chemical potential) dependence from the temperature (chemical potential) dependence of the x and y . The explicit temperature (chemical potential) dependence of the quark-antiquark potential in the grand potential gives rise to the term $(\delta m_{\alpha,ab}^{\text{T}})^2$ which remains the same in the QM, QMVT, and RQM models. The QMVT model meson mass matrix in the vacuum is written as

$$m_{\alpha,ab}^2 \Big|_{\text{QMVT}} = \frac{\partial^2 \Omega^{\Lambda}(x, y)}{\partial \xi_{\alpha,a} \partial \xi_{\alpha,b}} \Big|_{\text{min}} = (m_{\alpha,ab}^{\text{m}})^2 + (\delta m_{\alpha,ab}^{\text{v}})^2. \quad (171)$$

The QM model vacuum meson masses $m_{\alpha,ab}^2$ [evaluated in Refs. [18,19] from the second derivatives of the pure meson potential $U(x, y)$] as presented in Table I have been renamed in the above as $(m_{\alpha,ab}^{\text{m}})^2$ because the parameters will be different in the QMVT (RQM) model. The mass modifications $(\delta m_{\alpha,ab}^{\text{v}})^2$ caused by the one quark-loop vacuum correction are presented in the Appendix A. The renormalization scale Λ dependence of the parameter λ_2 in the QMVT model makes the mass expressions $(m_{\alpha,ab}^{\text{m}})^2$ scale dependent. The above dependence is completely cancelled by the scale Λ dependence present in the $(\delta m_{\alpha,ab}^{\text{v}})^2$. The scale-independent vacuum meson masses $m_{\alpha,ab}^2 \Big|_{\text{QMVT}}$ have been calculated in Appendix B of Ref. [59].

Mass modifications due to the quark-antiquark contributions at the finite temperature (chemical potential) are calculated by taking into account the complete dependences of all the scalar and pseudoscalar mesons in Eq. (4). Diagonalizing the resulting quark mass matrix, the finite temperature expressions of the mass modifications in the QM model were calculated in Ref. [19] as the following:

$$(\delta m_{\alpha,ab}^{\text{T}})^2 \Big|_{\text{QM}} = \frac{\partial^2 \Omega_{q\bar{q}}^{\text{T}}(T, \mu, x, y)}{\partial \xi_{\alpha,a} \partial \xi_{\alpha,b}} \Big|_{\text{min}} \quad (172)$$

$$= 3 \sum_{f=x,y} \int \frac{d^3 p}{(2\pi)^3} \frac{1}{E_f} \left[(n_f^+ + n_f^-) \left(m_{f,ab}^2 - \frac{m_{f,a}^2 m_{f,b}^2}{2E_f^2} \right) + (b_f^+ + b_f^-) \left(\frac{m_{f,a}^2 m_{f,b}^2}{2E_f T} \right) \right]. \quad (173)$$

The notations n_f^{\pm} and b_f^{\pm} have the following definitions:

$$n_f^{\pm} = \frac{1}{1 + e^{E_f^{\pm}/T}} \quad \text{and} \quad b_f^{\pm} = n_f^{\pm} (1 - n_f^{\pm}). \quad (174)$$

The $m_{f,a}^2 \equiv \partial m_f^2 / \partial \xi_{\alpha,a}$ is the first partial derivative and the $m_{f,ab}^2 \equiv \partial^2 m_f^2 / \partial \xi_{\alpha,a} \partial \xi_{\alpha,b}$ is the second partial derivative of the squared quark mass with respect to the meson fields $\xi_{\alpha,b}$. Table III of Ref. [19] shows the calculated values of these derivatives.

The meson mass expressions at the finite temperature in the QM and QMVT model are written as

$$m_{\alpha,ab}^2 \Big|_{\text{T,QM}} = m_{\alpha,ab}^2 + (\delta m_{\alpha,ab}^{\text{T}})^2 \Big|_{\text{QM}}. \quad (175)$$

$$m_{\alpha,ab}^2 \Big|_{\text{T,QMVT}} = m_{\alpha,ab}^2 \Big|_{\text{QMVT}} + (\delta m_{\alpha,ab}^{\text{T}})^2 \Big|_{\text{QM}}. \quad (176)$$

The vacuum curvature masses and pole (physical) masses of the mesons are the same in the QM and QMVT mode, but the curvature masses of the mesons in the RQM model are different from their pole masses due to the on-shell parameter fixing in the RQM model. In the RQM model, the curvature meson mass matrix is calculated by taking the double derivative of Eq. (162) with respect to the meson fields ξ ,

$$m_{\alpha,ab}^2 \Big|_{\text{RQM}} = m_{\alpha,abc}^2 = \frac{\partial^2 \Omega_{\text{vac}}(\Delta_x, \Delta_y)}{\partial \xi_{\alpha,a} \partial \xi_{\alpha,b}} \Big|_{\text{min}} = (m_{\alpha,ab}^0)^2 + (\delta m_{\alpha,ab}^{\text{v,RQM}})^2. \quad (177)$$

Here c has been used to denote the curvature masses for the RQM model. The $(m_{\alpha,ab}^0)^2$ are evaluated from the double derivatives of $U(\Delta_x, \Delta_y)$ which is the pure meson potential written in terms of scale-independent masses. The expressions of the masses $(m_{\alpha,ab}^0)^2$ are the same as that of the vacuum masses $(m_{\alpha,ab})^2$ in the QM model, but here the superscript 0 signifies the fact that the parameters are evaluated in the $\overline{\text{MS}}$ scheme at the scale Λ_0 . Here it is relevant to point out that the finite part of the quark one-loop vacuum correction in the RQM model contains the terms $\frac{2N_c \Delta_x^4(3)}{(4\pi)^2(2)}$ and $\frac{N_c \Delta_y^4(3)}{(4\pi)^2(2)}$ in addition to the scale-dependent terms while in the QMVT model only scale-dependent terms have been considered as the finite part of the correction. Therefore the quark one-loop vacuum corrections to the curvature masses in the RQM model $(\delta m_{\alpha,ab}^{\text{v,RQM}})^2$ are different from the QMVT model vacuum corrections $(\delta m_{\alpha,ab}^{\text{v}})^2$. If one considers the QMVT model finite part of the quark one-loop vacuum corrections, exactly the same as those of the RQM model, the QMVT model parameters of the present calculation will change such that the resulting effective potential remains the same as in the present calculation. The RQM model quark one-loop vacuum corrections are defined as

$$\begin{aligned}
(\delta m_{\alpha,ab}^{\nu,\text{RQM}})^2 &= \left. \frac{\partial^2 \Omega_{\text{MS}}^{q,\text{vac:F}}}{\partial \xi_{\alpha,a} \partial \xi_{\alpha,b}} \right|_{\text{min}} \\
&= \frac{N_c}{8\pi^2} \sum_{f=u,d,s} \left[\left(\frac{\partial \Delta_f^2}{\partial \xi_{\alpha,a}} \right) \left(\frac{\partial \Delta_f^2}{\partial \xi_{\alpha,b}} \right) \ln \left(\frac{\Lambda^2}{\Delta_f^2} \right) \right. \\
&\quad \left. + \Delta_f^2 \left(1 + \ln \left(\frac{\Lambda^2}{\Delta_f^2} \right) \right) \frac{\partial^2 \Delta_f^2}{\partial \xi_{\alpha,a} \partial \xi_{\alpha,b}} \right], \quad (178)
\end{aligned}$$

where $f = u, d = x, \Delta_f = \Delta_x$, and for $f = s = y, \Delta_f = \Delta_y$. The first partial derivatives $\partial \Delta_f^2 / \partial \xi_{\alpha,a} \equiv \partial m_f^2 / \partial \xi_{\alpha,a}$ and the second partial derivatives $\partial^2 \Delta_f^2 / (\partial \xi_{\alpha,a} \partial \xi_{\alpha,b}) \equiv \partial^2 m_f^2 / (\partial \xi_{\alpha,a} \partial \xi_{\alpha,b})$ of the scale-independent squared quark masses with respect to the different meson fields $\xi_{\alpha,b}$ can be taken from Table III of Ref. [19]. Evaluating the above corrections using the condition in Eq. (153) for the $\Lambda = \Lambda_0$, the final expressions of the vacuum curvature masses in the RQM model are calculated and presented below:

$$(m_{\pi,c})^2 = m_0^2 + \lambda_{10}(x^2 + y^2) + \frac{\lambda_{20}}{2}x^2 - \frac{\sqrt{2}c_0}{2}y + \frac{N_c g^4}{32\pi^2}x^2 [1 + 2 \ln f_\pi - \mathcal{C}(m_\pi^2) - m_\pi^2 \mathcal{C}'(m_\pi^2) - 2 \ln x], \quad (179)$$

$$(m_{a_0,c})^2 = m_0^2 + \lambda_{10}(x^2 + y^2) + \frac{3\lambda_{20}}{2}x^2 + \frac{c_0 y}{\sqrt{2}} + \frac{N_c g^4}{32\pi^2}x^2 [1 + 6 \ln f_\pi - 3\mathcal{C}(m_\pi^2) - 3m_\pi^2 \mathcal{C}'(m_\pi^2) - 6 \ln x], \quad (180)$$

$$\begin{aligned}
(m_{K,c})^2 &= m_0^2 + \lambda_{10}(x^2 + y^2) + \frac{\lambda_{20}}{2}(x^2 - \sqrt{2}xy + 2y^2) - \frac{c_0}{2}x \\
&\quad + \frac{N_c g^4}{32\pi^2} \left[(x^2 - \sqrt{2}xy + 2y^2)(1 + 2 \ln f_\pi - \mathcal{C}(m_\pi^2) - m_\pi^2 \mathcal{C}'(m_\pi^2)) - \frac{2}{(x + \sqrt{2}y)} (x^3 \ln x + (\sqrt{2}y)^3 \ln \sqrt{2}y) \right], \quad (181)
\end{aligned}$$

$$\begin{aligned}
(m_{\text{p},00c})^2 &= m_0^2 + \lambda_{10}(x^2 + y^2) + \frac{\lambda_{20}}{3}(x^2 + y^2) + \frac{c_0}{3}(2x + \sqrt{2}y) \\
&\quad + \frac{N_c g^4}{48\pi^2} [(x^2 + y^2)(1 + 2 \ln f_\pi - \mathcal{C}(m_\pi^2) - m_\pi^2 \mathcal{C}'(m_\pi^2)) - 2(x^2 \ln x + y^2 \ln \sqrt{2}y)], \quad (182)
\end{aligned}$$

$$\begin{aligned}
(m_{\text{p},88c})^2 &= m_0^2 + \lambda_{10}(x^2 + y^2) + \frac{\lambda_{20}}{6}(x^2 + y^2) - \frac{c_0}{6}(4x - \sqrt{2}y) \\
&\quad + \frac{N_c g^4}{96\pi^2} [(x^2 + 4y^2)(1 + 2 \ln f_\pi - \mathcal{C}(m_\pi^2) - m_\pi^2 \mathcal{C}'(m_\pi^2)) - 2(x^2 \ln x + 4y^2 \ln \sqrt{2}y)], \quad (183)
\end{aligned}$$

$$\begin{aligned}
(m_{\text{p},08c})^2 &= \frac{\sqrt{2}\lambda_{20}}{6}(x^2 + y^2) - \frac{c_0}{6}(\sqrt{2}x - 2y) \\
&\quad + \frac{\sqrt{2}N_c g^4}{96\pi^2} [(x^2 - 2y^2)(1 + 2 \ln f_\pi - \mathcal{C}(m_\pi^2) - m_\pi^2 \mathcal{C}'(m_\pi^2)) - 2(x^2 \ln x - 2y^2 \ln \sqrt{2}y)], \quad (184)
\end{aligned}$$

$$\begin{aligned}
(m_{s,00c})^2 &= m_0^2 + \frac{\lambda_{10}}{3}(7x^2 + 4\sqrt{2}xy + 5y^2) + \lambda_{20}(x^2 + y^2) - \frac{\sqrt{2}c_0}{3}(\sqrt{2}x + y) \\
&\quad + \frac{N_c g^4}{48\pi^2} [(x^2 + y^2)(1 + 6 \ln f_\pi - 3\mathcal{C}(m_\pi^2) - 3m_\pi^2 \mathcal{C}'(m_\pi^2)) - 6(x^2 \ln x + y^2 \ln \sqrt{2}y)], \quad (185)
\end{aligned}$$

$$\begin{aligned}
(m_{s,88c})^2 &= m_0^2 + \frac{\lambda_{10}}{3}(5x^2 - 4\sqrt{2}xy + 7y^2) + \lambda_{20} \left(\frac{x^2}{2} + 2y^2 \right) + \frac{\sqrt{2}c_0}{3} \left(\sqrt{2}x - \frac{y}{2} \right) \\
&\quad + \frac{N_c g^4}{96\pi^2} [(x^2 + 4y^2)(1 + 6 \ln f_\pi - 3\mathcal{C}(m_\pi^2) - 3m_\pi^2 \mathcal{C}'(m_\pi^2)) - 6(x^2 \ln x + 4y^2 \ln \sqrt{2}y)], \quad (186)
\end{aligned}$$

$$\begin{aligned}
(m_{s,08c})^2 &= \frac{2\lambda_{10}}{3}(\sqrt{2}x^2 - xy - \sqrt{2}y^2) + \sqrt{2}\lambda_{20} \left(\frac{x^2}{2} - y^2 \right) + \frac{c_0}{3\sqrt{2}}(x - \sqrt{2}y) \\
&\quad + \frac{N_c \sqrt{2}g^4}{96\pi^2} [(x^2 - 2y^2)(1 + 6 \ln f_\pi - 3\mathcal{C}(m_\pi^2) - 3m_\pi^2 \mathcal{C}'(m_\pi^2)) - 6(x^2 \ln x - 2y^2 \ln \sqrt{2}y)]. \quad (187)
\end{aligned}$$

We have checked that in vacuum for $x = f_\pi$ and $y = \frac{(2f_K - f_\pi)}{\sqrt{2}}$, $m_{p,11c}^2$ becomes equal to the pion curvature mass $m_{\pi,c}^2$ calculated from Eq. (165) and $m_{p,44c}^2 = m_{K,c}^2$ is equal to the kaon curvature mass calculated from Eq. (166). $m_{s,11c}^2 = m_{a_0,c}^2$. The curvature masses of the scalar σ and pseudoscalar η are obtained as

$$m_{\sigma(\eta),c}^2 = \frac{1}{2} \left[(m_{s(p),00c}^2 + m_{s(p),88c}^2) - \sqrt{(m_{s(p),00c}^2 - m_{s(p),88c}^2)^2 + 4m_{s(p),08c}^4} \right]. \quad (188)$$

The pseudoscalar η' meson curvature mass is given by

$$m_{\eta',c}^2 = \frac{1}{2} \left[(m_{p,00c}^2 + m_{p,88c}^2) + \sqrt{(m_{p,00c}^2 - m_{p,88c}^2)^2 + 4m_{p,08c}^4} \right]. \quad (189)$$

The curvature masses of the mesons at finite temperature (chemical potential) in the RQM model are obtained as

$$m_{a,ab}^2|_{T,RQM} = m_{a,abc}^2 + (\delta m_{a,ab}^T)^2|_{QM}. \quad (190)$$

VI. RESULTS AND DISCUSSION

Table II presents the parameters of the different models when the σ masses are different. The pion decay constant f_π , the kaon decay constant f_K , and the Yukawa coupling g do not get any correction at the scale Λ_0 in the RQM model. Therefore, the RQM model minimum of the vacuum effective potential at $\Delta_x = m_{u/d} = 300.3$ MeV and $\Delta_y = m_s = 433.34$ MeV (as $x = f_\pi = 92.4$ MeV

and $y = \frac{(2f_K - f_\pi)}{\sqrt{2}} = 94.5$ MeV) does not change from its corresponding position in the QM and the QMVT model. The curvature masses of the pion and kaon are the same as their physical (pole) masses in the QM and QMVT model. Due to the consistent on-shell parameter fixing in the RQM model, the curvature mass of the pion calculated from Eq. (165) $m_{\pi,c} = 135.95$ MeV is different (and 2.05 MeV smaller) from its physical mass $m_\pi = 138.0$ MeV while the kaon curvature mass obtained from Eq. (166) $m_{K,c} = 467.99$ MeV is 28.01 MeV smaller than its pole mass $m_K = 496.0$ MeV. We point out that the respective explicit symmetry breaking strengths h_x and h_y in the nonstrange and strange directions which do not change in the QMVT model, get modified (reduced) by the consistent on-shell treatment of the quark one-loop vacuum fluctuation in the RQM model. The consistency and exactness of the RQM model results are buttressed by the findings in Table II which show that the strength h_x gets reduced by a small amount when compared to its QM model reference value while the strength h_y gets reduced by a relatively large amount. The above-mentioned changes are expected because f_π and f_K do not change while the pion and kaon curvature masses get reduced respectively by a small and a relatively large amount. Another important result in Table II worth pointing out is the noteworthy increase of the coefficient c of the 't Hooft determinant term for the $2 + 1$ RQM model. Thus due to the modification caused by the fermionic one-loop vacuum fluctuation, the $U_A(1)$ anomaly gets enhanced in the RQM model. The modifications of the $U_A(1)$ anomaly caused by the vacuum fluctuations and its enhancement caused by the meson vacuum fluctuations have already been reported in Refs. [75–79].

TABLE II. Parameters of the different model scenarios. The RQM model parameters are obtained by putting $\Lambda = \Lambda_0$ in Eqs. (126)–(131).

Model	m_σ (MeV)	λ_2	c (MeV ²)	λ_1	m^2 (MeV ²)	h_x (MeV ³)	h_y (MeV ³)
QM	400	46.43	4801.82	-5.89	(494.549) ²	(120.73) ³	(336.43) ³
	500	46.43	4801.82	-2.69	(434.305) ²	(120.73) ³	(336.43) ³
	600	46.43	4801.82	1.141	(342.139) ²	(120.73) ³	(336.43) ³
	648	46.43	4801.82	3.75	(275.92) ²	(120.73) ³	(336.43) ³
	700	46.43	4801.82	6.63	(160.93) ²	(120.73) ³	(336.43) ³
QMVT	400	46.43	4801.82	-8.17	(282.338) ²	(120.73) ³	(336.43) ³
	500	46.43	4801.82	-5.28	(171.167) ²	(120.73) ³	(336.43) ³
	600	46.43	4801.82	-1.66	-(184.28) ²	(120.73) ³	(336.43) ³
	648	46.43	4801.82	0.369	-(263.494) ²	(120.73) ³	(336.43) ³
	700	46.43	4801.82	2.82	-(334.918) ²	(120.73) ³	(336.43) ³
RQM	400	34.88	7269.20	1.45	(442.447) ²	(119.53) ³	(323.32) ³
	500	34.88	7269.20	3.676	(396.075) ²	(119.53) ³	(323.32) ³
	600	34.88	7269.20	8.890	(256.506) ²	(119.53) ³	(323.32) ³
	648	34.88	7269.20	13.905	-(147.619) ²	(119.53) ³	(323.32) ³
	700	34.88	7269.20	19.23	-(338.906) ²	(119.53) ³	(323.32) ³

A. Comparing the effective potentials, the order parameters, and the phase diagrams

The normalized vacuum effective potential difference $\frac{\{\Omega_{\text{vac}}(\Delta_x, 334.43) - \Omega_{\text{vac}}(0, 334.43)\}}{f_\pi^4}$ versus the scale-independent non-strange constituent quark mass Δ_x , has been plotted in Fig. 5(a) when $m_\sigma = 400$ MeV and the strange quark constituent mass Δ_y is fixed at the 433.34 MeV. The most shallow nonstrange direction effective potential for the s-MFA QM model becomes deeper and deepest respectively in the RQM and the QMVT models. The same trend is repeated in the plots of Fig. 6(a) where the effective potentials for all of the models become deeper due to the increased $m_\sigma = 500$ MeV. The RQM model effective potential coincides with that of the QMVT model when the

m_σ becomes 658.8 MeV in Fig. 6(b) and the trend of Fig. 6(a) gets reversed in Fig. 6(c) where the RQM model effective potential becomes deepest for $m_\sigma = 700$ MeV (>658.8 MeV). It is to be noted that such trend reversal in the effective potential of the two flavor case [74] occurs at a lower sigma meson mass when $m_\sigma > 616$ MeV.

Emphasizing the important difference in the plots of Fig. 7(a) for the strange direction Δ_y -dependent variations of the normalized vacuum effective potential difference $\frac{\{\Omega_{\text{vac}}(300.3, \Delta_y) - \Omega_{\text{vac}}(300.3, 0)\}}{f_\pi^4}$, we note that the RQM model effective potential is shallower even than the QM Model plot while the plot of the QMVT model is deepest when $m_\sigma = 500$ MeV. This happens because the explicit symmetry breaking strength h_y becomes more weak in the

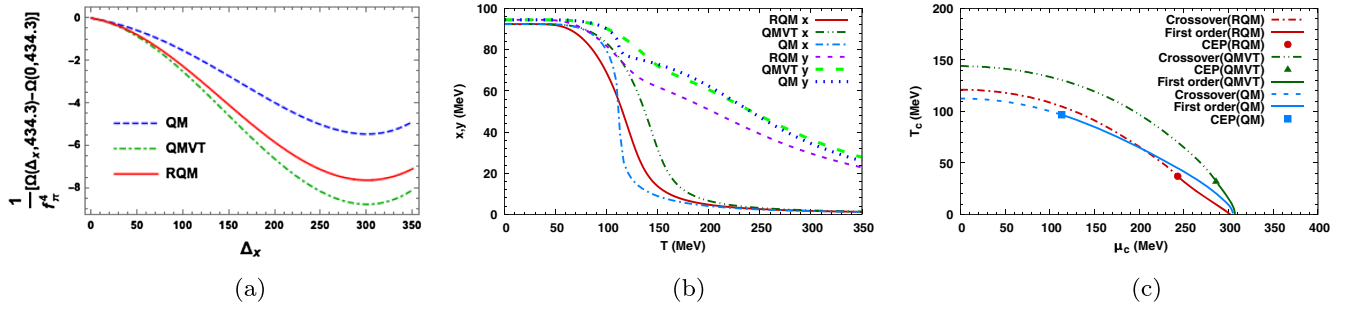


FIG. 5. (a) Effective potential in nonstrange direction for $m_\sigma = 400$ MeV. (b) Nonstrange and strange order parameter for $m_\sigma = 400$ MeV. (c) Phase diagram for $m_\sigma = 400$ MeV.

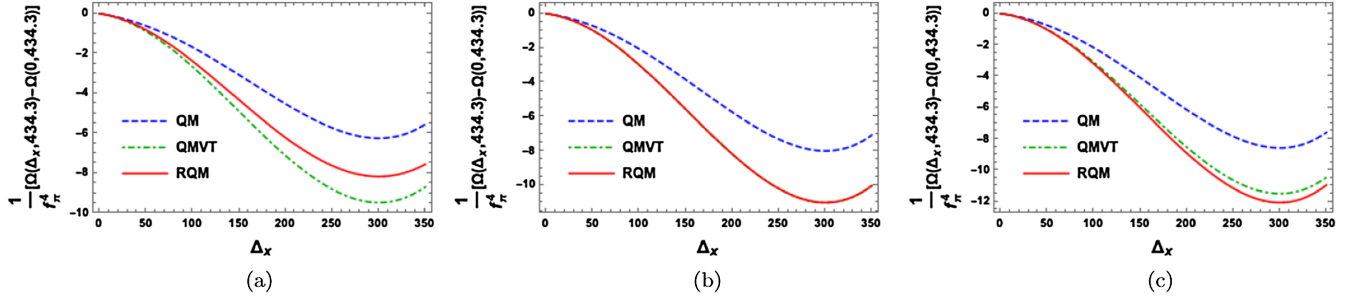


FIG. 6. Normalized effective potential difference in the nonstrange direction for the QM, RQM, and QMVT model. (a) $m_\sigma = 500$ MeV. (b) $m_\sigma = 658.8$ MeV. (c) $m_\sigma = 700$ MeV.

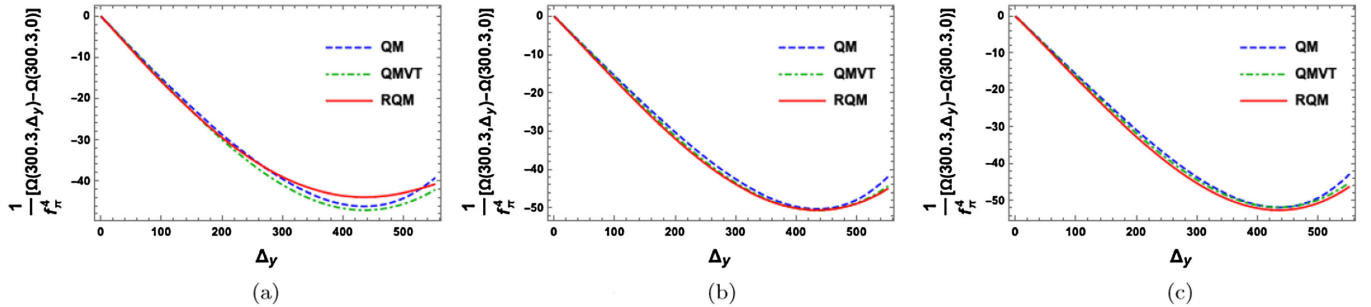


FIG. 7. Normalized effective potential difference in the strange direction for the QM, RQM, and QMVT models. (a) $m_\sigma = 500$ MeV. (b) $m_\sigma = 785$ MeV. (c) $m_\sigma = 850$ MeV.

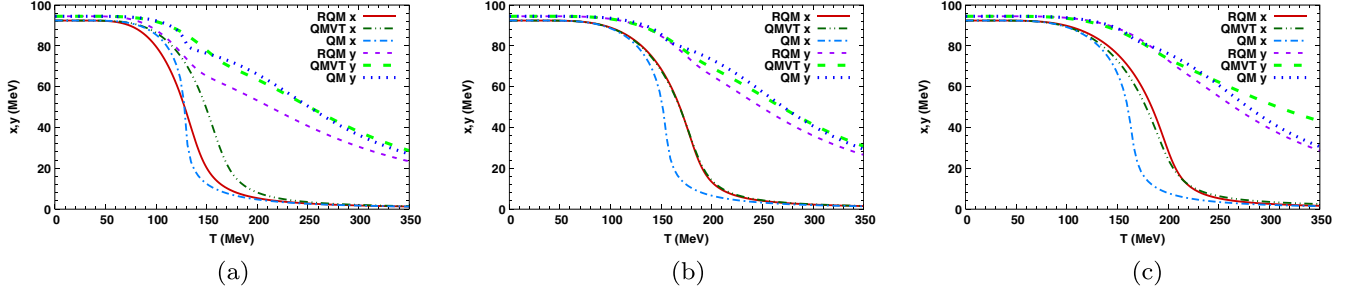


FIG. 8. Temperature variation of the nonstrange and strange order parameter. (a) $m_\sigma = 500$ MeV. (b) $m_\sigma = 648$ MeV. (c) $m_\sigma = 700$ MeV.

strange direction due to the on-shell parameter fixing in the RQM model (as is evident from Table II), and its effect on the strange direction effective potential is more dominant than the smoothing effect of the quark one-loop vacuum correction for the smaller $m_\sigma = 500$ MeV, while the use of the curvature masses for fixing the model parameters does not affect the h_y in the QMVT model. The strange direction effective potentials for all of the models become deeper with the increasing σ mass and, as shown in Fig. 7(b), the strange direction variation of the RQM model effective potential becomes degenerate with that of the QMVT model when m_σ becomes 785.0 MeV. The trend of Fig. 7(a) gets reversed in Fig. 7(c) for $m_\sigma = 850$ MeV (>785.0 MeV) as the strange direction effective potential for the RQM model becomes deepest while the QM model effective potential is most shallow.

The temperature variations of the nonstrange and strange quark condensates x and y (obtained from Δ_x and Δ_y since the renormalization does not change the Yukawa coupling g) at $\mu = 0$ MeV are plotted in Figs. 5(b), 8(a)–8(c) respectively for $m_\sigma = 400, 500, 648,$ and 700 MeV. The temperature derivative of the condensate in the nonstrange and the strange direction when $\mu = 0$ MeV defines the chiral crossover transition temperature (called the pseudocritical temperature) T_c^x for the nonstrange direction and T_c^y for the strange direction. Table III gives the summary of the pseudocritical temperatures T_c^x and T_c^y for the chiral crossover transition in the nonstrange and strange direction for the different values $m_\sigma = 400, 500, 600, 648,$ and 700 MeV. The sharpest QM model temperature variation of the nonstrange quark condensate x in Fig. 5(b) when $m_\sigma = 400$ MeV gives rise to an early chiral crossover

transition at $T_c^x = 112.5$ MeV and a smoother condensate variation generates a smooth chiral transition for the RQM model occurring at $T_c^x = 121.1$ MeV while a most smooth temperature variation of the condensate causes quite a delayed chiral crossover transition at $T_c^x = 144.1$ MeV in the QMVT model. The above trends for the nonstrange chiral condensate temperature variations in the QM, RQM, and QMVT models are repeated in Fig. 8(a) when $m_\sigma = 500$ MeV and the chiral crossover transition occurs respectively at $T_c^x = 129.0, 133.6,$ and 156.8 MeV in the QM, RQM, and QMVT models.

The RQM model temperature variation of the nonstrange quark condensate merges with that of the QMVT model when $m_\sigma = 648$ MeV in Fig. 8(b) and the $\mu = 0$ chiral crossover transition in the nonstrange sector occurs at $T_c^x = 178.1$ MeV in both models. This pattern is a consequence of the coincidence of the RQM model plot of the normalized vacuum effective potential difference $\frac{\{\Omega_{\text{vac}}(\Delta_x, 0.334, 4.3) - \Omega_{\text{vac}}(0, 0.334, 4.3)\}}{f_\pi^4}$ with the corresponding plot in the QMVT model in Fig. 6(b) for the $m_\sigma = 658.8$ MeV case. Here, it is relevant to remind the reader that in the recent two flavor work [74], it was shown that the constituent quark mass (Δ) dependent variation of the vacuum effective potential and the temperature variation of the chiral order parameter for the on-shell parameter fixing scheme in the RQM model completely merges with the corresponding variations computed with the curvature mass parametrization in the QMVT model. In the present $2 + 1$ flavor work, since the vacuum effective potential depends on the nonstrange and strange constituent quark mass parameters Δ_x and Δ_y variations in the two independent

TABLE III. Critical temperature in MeV of the chiral crossover transition at $\mu = 0$ MeV for the nonstrange sector T_c^x and the strange sector T_c^y for $m_\sigma = 400, 500, 600, 648,$ and 700 MeV.

m_σ (MeV)	QM T_c^x	RQM T_c^x	QMVT T_c^x	QM T_c^y	RQM T_c^y	QMVT T_c^y
400	112.5	121.1	144.1	231.6	210.1	236.1
500	129.0	133.6	156.8	238.6	213.3	241.1
600	146.1	158.6	170.8	248.3	220.6	247.8
648	154.5	178.1	178.1	254.8	229.1	251.8
700	163.9	195.8	186.3	261.7	240.3	256.7

directions, the Δ_x variation of the effective potential is somewhat influenced by its Δ_y variation. Hence even though the RQM model nonstrange direction variation of the vacuum effective potential $\frac{\{\Omega_{\text{vac}}(\Delta_y, 334.43) - \Omega_{\text{vac}}(0, 334.43)\}}{f_\pi^4}$ coincides with the corresponding effective potential variation in the QMVT model for $m_\sigma = 658.8$ MeV, the consequential coincidence of the nonstrange order parameter temperature variations for both model settings of the RQM and QMVT occurs when the σ mass is smaller by about 10 MeV, i.e. $m_\sigma = 648$ MeV.

Figure 8(c) for $m_\sigma = 700$ MeV shows that the most smooth nonstrange quark condensate temperature variation takes place in the RQM model and the $\mu = 0$ chiral crossover transition occurring at $T_c^x = 195.8$ MeV is very delayed while a less smooth chiral crossover transition is noticed in the QMVT model occurring earlier at $T_c^x = 186.3$ MeV. Note that the above trend for $m_\sigma = 700$ MeV is opposite of what one observes in Fig. 8(a) for the $m_\sigma = 500$ MeV case. This happens because the nonstrange direction effective potential in the RQM model becomes deepest for the $m_\sigma = 700$ MeV (>658.8 MeV) case while it is shallower than that of the QMVT model for $m_\sigma = 500$ MeV (<658.8 MeV).

The temperature variations of the strange quark condensate y have been plotted by the purple dashed line for the RQM model, the dotted blue line for the QM model, and the thick dashed green line for the QMVT model in Figs. 5(b), 8(a)–8(c) respectively for $m_\sigma = 400, 500, 648,$ and 700 MeV. The temperature variations of the strange condensate in Figs. 5(b) and 8(a) develop a small kink-like region near the T_c^x due to the sharper and the faster chiral transition occurring in the nonstrange direction of the QM Model. The above kink-like structure gets smoothed out due to the quark one-loop vacuum correction in the RQM and QMVT models. The strange condensate melting in the QMVT model for the 160–240 MeV temperature range is larger than that of the QM model result. When the temperature variations of the strange condensate y for all three model scenarios are compared, its melting is most significant in the RQM model. Due to a significantly large and early melting of the strange condensate, the pseudocritical temperatures T_c^s for the different m_σ values are found to be significantly smaller in the RQM model by about 21

to 28 MeV when those are compared with corresponding values of T_c^s in the QM and QMVT models as is evident from Table III. The RQM model strange condensate melting comes closer to its temperature variation in the QM model for the large $m_\sigma = 700$ MeV case. The significantly large melting of the strange condensate in the $2 + 1$ flavor RQM model gets explained when one notes that the on-shell parameter fixing gives rise to a relatively large reduction in the explicit symmetry breaking strength h_y in the strange direction while the nonstrange direction strength h_x is reduced by a small amount.

Figure 5(c) depicts the phase diagram for the $m_\sigma = 400$ MeV case where the line types for different models are labeled. The QM model critical end point (CEP) at $(T_{\text{CEP}}, \mu_{\text{CEP}}) = (96.76, 113.3)$ MeV shifts significantly (as also reported in [53–55, 57, 58]) to a far right position in the lower corner of the μ - T plane at $(T_{\text{CEP}}, \mu_{\text{CEP}}) = (32.23, 285.91)$ MeV for the QMVT model. Note that the CEP moves higher up in the phase diagram at $(T_{\text{CEP}}, \mu_{\text{CEP}}) = (37.03, 243.12)$ for the RQM model. The phase diagrams for $m_\sigma = 500$ MeV have been presented in the μ - T plane of Fig. 9(a). The QM and RQM model phase diagrams stand in close proximity of each other. Here also, the CEP of the QM model at $(T_{\text{CEP}}, \mu_{\text{CEP}}) = (97.52, 165.24)$ MeV shifts to a far right lower corner of the phase diagram at $(T_{\text{CEP}}, \mu_{\text{CEP}}) = (19.8, 311.85)$ MeV in the QMVT model. The robust shift in the present $2 + 1$ flavor QMVT model is quite large (i.e. μ_{CEP} is larger by 11 MeV and T_{CEP} is smaller by about 10 MeV) when it is compared with the corresponding shift reported [74] for the two flavor QMVT model setting. The CEP in the RQM model moves to a significantly higher position in the phase diagram at $(T_{\text{CEP}}, \mu_{\text{CEP}}) = (38.71, 265.42)$ MeV when it is compared with the position of the CEP in the QMVT model. Similar to the two flavor [74] result, here also in the $2 + 1$ flavor investigation, the RQM model and the QMVT model phase diagrams (crossover lines in the entire μ - T plane) merge with each other in Fig. 9(b) for $m_\sigma = 648$ MeV. The above overlap is a consequence of the coincidence that occurs in the normalized vacuum effective potential difference and the nonstrange order parameter plots respectively in Figs. 6(b) and 8(b) for both

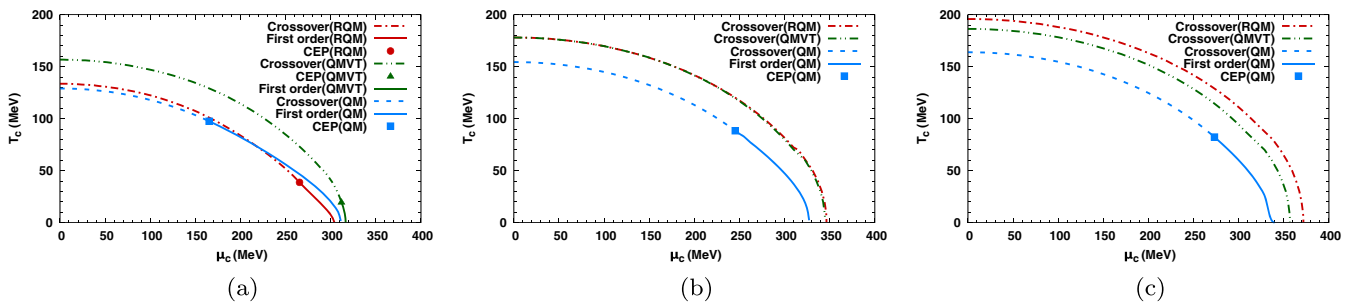


FIG. 9. Phase diagrams for different m_σ . (a) $m_\sigma = 500$ MeV. (b) $m_\sigma = 648$ MeV. (c) $m_\sigma = 700$ MeV.

models RQM and QMVT. The QM model CEP is at $(T_{\text{CEP}}, \mu_{\text{CEP}}) = (88.37, 223.3)$ MeV in Fig. 9(b). For the $m_\sigma = 700$ MeV case in Fig. 9(c), the phase diagrams for the RQM and QMVT models are crossover lines in the entire μ - T plane and here again, the familiar trend reversal is witnessed as instead of the RQM model phase diagram, the phase diagram of the QMVT model stands closer to the QM model phase boundary. The first order line gets terminated at the CEP position $(T_{\text{CEP}}, \mu_{\text{CEP}}) = (82.3, 273.12)$ for the QM model phase diagram.

B. Differences with the two flavor results

Here, we discuss and underline the important differences that exist between the results of the present 2 + 1 flavor QM, QMVT, and RQM model studies and the results of Ref. [74] for the corresponding two flavor model investigations. Table IV presents the comparison of the pseudocritical temperature data of the chiral crossover transition at $\mu = 0$ for the two flavor (data taken from Table II in Ref. [74]) and the 2 + 1 flavor of the QM, QMVT, and RQM models. Denoting the chiral crossover transition temperature by $(T_c^\chi)_{2F}$ and $(T_c^\chi)_{(2+1)F}$ respectively for the two and the 2 + 1 flavor models, the difference $\Delta T_c^\chi = (T_c^\chi)_{2F} - (T_c^\chi)_{(2+1)F}$ for each model has also been tabulated in Table IV for comparison. Note that the chiral transition temperatures in the 2 + 1 flavor models are in general smaller than those in the two flavor models and the difference ΔT_c^χ is positive for all m_σ except for $m_\sigma = 400$ MeV in the QMVT model where the $\Delta T_c^\chi = -0.5$ MeV is marginally negative. Table IV clearly shows

that the difference $\Delta T_c^\chi = 10.7, 12.0,$ and 10.7 MeV respectively for $m_\sigma = 400, 500,$ and 600 MeV between the two flavor and the 2 + 1 flavor chiral transition temperature is highest for the RQM model while the corresponding difference ΔT_c^χ for the QM and QMVT models is very small (i.e. two flavor and 2 + 1 flavor chiral transitions at $\mu = 0$ are almost overlapping).

Table V compares the crucial differences that exist between the location of the CEP in the two flavor (taken from Ref. [74]) and the 2 + 1 flavor calculations of the QM, QMVT, and RQM models when $m_\sigma = 500$ MeV. The location of the CEP in the 2 + 1 flavor computation coincides with that of the two flavor calculation for the QM model. In the QMVT model, the two flavor position of the CEP at $(T_{\text{CEP}}, \mu_{\text{CEP}})_{2F} = (29.48, 299.6)$ MeV goes down and after registering a decrease (increase) of about 10 MeV (12 MeV) in the temperature (chemical potential) direction, the CEP gets located at $(T_{\text{CEP}}, \mu_{\text{CEP}})_{(2+1)F} = (19.8, 311.85)$ MeV in the 2 + 1 flavor calculation. In complete contrast to the QMVT model result, the two flavor location of the CEP in the RQM model at $(T_{\text{CEP}}, \mu_{\text{CEP}})_{2F} = (36.2, 277.3)$ MeV moves up leftward and after registering an increase (decrease) of the 2.51 MeV (about 12 MeV) in the temperature (chemical potential) direction, the CEP gets located at $(T_{\text{CEP}}, \mu_{\text{CEP}})_{(2+1)F} = (38.71, 265.42)$ MeV in the 2 + 1 flavor RQM model calculation. The CEP locations for the two and the 2 + 1 flavor have been compared in the RQM model also when the $m_\sigma = 400$ and 600 MeV in Table V. When $m_\sigma = 400$ and 600 MeV, the shift in the location of the CEP from the two flavor calculation

TABLE IV. The $\mu = 0$ MeV chiral crossover transition pseudocritical temperature is denoted by $(T_c^\chi)_{2F}$ (data has been taken from Table II in Ref. [74]) for the two quark flavor and the $(T_c^\chi)_{(2+1)F}$ (data from Table III) for the 2 + 1 quark flavor of the QM, QMVT, and RQM models when $m_\sigma = 400, 500, 600,$ and 700 MeV. $\Delta T_c^\chi = (T_c^\chi)_{2F} - (T_c^\chi)_{(2+1)F}$.

m_σ (MeV)	QM (MeV)			QMVT (MeV)			RQM (MeV)		
	T_{c2F}^χ	$T_{c(2+1)F}^\chi$	ΔT_c^χ	T_{c2F}^χ	$T_{c(2+1)F}^\chi$	ΔT_c^χ	T_{c2F}^χ	$T_{c(2+1)F}^\chi$	ΔT_c^χ
400	113.3	112.5	0.8	143.6	144.1	-0.5	131.8	121.1	10.7
500	130.2	129.0	1.2	157.3	156.8	0.5	145.6	133.6	12.0
600	147.8	146.1	1.7	173.1	170.8	2.3	169.3	158.6	10.7
700	166.1	163.9	2.2	189.8	186.3	3.5	203.6	195.8	7.8

TABLE V. The position of the critical end point in the phase diagram has been denoted as $(T_{\text{CEP}}, \mu_{\text{CEP}})_{2F}$ for the two quark flavor and $(T_{\text{CEP}}, \mu_{\text{CEP}})_{(2+1)F}$ for the 2 + 1 quark flavor of the QM, QMVT, and RQM models. $m_\sigma = 400, 500,$ and 600 MeV.

m_σ (MeV)	QM (MeV)		QMVT (MeV)		RQM (MeV)	
	$(T_{\text{CEP}}, \mu_{\text{CEP}})_{2F}$	$(T_{\text{CEP}}, \mu_{\text{CEP}})_{(2+1)F}$	$(T_{\text{CEP}}, \mu_{\text{CEP}})_{2F}$	$(T_{\text{CEP}}, \mu_{\text{CEP}})_{(2+1)F}$	$(T_{\text{CEP}}, \mu_{\text{CEP}})_{2F}$	$(T_{\text{CEP}}, \mu_{\text{CEP}})_{(2+1)F}$
400	...	(96.76, 113.30)	...	(32.23, 285.91)	(38.20, 253.50)	(37.03, 243.12)
500	(97.70, 165.20)	(97.52, 165.24)	(29.48, 299.60)	(19.80, 311.85)	(36.20, 277.30)	(38.71, 265.42)
600	(7.20, 322.50)	(17.70, 317.45)

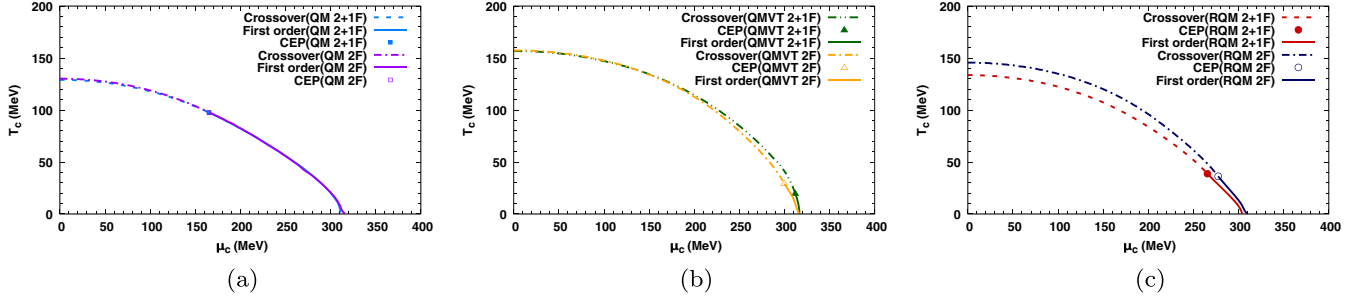


FIG. 10. Phase diagrams of the present 2 + 1 flavor calculations are compared with the two flavor phase diagrams for the QM, QMVT, and RQM model calculations taken from Ref. [74] when $m_\sigma = 500$ MeV.

to the 2 + 1 flavor calculation in the RQM model follows the same pattern that has been observed for the $m_\sigma = 500$ MeV case.

The above discussed findings of Tables IV and V are confirmed when one compares the two flavor and the 2 + 1 flavor model phase diagrams in Figs. 10(a)–10(c) respectively for the QM, QMVT, and RQM models. The phase boundary and the location of the CEP for the two flavor QM model completely coincide with those of the 2 + 1 flavor QM model in Fig. 10(a). The two flavor phase diagram in the QMVT model nearly coincides with that of the 2 + 1 flavor QMVT model up to $\mu = 180$ MeV and the 2 + 1 flavor phase boundary shifts rightwards after crossing the two flavor phase boundary near $\mu \sim 200$ MeV in Fig. 10(b). Further, it is noticed that the CEP location for the 2 + 1 flavor case registers a noticeable downward shift towards the right side of the phase diagram (as also discussed in the preceding paragraph) when it gets compared with the CEP of the two flavor QMVT model. Our findings in the exact on-shell renormalized RQM model are worth emphasizing, because unlike the QM and in complete contrast to the QMVT model, the 2 + 1 flavor RQM model phase boundary lies at a noticeable distance below the two flavor RQM model phase boundary in Fig. 10(c) and the CEP for the 2 + 1 flavor RQM model gets located upward on the left side of the location of the two flavor CEP and phase boundary in the RQM model. The above-mentioned findings are corroborated in Fig. 11 where the two flavor and the 2 + 1 flavor phase diagrams for the RQM model have been plotted when $m_\sigma = 400, 600,$ and 700 MeV.

The well separated 2 + 1 flavor RQM model phase boundary gets located to the left of the two flavor phase boundary and remains below it even when the two and 2 + 1 flavor phase transitions become crossover in the entire μ - T plane for the $m_\sigma = 700$ MeV case. The temperature direction upward shift of the 10.5 MeV (while the chemical potential decreases by 5.05 MeV) is noticeable when the two flavor RQM model CEP at $(T_{\text{CEP}}, \mu_{\text{CEP}})_{2F} = (7.20, 322.50)$ MeV moves up in the phase diagram for the $m_\sigma = 600$ MeV case and gets located at $(T_{\text{CEP}}, \mu_{\text{CEP}})_{(2+1)F} = (17.70, 317.45)$ MeV in the 2 + 1 flavor calculation.

It is clear from Figs. 10(c) and 11 that when the σ meson mass increases, the downward shift in the location of the CEP is smaller in the 2 + 1 flavor case if it is compared with that of the two flavor case of the RQM model. It means that the difference between the two flavor and the 2 + 1 flavor location of the CEP in the temperature direction increases with the increasing m_σ . The above behavior in the 2 + 1 flavor RQM model is caused by a relatively large reduction in the explicit symmetry breaking strength h_y while h_x gets reduced by the same small amount in both the 2 + 1 and the two flavor RQM models. Recall that h_x and h_y do not change in the curvature mass parameter fixing of the QMVT model where one gets an opposite trend of what one observes in the RQM model when the CEP for the 2 + 1 flavor QMVT model shifts noticeably down in reference to the CEP of the two flavor case.

C. Modification of the $U_A(1)$ restoration pattern

The temperature and chemical potential variations of the meson masses have been computed and the results obtained in the RQM model have been compared with the corresponding results in the QMVT model. We have taken $m_\sigma = 600$ MeV in all of these computations. Figures 12(a) and 12(b) depict the respective plots in the RQM and

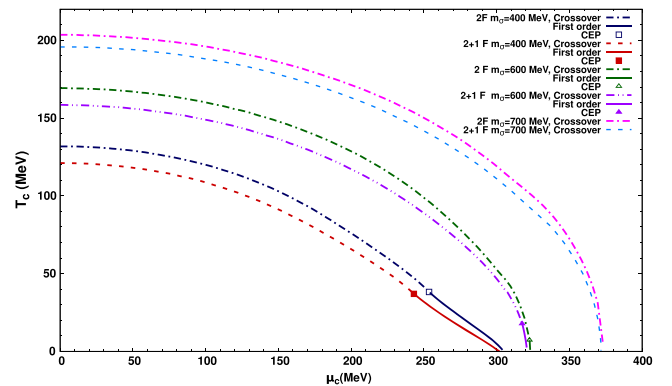


FIG. 11. Phase diagrams of the present 2 + 1 flavor calculations are compared with the two flavor phase diagrams for the RQM model calculations taken from Ref. [74] when $m_\sigma = 400, 600,$ and 700 MeV.

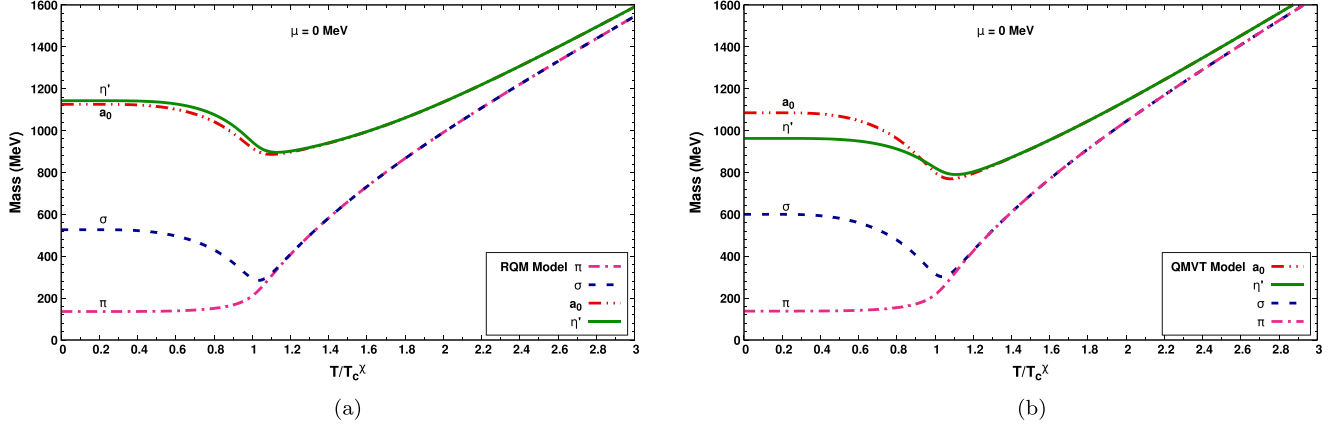


FIG. 12. The reduced temperature scale variations of a_0 , σ , π , and η' meson masses for $\mu = 0$ MeV and $m_\sigma = 600$ MeV.

QMVT models for the temperature variations of the a_0 , σ , π , and η' meson masses on the reduced temperature scale at zero chemical potential. Note that the chiral crossover transition temperature is $T_c^\chi = 158.6$ MeV in the RQM model while it is 170.8 MeV in the QMVT model. In the RQM model calculation, we have found that the curvature mass of the η' meson $m_{\eta',c} = 1142.48$ MeV in the vacuum (at $T, \mu = 0$ MeV) is significantly larger than its pole mass of $m_{\eta'} = 968.89$ MeV. A significant enhancement in the vacuum curvature mass of the a_0 meson has also been obtained in the RQM model as $m_{a_0,c} = 1125.46$ MeV while the vacuum curvature mass of σ gets noticeably reduced to $m_{\sigma,c} = 526.8$ MeV from its pole mass value of $m_\sigma = 600$ MeV, and the curvature mass of π gets reduced to $m_{\pi,c} = 135.95$ MeV. The sizeable increase in the vacuum curvature masses of the η' and a_0 mesons and the noticeable reduction in the vacuum curvature masses of the σ and π mesons are explained when one notes that the quark one-loop vacuum correction causes significant enhancement in the coefficient c (see Table II) of the 't Hooft determinant term for the $2 + 1$ RQM model.

When $\frac{T}{T_c^\chi} = 1$, the masses of the chiral partners (σ, π) and (a_0, η') become degenerate because of the chiral symmetry restoration. One can clearly see from Figs. 12(a) and 12(b) that the mass difference between $m_\sigma = m_\pi$ and $m_{a_0} = m_{\eta'}$ at $\frac{T}{T_c^\chi} = 1$ is significantly larger in the RQM model when it is compared with that of the QMVT model. Thus at the chiral transition temperature, the $U_A(1)$ anomaly is significantly larger in the RQM model. The $U_A(1)$ symmetry restoration will take place for $\frac{T}{T_c^\chi} > 1$ when the degenerate temperature variations of the σ and π meson masses coincide with the degenerate temperature variations of the a_0 and η' meson masses. The nature of the $U_A(1)$ symmetry restoration pattern for $\frac{T}{T_c^\chi} > 1$ can be inferred by noticing how the merged temperature variation lines for σ and π masses are approaching the coincident temperature variations of the a_0 and η' meson masses. We find that the degenerate temperature variation lines for $m_{\eta',c}$ and $m_{a_0,c}$ on

the reduced temperature scale for $\frac{T}{T_c^\chi} > 1$ approach the degenerate temperature variations of $m_{\sigma,c}$ and $m_{\pi,c}$ quite slowly in the RQM model in Fig. 12(a) when the results are compared with the corresponding results for the QMVT model in Fig. 12(b). Thus it is inferred that the $U_A(1)$ restoration gets delayed and a sizable $U_A(1)$ anomaly persists even up to $\frac{T}{T_c^\chi} = 2.6$ due to the quark one-loop vacuum correction when the parameters are fixed by the exact on-shell method in the RQM model. We point out that the vacuum curvature mass of the a_0 meson increases in the QMVT model also as $m_{a_0} = 1086.26$ MeV, but this increase (of about 60 MeV over $m_{a_0} = 1028$ MeV) is noticeably less than the increase calculated in the RQM model. The modifications of the $U_A(1)$ anomaly caused by the vacuum fluctuations and its enhancement caused by the meson vacuum fluctuations have been investigated in the functional renormalization group framework and reported in Refs. [75–79].

The RQM and QMVT model plots for a_0 , σ , π , and η' meson mass variations on the reduced chemical potential scale are shown respectively in Figs. 13(a) and 13(b) when the temperature is $T = 30$ MeV. The pseudocritical chemical potential for the chiral crossover transition is $\mu_c = 312.2$ MeV in the RQM model while the chiral crossover in the QMVT model occurs at $\mu_c = 328.5$ MeV. One notices that the masses of mesons are nearly constant up to $\frac{\mu}{\mu_c} = 0.8$ and the masses register a rapid drop afterwards and attain their minimum at $\frac{\mu}{\mu_c} = 1$. The m_σ variation in the RQM model in Fig. 13(a) shows a very sharp drop as it becomes 92.7 MeV at the chiral crossover transition when $\frac{\mu}{\mu_c} = 1$, while correspondingly for the QMVT model in Fig. 13(b), the m_σ variation drops to the minimum of 165.6 MeV. The above behavior is expected because in the RQM model we are near the critical end point as we recall that in the RQM model the CEP lies at $(T_{\text{CEP}} = 17.7, \mu_{\text{CEP}} = 317.45)$ MeV, while the chiral phase transition in the QMVT model for $m_\sigma = 600$ MeV is a crossover in the entire T - μ plane and the model does not have a CEP. The scalar susceptibility

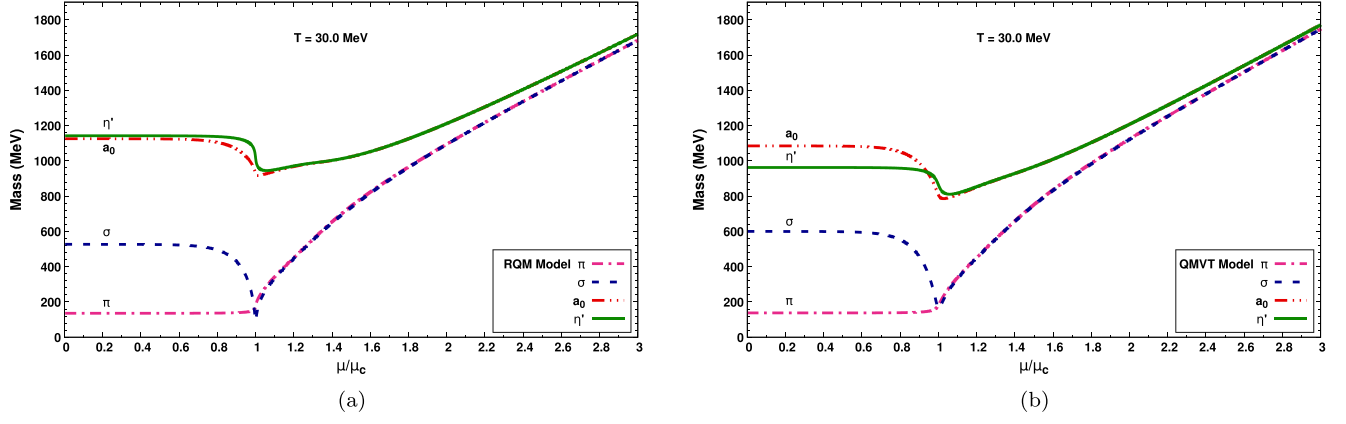


FIG. 13. The reduced chemical potential scale variations of m_{a_0} , m_σ , m_π , and $m_{\eta'}$ at $T = 30$ MeV. $m_\sigma = 600$ MeV.

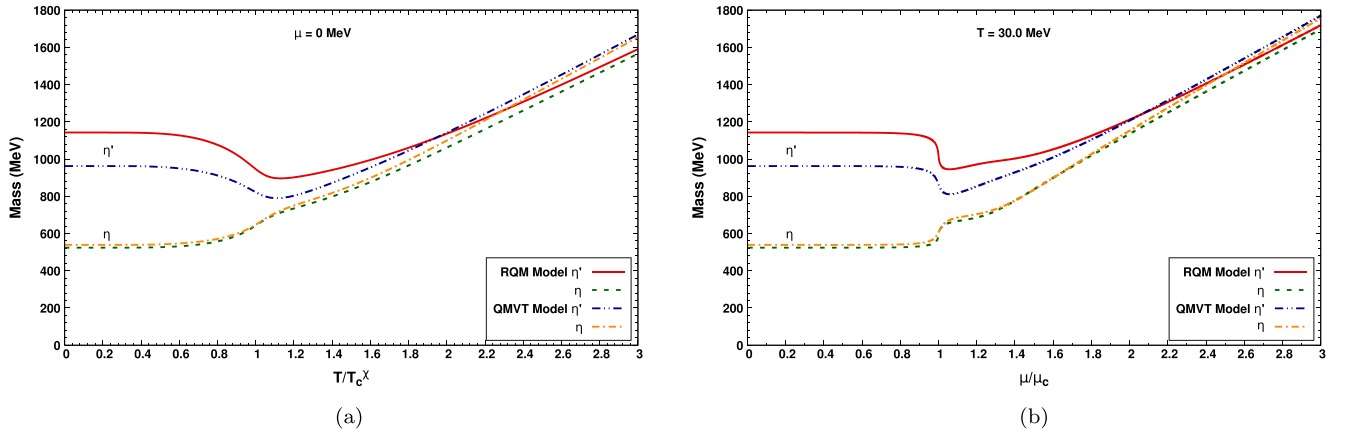


FIG. 14. (a) Reduced temperature scale variations of η and η' meson masses at $\mu = 0$. (b) Reduced chemical potential scale variations of η and η' meson masses for $T = 30$ MeV. $m_\sigma = 600$ MeV.

behaves as $\sim \frac{1}{m_\sigma^2}$ and it diverges at the CEP where m_σ becomes zero. Similar to the case of temperature variation, it is evident that the $U_A(1)$ anomaly is significantly larger in the RQM model when $\frac{\mu}{\mu_c} = 1$. It is also clear that the larger $U_A(1)$ anomaly persists in the RQM model even when $\frac{\mu}{\mu_c}$ becomes 3. Thus the $U_A(1)$ anomaly restoration with respect to the increasing chemical potential also gets delayed in the RQM model.

Figure 14(a) depicts the reduced temperature scale variations of the η and η' meson masses at $\mu = 0$ while Fig. 14(b) plots the variations of the η and η' meson masses on the reduced chemical potential scale for $T = 30$ MeV. The vacuum curvature mass of the η meson in the RQM model is $m_{\eta,c} = 523.97$ MeV which shows a slight decrease from its pole mass $m_\eta = 527.58$ MeV. The difference between the vacuum masses of η' and η mesons is $(m_{\eta',c} - m_{\eta,c}) = 618.5$ MeV in the RQM model while it is $(m_{\eta'} - m_\eta) = 423.6$ MeV in the QMVT model. The η' meson mass initially decreases and its minimum in the RQM model occurs at the $\frac{T}{T_c^x} = 1.13$ where the mass

difference becomes $(m_{\eta',c} - m_{\eta,c}) = 183.7$ MeV. The corresponding minimum in $m_{\eta'}$ occurs in the QMVT model at $\frac{T}{T_c^x} = 1.11$ where the η and η' mass difference is $(m_{\eta'} - m_\eta) = 76.7$ MeV. The significantly larger mass difference between η and η' masses in the RQM model at $\frac{T}{T_c^x} = 1.13$ tells us that the $U_A(1)$ anomaly is quite large in the RQM model even after the chiral crossover transition has taken place. The above findings corroborate our earlier conclusion that the enhanced $U_A(1)$ anomaly persists in the RQM model even up to $\frac{T}{T_c^x} = 3$ and $U_A(1)$ axial symmetry restoration gets delayed in the RQM model. The above trend becomes stronger if we consider η and η' mass variations on the reduced chemical potential scale in Fig. 14(b) as the mass difference is $(m_{\eta',c} - m_{\eta,c}) = 287.6$ MeV in the RQM model, while in the QMVT model $(m_{\eta'} - m_\eta) = 137.93$ MeV when $\frac{\mu}{\mu_c} = 1.06$. For $\frac{\mu}{\mu_c} > 1.06$, the η' and η mass difference in the RQM model keeps on getting reduced as it gradually approaches the corresponding mass difference in the QMVT model.

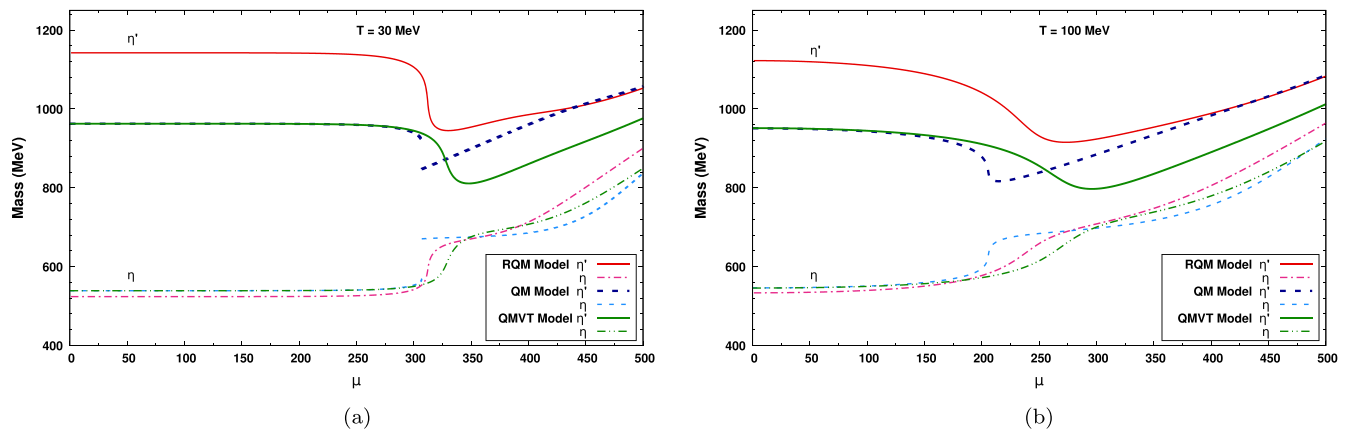


FIG. 15. RQM and QMVT model results have been compared with that of the QM Model. (a) Plots of m_η and $m_{\eta'}$ with respect to the chemical potential at $T = 30$ MeV. (b) Plots of m_η and $m_{\eta'}$ versus the chemical potential for $T = 100$ MeV. $m_\sigma = 600$ MeV.

The QM, RQM, and QMVT model plots of η' and η meson masses with respect to the quark chemical potential are presented in Figs. 15(a) and 15(b) for the respective cases of $T = 30$ MeV and 100 MeV. Comparing the η' and η mass splitting in the QM model with that of the RQM and QMVT models, one can see the effect of the quark one-loop vacuum correction on the $U_A(1)$ symmetry restoration pattern at high baryon densities/chemical potentials. Since the coefficient c of the 't Hooft determinant term increases significantly due to the consistent on-shell parameter fixing, one gets the largest $(m_{\eta',c} - m_{\eta,c})$ for the RQM model in the vacuum and near the chiral transition ($\mu_c = 312.2$ MeV). It is worth emphasizing that when $\mu = 400$ MeV in Fig. 15(a), the mass splitting $(m_{\eta',c} - m_{\eta,c}) = 272.3$ MeV in the RQM model becomes smaller than that of the QM model which is 274.7 MeV. The above behavior is caused by the fastest growth of $m_{\eta,c}$ in the RQM model for the $\mu > \mu_c$. The largest mass splitting is observed in the QM model with respect to the increasing chemical potential. When $\mu = 500$ MeV, the respective values of the $(m_{\eta',c} - m_{\eta,c})$ in the QM, RQM, and QMVT models are 220, 152, and 127 MeV. One gets a mass gap in the η' and η masses at $\mu_c = 306.9$ because the chiral phase transition is first order in the QM model when $T = 30$ MeV. The chiral transition is a crossover for the QM, RQM, and QMVT models for $T = 100$ MeV in Fig. 15(b) and the respective values of pseudocritical chemical potential μ_c in the QM, RQM, and QMVT models are 205.6, 238.3, and 265.2 MeV. Figure 15(b) shows that for higher temperature $T = 100$ MeV, 209.4 MeV of equal mass splitting $(m_{\eta',c} - m_{\eta,c})$ is observed in both the QM and RQM models at a smaller chemical potential $\mu = 336$ MeV. For $\mu > 336$ MeV, the mass splitting becomes largest in the QM model. The respective values of $(m_{\eta',c} - m_{\eta,c})$ in the QM, RQM, and QMVT models are 162, 119, and 94 MeV when $\mu = 500$ MeV.

The masses of m_η and $m_{\eta'}$ versus the baryon chemical potential μ_B have been plotted in Fig. 3 of Ref. [83] for the QM model (for $m_\sigma = 550$ MeV) where the maximum μ_B is 1.5 GeV which gives the quark chemical potential $\mu = 500$ MeV. The results of Fig. 3 (middle panel for $T = .1$ GeV) in Ref. [83] are very similar to the QM model result of the present work in Fig. 15(b) where it has been shown that $(m_{\eta',c} - m_{\eta,c})$ is significantly large in the QM model. The results [in Figs. 15(a) and 15(b)] discussed in the preceding paragraph enable one to conclude that the fermionic vacuum one-loop correction even in the RQM model calculations facilitates the $U_A(1)$ symmetry restoration at high baryon densities $\mu \geq 350$ MeV. The $U_A(1)$ symmetry restoration pattern sets up quite early (on the chemical potential scale) in the QMVT model after the chiral transition but some $U_A(1)$ axial breaking persists even for very large chemical potentials. It is worthwhile to point out that Ref. [83] has calculated the topological susceptibility as an alternative observable of the $U_A(1)$ symmetry restoration at high baryon density. The topological susceptibility has two components: the condensate controlled one and the meson fluctuation one and the $U_A(1)$ restoration is governed by their competition. The condensates melt at high temperatures but the fluctuations are enhanced. Therefore the $U_A(1)$ symmetry restoration cannot be achieved by the temperature effect alone. Since the baryon density reduces both the condensates and fluctuation, the authors of Ref. [83] reach apparently a model-independent qualitative conclusion that the $U_A(1)$ symmetry can only be restored in dense or dense and hot mediums. However they have pointed out that the quarks and mesons in their work have been treated in mean field approximation while the susceptibility has been calculated above the mean field by including the thermal fluctuation. In their calculation the above kind of perturbative treatment may bring in some inconsistency.

VII. SUMMARY AND CONCLUSION

This work presents the consistent calculation of the effective potential in the QCD-like framework of the $2 + 1$ flavor renormalized quark-meson model where the quark one-loop vacuum fluctuation is properly renormalized when it is included in the $2 + 1$ flavor quark-meson model. The seven running parameters of the model $\lambda_1, \lambda_2, c, m^2, h_x, h_y,$ and g are determined by relating the $\overline{\text{MS}}$, on-shell schemes, and the experimental values of the pion decay constant f_π , the kaon decay constant f_K , the scalar σ meson mass m_σ , the pseudoscalar pion, kaon, eta, and eta-prime meson masses $m_\pi, m_K, m_\eta, m_{\eta'}$, and the nonstrange as well as the strange constituent quark masses. The computed effective potentials, order parameters, and the phase diagrams for the RQM model have been compared respectively with the corresponding calculations in the quark-meson model without the vacuum term and the quark-meson model with the vacuum term where the curvature meson masses have been used for fixing the model parameters. The pion, kaon decay constant f_π, f_K , the Yukawa coupling g , and the position of the minimum of the effective potential do not change after the renormalization in the RQM model. In contrast to the QMVT model where the explicit symmetry breaking strengths h_x and h_y do not change, the strength h_x is reduced by a small amount while the strength h_y gets reduced by a relatively large amount in the RQM model because the pion curvature mass $m_{\pi,c} = 135.95$ MeV is 2.05 MeV smaller than its physical mass $m_\pi = 138.0$ MeV and the kaon curvature mass $m_{K,c} = 467.99$ MeV is 28.01 MeV smaller than its pole mass $m_K = 496.0$ MeV. Due to the above-mentioned reason, the $2 + 1$ flavor phase diagrams and the CEP location in the RQM model differ noticeably from the existing results of the two flavor RQM model. Noteworthy increase of the 't Hooft coupling c has also been found in the RQM model. The increase of the $U_A(1)$ anomaly due to the meson vacuum fluctuations has already been reported in Refs. [75,76].

The σ meson mass dependent similarities and differences are observed in the plots of the vacuum effective potentials, the nonstrange and strange order parameters, and the phase diagrams for the QM, QMVT, and RQM models. The normalized vacuum effective potential difference in the nonstrange direction is most shallow in the QM model and becomes deeper in the RQM model; it turns deepest in the QMVT model when $m_\sigma = 400$ and 500 MeV. The sharpest chiral transition occurring in the nonstrange direction of the QM model becomes quite smooth in the RQM model while the excessively smooth and delayed chiral transition is witnessed in the QMVT model. The RQM model vacuum effective potential difference in the nonstrange direction coincides with that of the QMVT model when $m_\sigma = 658.8$ MeV while the temperature variation of the nonstrange condensate and the phase diagrams for both models

coincide with each other when the mass of the σ meson is 10 MeV smaller, i.e. $m_\sigma = 648.0$ MeV.

The above behavior gets explained when one notes that in addition to its Δ_x -dependent variation, the vacuum effective potential depends also on the strange constituent quark mass parameter Δ_y . For the higher $m_\sigma = 700 (> 658.8)$ MeV, the trends that one obtain for the respective plots of the nonstrange direction effective potential, order parameter, and the phase diagram for the $m_\sigma = 500$ MeV case get reversed and the deepest effective potential together with an excessively smooth order parameter temperature variation is noticed in the RQM model, and the QMVT model phase boundary stands close to that of the QM model. Since the explicit symmetry breaking strength h_y becomes weaker, the strange direction vacuum effective potential difference looks most shallow in the RQM model while it is deeper in the QM model and deepest in the QMVT model for $m_\sigma = 500$ MeV. The above nature of the effective potential causes a significantly large melting of the strange condensate in the RQM model. On increasing the m_σ , the RQM model effective potential becomes deeper in the strange direction and merges with the rising QMVT model effective potential when $m_\sigma = 785$ MeV. Here, the trend of the effective potential plot for the $m_\sigma = 500$ MeV case gets reversed for quite large $m_\sigma = 850$ MeV when the effective potential becomes shallower (deepest) in the QMVT (RQM) model.

The phase boundary and the CEP for the $2 + 1$ flavor and the two flavor calculations overlap with each other in the QM model. The $2 + 1$ flavor phase boundary in the QMVT model separates from that of the two flavor case near $\mu \sim 200$ MeV and the $2 + 1$ flavor CEP shifts noticeably down to the right side of the phase diagram when it gets compared with the two flavor CEP for $m_\sigma = 500$ MeV. Unlike the QM and opposite to that of the QMVT model, the phase boundary obtained in the $2 + 1$ flavor RQM model lies at a noticeable distance below the two flavor RQM model phase boundary and the $2 + 1$ flavor case CEP moves upward on the left side the phase boundary (and the CEP) that one gets in the two flavor RQM model [74]. The above-mentioned findings are corroborated also when the $2 + 1$ flavor phase diagrams for the $m_\sigma = 400, 600,$ and 700 MeV cases are compared with the corresponding two flavor phase diagrams in the RQM model. Note that when m_σ increases, the downward shift of the $2 + 1$ flavor case CEP is smaller than the down shift of the two flavor CEP in the RQM model. The above behavior is again the consequence of the fact that the strength h_y for the $2 + 1$ flavor model becomes weaker by a relatively large amount while the strength h_x gets reduced by the same small amount in both the $2 + 1$ and the two flavor RQM model. Recall that h_x and h_y do not change in the QMVT model where one gets an opposite trend of what one observes in the RQM model when the CEP for the $2 + 1$ flavor QMVT model shifts noticeably down in reference to the CEP of the two flavor case.

The variation of a_0 , σ , π , η' , and η meson masses, with respect to the reduced temperature and chemical potential, tells us that the enhanced $U_A(1)$ anomaly persists in the RQM model even up to $\frac{T}{T_c} = 3$ and $\frac{\mu}{\mu_c} = 3$. The mass difference ($m_{\eta',c} - m_{\eta,c}$) between the curvature masses of the η and η' is significantly larger in the RQM model near the chiral transition when $\frac{T}{T_c} = 1.11$ and $\frac{\mu}{\mu_c} = 1.06$. Thus immediately after the chiral transition, significant $U_A(1)$ anomaly strength persists in the RQM model and the $U_A(1)$ axial symmetry restoration gets somewhat delayed in comparison to the QMVT model. The quark one-loop vacuum correction even in the RQM model calculations facilitates the $U_A(1)$ symmetry restoration at high baryon densities $\mu \geq 350$ MeV and the $U_A(1)$ restoration trend sets up early on the chemical potential scale in the RQM model when the results are compared with the QM model.

ACKNOWLEDGMENTS

I acknowledge the support of Dr. Pramod Kumar Shukla and Mr. Suraj Kumar Rai for making some figures, reading the manuscript, and suggesting corrections. Dr. Swatantra Kumar Tiwari is also thanked for reading the manuscript and suggesting corrections. Computational support of the computing facility which has been developed by the Nuclear Particle Physics group of the Department of Physics, University of Allahabad (UOA) under the Center of Advanced Studies (CAS) funding of UGC, India, is acknowledged. Department of Science and Technology, Government of India, DST-PURSE program Phase 2/43(C), financial support to the science faculty of the UOA is also acknowledged.

APPENDIX A: QMVT PARAMETER FIXING

This appendix presents a brief description of the parameter fixing procedure in the QMVT model as given in Ref. [59]. The vacuum meson mass matrix is written as

$$m_{\alpha,ab}^2|_{\text{QMVT}} = \frac{\partial^2 \Omega^\Lambda(x, y)}{\partial \xi_{\alpha,a} \partial \xi_{\alpha,b}} \Big|_{\min} = (m_{\alpha,ab}^m)^2 + (\delta m_{\alpha,ab}^v)^2. \quad (\text{A1})$$

Here, the $(m_{\alpha,ab}^m)^2$ expressions for $\alpha = s, p$ and $a, b = 0, 1, \dots, 8$ are the same as the vacuum values of the meson masses $m_{\alpha,ab}^2$ which were originally evaluated for the QM model under s-MFA in Refs. [18,19] by taking the second derivatives of the pure mesonic potential at its minimum.

The vacuum ($T = 0, \mu = 0$) mass modifications on account of the fermionic vacuum correction are given by

$$(\delta m_{\alpha,ab}^v)^2 = \frac{\partial^2 \Omega_{q\bar{q}}^{\text{vac}}}{\partial \xi_{\alpha,a} \partial \xi_{\alpha,b}} \Big|_{\min} = -\frac{N_c}{8\pi^2} \sum_f \left[\left(2 \ln \left(\frac{m_f}{\Lambda} \right) + \frac{3}{2} \right) \left(\frac{\partial m_f^2}{\partial \xi_{\alpha,a}} \right) \left(\frac{\partial m_f^2}{\partial \xi_{\alpha,b}} \right) + \left(\frac{m_f^2}{2} + 2m_f^2 \ln \left(\frac{m_f}{\Lambda} \right) \right) \frac{\partial^2 m_f^2}{\partial \xi_{\alpha,a} \partial \xi_{\alpha,b}} \right]. \quad (\text{A2})$$

Here $|_{\min}$ denotes the global minimum of the full grand potential in Eq. (10). The first $m_{f,a}^2 \equiv \partial m_f^2 / \partial \xi_{\alpha,a}$ and second $m_{f,ab}^2 \equiv \partial^2 m_f^2 / \partial \xi_{\alpha,a} \partial \xi_{\alpha,b}$ partial derivatives of the squared quark mass with respect to the different meson fields are evaluated in Ref. [19] in the nonstrange-strange basis. The values of these derivatives can be found from Table III of Refs. [19,59]. The mass modifications given in Eq. (A2) due to the fermionic vacuum correction were evaluated in Ref. [59] and different expressions of $(\delta m_{\alpha,ab}^v)^2$ are presented in Table VI for all the mesons of the scalar and pseudoscalar nonet.

In the QMVT model calculations, the vacuum mass expressions in Eq. (A1) that determine λ_2 and c are $m_\pi^2 = (m_\pi^m)^2 + (\delta m_{p,11}^v)^2$, $m_K^2 = (m_K^m)^2 + (\delta m_{p,44}^v)^2$, and $m_\eta^2 + m_{\eta'}^2 = m_{p,00}^2 + m_{p,88}^2$ where $m_{p,00}^2 = (m_{p,00}^m)^2 + (\delta m_{p,00}^v)^2$ and $m_{p,88}^2 = (m_{p,88}^m)^2 + (\delta m_{p,88}^v)^2$. We can write $m_\eta^2 + m_{\eta'}^2 = (m_\eta^m)^2 + (m_{\eta'}^m)^2 + (\delta m_{p,00}^v)^2 + (\delta m_{p,88}^v)^2$ where $(m_\eta^m)^2 + (m_{\eta'}^m)^2 = (m_{p,00}^m)^2 + (m_{p,88}^m)^2$. Using mass modification expressions $(\delta m_{\alpha,ab}^v)^2$ given in Table VI, one writes

$$\begin{aligned} (m_K^m)^2 &= m_K^2 + \frac{N_c g^4}{64\pi^2} \left(\frac{x - \sqrt{2}y}{x^2 - 2y^2} \right) (x^3 X + 2\sqrt{2}y^3 Y); \\ (m_\pi^m)^2 &= m_\pi^2 + \frac{N_c g^4}{64\pi^2} x^2 X \quad \text{and} \\ (m_\eta^m)^2 + (m_{\eta'}^m)^2 &= (m_\eta^2 + m_{\eta'}^2) + \frac{N_c g^4}{192\pi^2} (3x^2 X + 6y^2 Y). \end{aligned} \quad (\text{A3})$$

f_π and f_K give vacuum condensates according to the partially conserved axial vector current (PCAC) relation. $x = f_\pi$ and $y = \frac{(2f_K - f_\pi)}{\sqrt{2}}$ at $T = 0$. The parameters λ_2 and c in vacuum are obtained as

$$\lambda_2 = \frac{3(2f_K - f_\pi)(m_K^m)^2 - (2f_K + f_\pi)(m_\pi^m)^2 - 2((m_\eta^m)^2 + (m_{\eta'}^m)^2)(f_K - f_\pi)}{(3f_\pi^2 + 8f_K(f_K - f_\pi))(f_K - f_\pi)}, \quad (\text{A4})$$

TABLE VI. The superscript m in $(m_{\alpha,ab}^m)^2$ symbolizes the meson curvature masses calculated from the second derivatives of the pure mesonic potential $U(x, y)$. The mass modifications $(\delta m_{\alpha,ab}^v)^2$ due to the fermionic vacuum correction are shown in the right half. Symbols used in the expressions are defined as $X = \{1 + 4 \ln(\frac{gX}{2\Lambda})\}$ and $Y = \{1 + 4 \ln(\frac{gY}{\sqrt{2}\Lambda})\}$.

Meson masses calculated from pure mesonic potential		Fermionic vacuum correction in meson masses	
$(m_{a_0}^m)^2$	$m^2 + \lambda_1(x^2 + y^2) + \frac{3\lambda_2}{2}x^2 + \frac{\sqrt{2}c}{2}y$	$(\delta m_{s,11}^v)^2$	$-\frac{N_c g^4}{64\pi^2} x^2(4 + 3X)$
$(m_K^m)^2$	$m^2 + \lambda_1(x^2 + y^2) + \frac{\lambda_2}{2}(x^2 + \sqrt{2}xy + 2y^2) + \frac{\epsilon}{2}x$	$(\delta m_{s,44}^v)^2$	$-\frac{N_c g^4}{64\pi^2} (\frac{x+\sqrt{2}y}{x^2-2y^2})(x^3X - 2\sqrt{2}y^3Y)$
$(m_{s,00}^m)^2$	$m^2 + \frac{\lambda_1}{3}(7x^2 + 4\sqrt{2}xy + 5y^2) + \lambda_2(x^2 + y^2) - \frac{\sqrt{2}c}{3}(\sqrt{2}x + y)$	$(\delta m_{s,00}^v)^2$	$-\frac{N_c g^4}{96\pi^2} \{3(x^2X + y^2Y) + 4(x^2 + y^2)\}$
$(m_{s,88}^m)^2$	$m^2 + \frac{\lambda_1}{3}(5x^2 - 4\sqrt{2}xy + 7y^2) + \lambda_2(\frac{x^2}{2} + 2y^2) + \frac{\sqrt{2}c}{3}(\sqrt{2}x - \frac{y}{2})$	$(\delta m_{s,88}^v)^2$	$-\frac{N_c g^4}{96\pi^2} \{\frac{3}{2}(x^2X + 4y^2Y) + 2(x^2 + 4y^2)\}$
$(m_{s,08}^m)^2$	$\frac{2\lambda_1}{3}(\sqrt{2}x^2 - xy - \sqrt{2}y^2) + \sqrt{2}\lambda_2(\frac{x^2}{2} - y^2) + \frac{c}{3\sqrt{2}}(x - \sqrt{2}y)$	$(\delta m_{s,08}^v)^2$	$-\frac{N_c g^4}{8\sqrt{2}\pi^2} \{\frac{1}{4}(x^2X - 2y^2Y) + \frac{1}{3}(x^2 - 2y^2)\}$
$(m_\pi^m)^2$	$m^2 + \lambda_1(x^2 + y^2) + \frac{\lambda_2}{2}x^2 - \frac{\sqrt{2}c}{2}y$	$(\delta m_{p,11}^v)^2$	$-\frac{N_c g^4}{64\pi^2} x^2X$
$(m_K^m)^2$	$m^2 + \lambda_1(x^2 + y^2) + \frac{\lambda_2}{2}(x^2 - \sqrt{2}xy + 2y^2) - \frac{\epsilon}{2}x$	$(\delta m_{p,44}^v)^2$	$-\frac{N_c g^4}{64\pi^2} (\frac{x-\sqrt{2}y}{x^2-2y^2})(x^3X + 2\sqrt{2}y^3Y)$
$(m_{p,00}^m)^2$	$m^2 + \lambda_1(x^2 + y^2) + \frac{\lambda_2}{3}(x^2 + y^2) + \frac{\epsilon}{3}(2x + \sqrt{2}y)$	$(\delta m_{p,00}^v)^2$	$-\frac{N_c g^4}{96\pi^2} (x^2X + y^2Y)$
$(m_{p,88}^m)^2$	$m^2 + \lambda_1(x^2 + y^2) + \frac{\lambda_2}{6}(x^2 + 4y^2) - \frac{\epsilon}{6}(4x - \sqrt{2}y)$	$(\delta m_{p,88}^v)^2$	$-\frac{N_c g^4}{192\pi^2} (x^2X + 4y^2Y)$
$(m_{p,08}^m)^2$	$\frac{\sqrt{2}\lambda_2}{6}(x^2 - 2y^2) - \frac{\epsilon}{6}(\sqrt{2}x - 2y)$	$(\delta m_{p,08}^v)^2$	$-\frac{N_c g^4}{96\sqrt{2}\pi^2} (x^2X - 2y^2Y)$

$$c = \frac{(m_K^m)^2 - (m_\pi^m)^2}{f_K - f_\pi} - \lambda_2(2f_K - f_\pi). \quad (\text{A5})$$

When expressions of $(m_\pi^m)^2$, $(m_K^m)^2$, and $((m_\eta^m)^2 + (m_{\eta'}^m)^2)$ from Eq. (A3) are substituted in Eq. (A4), Eq. (A5) and the vacuum value of the condensates are used, the final rearrangement of terms yields:

$$\lambda_2 = \lambda_{2s} + n + \lambda_{2+} + \lambda_{2\Lambda} \quad \text{where } \lambda_{2s} = \frac{3(2f_K - f_\pi)m_K^2 - (2f_K + f_\pi)m_\pi^2 - 2(m_\eta^2 + m_{\eta'}^2)(f_K - f_\pi)}{(3f_\pi^2 + 8f_K(f_K - f_\pi))(f_K - f_\pi)},$$

$$n = \frac{N_c g^4}{32\pi^2}, \quad \lambda_{2+} = \frac{nf_\pi^2}{f_K(f_K - f_\pi)} \ln\left(\frac{2f_K - f_\pi}{f_\pi}\right) \text{ and scale dependent part } \lambda_{2\Lambda} = 4n \ln\left(\frac{g(2f_K - f_\pi)}{2\Lambda}\right), \quad (\text{A6})$$

$$c = \frac{m_K^2 - m_\pi^2}{f_K - f_\pi} - \lambda_{2s}(2f_K - f_\pi). \quad (\text{A7})$$

Note that λ_{2s} is the old λ_2 parameter fixed in the QM/PQM model calculations in Refs. [18,19,48]. Here, the curvature mass parametrization in the QMVT model generates an addition of $(n + \lambda_{2+})$ to λ_{2s} and further, one gets a scale

Λ -dependent addition $\lambda_{2\Lambda}$ to the expression of the λ_2 in Eq. (A6). The Λ dependence completely cancels in the evaluation of c and its value remains the same as in the QM model. The parameter m^2 can be expressed in terms of λ_1 using the scale Λ -independent formula of m_σ^2 (given in Appendix B of Ref. [59]), and putting $x = f_\pi$ and $y = (\frac{2f_K - f_\pi}{\sqrt{2}})$, one gets

$$m^2 = m_\pi^2 - \lambda_1 \left\{ f_\pi^2 + \frac{(2f_K - f_\pi)^2}{2} \right\} - \frac{f_\pi^2}{2} \left[\lambda_{2v} - 4 \ln \left\{ \frac{f_\pi}{(2f_K - f_\pi)} \right\} \right] + \frac{c}{2}(2f_K - f_\pi). \quad (\text{A8})$$

When the formula of m_σ^2 (given in Table I) is used with the vacuum values of the masses $m_{s,00}^2$, $m_{s,88}^2$, $m_{s,08}^2$ and the above expression of m^2 is substituted in it, one gets the numerical value of λ_1 for different values of m_σ . The fermionic vacuum correction does not change the explicit symmetry breaking parameters h_x and h_y .

APPENDIX B: TADPOLE TERMS

The expressions of tadpole contributions in the self-energies are

$$\begin{aligned}\Sigma_{s,00}^{\text{tad}} &= 4\sqrt{\frac{2}{3}}N_c g \left[\frac{1}{m_{s,00}^2} \left\{ 3 \left(\lambda_1 + \frac{\lambda_2}{3} \right) \bar{\sigma}_0 - \frac{c}{2} \sqrt{\frac{2}{3}} \right\} + \frac{1}{3m_{s,08}^2} (\lambda_1 + \lambda_2) (\bar{\sigma}_8) \right] \mathcal{F}(m_u, m_s) \\ &+ \frac{8}{\sqrt{3}} N_c g \left[\frac{1}{m_{s,08}^2} \left\{ 3 \left(\lambda_1 + \frac{\lambda_2}{3} \right) \bar{\sigma}_0 - \frac{c}{2} \sqrt{\frac{2}{3}} \right\} + \frac{1}{3m_{s,88}^2} (\lambda_1 + \lambda_2) \bar{\sigma}_8 \right] \mathcal{G}(m_u, m_s),\end{aligned}\quad (\text{B1})$$

$$\begin{aligned}\Sigma_{s,88}^{\text{tad}} &= 4\sqrt{\frac{2}{3}}N_c g \left[\frac{1}{3m_{s,00}^2} \left\{ (\lambda_1 + \lambda_2) \bar{\sigma}_0 - \frac{\lambda_2}{\sqrt{2}} \bar{\sigma}_8 + \frac{c}{4} \sqrt{\frac{2}{3}} \right\} + \frac{1}{m_{s,08}^2} \left\{ \frac{-\lambda_2}{\sqrt{2}} \bar{\sigma}_0 + 3 \left(\lambda_1 + \frac{\lambda_2}{2} \right) \bar{\sigma}_8 + \frac{c}{2\sqrt{3}} \right\} \right] \mathcal{F}(m_u, m_s) \\ &+ \frac{8}{\sqrt{3}} N_c g \left[\frac{1}{3m_{s,08}^2} \left\{ (\lambda_1 + \lambda_2) \bar{\sigma}_0 - \frac{\lambda_2}{\sqrt{2}} \bar{\sigma}_8 + \frac{c}{4} \sqrt{\frac{2}{3}} \right\} + \frac{1}{m_{s,88}^2} \left\{ \frac{-\lambda_2}{\sqrt{2}} \bar{\sigma}_0 + 3 \left(\lambda_1 + \frac{\lambda_2}{2} \right) \bar{\sigma}_8 + \frac{c}{2\sqrt{3}} \right\} \right] \mathcal{G}(m_u, m_s),\end{aligned}\quad (\text{B2})$$

$$\begin{aligned}\Sigma_{s,08}^{\text{tad}} &= 4\sqrt{\frac{2}{3}}N_c g \left[\frac{1}{3m_{s,00}^2} (\lambda_1 + \lambda_2) \bar{\sigma}_8 + \frac{1}{3m_{s,08}^2} \left\{ (\lambda_1 + \lambda_2) \bar{\sigma}_0 - \frac{\lambda_2}{\sqrt{2}} \bar{\sigma}_8 + \frac{c}{4} \sqrt{\frac{2}{3}} \right\} \right] \mathcal{F}(m_u, m_s) \\ &+ \frac{8}{\sqrt{3}} N_c g \left[\frac{1}{3m_{s,08}^2} (\lambda_1 + \lambda_2) \bar{\sigma}_8 + \frac{1}{3m_{s,88}^2} \left\{ (\lambda_1 + \lambda_2) \bar{\sigma}_0 - \frac{\lambda_2}{\sqrt{2}} \bar{\sigma}_8 + \frac{c}{4} \sqrt{\frac{2}{3}} \right\} \right] \mathcal{G}(m_u, m_s),\end{aligned}\quad (\text{B3})$$

$$\begin{aligned}\Sigma_{p,00}^{\text{tad}} &= 4\sqrt{\frac{2}{3}}N_c g \left[\frac{1}{m_{s,00}^2} \left\{ \left(\lambda_1 + \frac{\lambda_2}{3} \right) \bar{\sigma}_0 + \frac{c}{2} \sqrt{\frac{2}{3}} \right\} + \frac{1}{m_{s,08}^2} \left(\lambda_1 + \frac{\lambda_2}{3} \right) \bar{\sigma}_8 \right] \mathcal{F}(m_u, m_s) \\ &+ \frac{8}{\sqrt{3}} N_c g \left[\frac{1}{m_{s,08}^2} \left\{ \left(\lambda_1 + \frac{\lambda_2}{3} \right) \bar{\sigma}_0 + \frac{c}{2} \sqrt{\frac{2}{3}} \right\} + \frac{1}{m_{s,88}^2} \left(\lambda_1 + \frac{\lambda_2}{3} \right) \bar{\sigma}_8 \right] \mathcal{G}(m_u, m_s),\end{aligned}\quad (\text{B4})$$

$$\begin{aligned}\Sigma_{p,88}^{\text{tad}} &= 4\sqrt{\frac{2}{3}}N_c g \left[\frac{1}{m_{s,00}^2} \left\{ \left(\lambda_1 + \frac{\lambda_2}{3} \right) \bar{\sigma}_0 - \frac{\lambda_2}{3\sqrt{2}} \bar{\sigma}_8 - \frac{c}{4} \sqrt{\frac{2}{3}} \right\} + \frac{1}{m_{s,08}^2} \left\{ \left(\lambda_1 + \frac{\lambda_2}{2} \right) \bar{\sigma}_8 - \frac{\lambda_2}{3\sqrt{2}} \bar{\sigma}_0 - \frac{c}{2\sqrt{3}} \right\} \right] \mathcal{F}(m_u, m_s) \\ &+ \frac{8}{\sqrt{3}} N_c g \left[\frac{1}{m_{s,08}^2} \left\{ \left(\lambda_1 + \frac{\lambda_2}{3} \right) \bar{\sigma}_0 - \frac{\lambda_2}{3\sqrt{2}} \bar{\sigma}_8 - \frac{c}{4} \sqrt{\frac{2}{3}} \right\} + \frac{1}{m_{s,88}^2} \left\{ \left(\lambda_1 + \frac{\lambda_2}{2} \right) \bar{\sigma}_8 - \frac{\lambda_2}{3\sqrt{2}} \bar{\sigma}_0 - \frac{c}{2\sqrt{3}} \right\} \right] \mathcal{G}(m_u, m_s),\end{aligned}\quad (\text{B5})$$

$$\begin{aligned}\Sigma_{p,08}^{\text{tad}} &= 4\sqrt{\frac{2}{3}}N_c g \left[\frac{1}{m_{s,00}^2} \left(\lambda_1 + \frac{\lambda_2}{3} \right) \bar{\sigma}_8 + \frac{1}{m_{s,08}^2} \left\{ \left(\lambda_1 + \frac{\lambda_2}{3} \right) \bar{\sigma}_0 - \frac{\lambda_2}{3\sqrt{2}} \bar{\sigma}_8 - \frac{c}{4} \sqrt{\frac{2}{3}} \right\} \right] \mathcal{F}(m_u, m_s) \\ &+ \frac{8}{\sqrt{3}} N_c g \left[\frac{1}{m_{s,08}^2} \left(\lambda_1 + \frac{\lambda_2}{3} \right) \bar{\sigma}_8 + \frac{1}{m_{s,88}^2} \left\{ \left(\lambda_1 + \frac{\lambda_2}{3} \right) \bar{\sigma}_0 - \frac{\lambda_2}{3\sqrt{2}} \bar{\sigma}_8 - \frac{c}{4} \sqrt{\frac{2}{3}} \right\} \right] \mathcal{G}(m_u, m_s),\end{aligned}\quad (\text{B6})$$

$$\begin{aligned}\Sigma_{p,11}^{\text{tad}} &= 4\sqrt{\frac{2}{3}}N_c g \left[\frac{1}{m_{s,00}^2} \left\{ \left(\lambda_1 + \frac{\lambda_2}{3} \right) \bar{\sigma}_0 + \frac{\sqrt{2}}{6} \lambda_2 \bar{\sigma}_8 - \frac{c}{4} \sqrt{\frac{2}{3}} \right\} + \frac{1}{m_{s,08}^2} \left\{ \frac{\sqrt{2}}{6} \lambda_2 \bar{\sigma}_0 + \left(\lambda_1 + \frac{\lambda_2}{6} \right) \bar{\sigma}_8 + \frac{c}{2\sqrt{3}} \right\} \right] \mathcal{F}(m_u, m_s) \\ &+ \frac{8}{\sqrt{3}} N_c g \left[\frac{1}{m_{s,08}^2} \left\{ \left(\lambda_1 + \frac{\lambda_2}{3} \right) \bar{\sigma}_0 + \frac{\sqrt{2}}{6} \lambda_2 \bar{\sigma}_8 - \frac{c}{4} \sqrt{\frac{2}{3}} \right\} + \frac{1}{m_{s,88}^2} \left\{ \frac{\sqrt{2}}{6} \lambda_2 \bar{\sigma}_0 + \left(\lambda_1 + \frac{\lambda_2}{6} \right) \bar{\sigma}_8 + \frac{c}{2\sqrt{3}} \right\} \right] \mathcal{G}(m_u, m_s),\end{aligned}\quad (\text{B7})$$

$$\begin{aligned}\Sigma_{p,44}^{\text{tad}} &= 4\sqrt{\frac{2}{3}}N_c g \left[\frac{1}{m_{s,00}^2} \left\{ \left(\lambda_1 + \frac{\lambda_2}{3} \right) \bar{\sigma}_0 - \frac{\lambda_2}{6\sqrt{2}} \bar{\sigma}_8 - \frac{c}{4} \sqrt{\frac{2}{3}} \right\} + \frac{1}{m_{s,08}^2} \left\{ -\frac{\lambda_2}{6\sqrt{2}} \bar{\sigma}_0 + \left(\lambda_1 + \frac{7\lambda_2}{6} \right) \bar{\sigma}_8 - \frac{c}{4\sqrt{3}} \right\} \right] \mathcal{F}(m_u, m_s) \\ &+ \frac{8}{\sqrt{3}} N_c g \left[\frac{1}{m_{s,08}^2} \left\{ \left(\lambda_1 + \frac{\lambda_2}{3} \right) \bar{\sigma}_0 - \frac{\lambda_2}{6\sqrt{2}} \bar{\sigma}_8 - \frac{c}{4} \sqrt{\frac{2}{3}} \right\} + \frac{1}{m_{s,88}^2} \left\{ -\frac{\lambda_2}{6\sqrt{2}} \bar{\sigma}_0 + \left(\lambda_1 + \frac{7\lambda_2}{6} \right) \bar{\sigma}_8 - \frac{c}{4\sqrt{3}} \right\} \right] \mathcal{G}(m_u, m_s),\end{aligned}\quad (\text{B8})$$

where $\mathcal{F}(m_u, m_s) = 2m_u\mathcal{A}(m_u^2) + m_s\mathcal{A}(m_s^2)$ and $\mathcal{G}(m_u, m_s) = m_u\mathcal{A}(m_u^2) - m_s\mathcal{A}(m_s^2)$. Substituting $\bar{\sigma}_0 = \frac{\sqrt{2}x+y}{\sqrt{3}}$ and $\bar{\sigma}_8 = \frac{x-\sqrt{2}y}{\sqrt{3}}$ in Eqs. (B1)–(B8) and rearranging the terms, one gets the following x - and y -dependent expressions of self-energies for the tadpole terms:

$$\begin{aligned} \Sigma_{s,00}^{\text{tad}} = & \frac{8N_c g m_u \mathcal{A}(m_u^2)}{3} \left[-c \left(\frac{1}{m_{s,00}^2} + \frac{1}{\sqrt{2}m_{s,88}^2} \right) + x \left\{ \frac{2(3\lambda_1 + \lambda_2)}{m_{s,00}^2} + \frac{(\lambda_1 + \lambda_2)}{3m_{s,88}^2} + \frac{2\sqrt{2}(2\lambda_1 + \lambda_2)}{3m_{s,08}^2} \right\} \right. \\ & + y \left\{ \sqrt{2} \left(\frac{1}{m_{s,00}^2} - \frac{1}{3m_{s,88}^2} \right) (3\lambda_1 + \lambda_2) + \frac{(\lambda_1 - \lambda_2)}{3m_{s,08}^2} \right\} \left. \right] + \frac{4N_c g m_s \mathcal{A}(m_s^2)}{3} \left[-c \left(\frac{1}{m_{s,00}^2} - \frac{\sqrt{2}}{m_{s,08}^2} \right) \right. \\ & + x \left\{ \frac{2(3\lambda_1 + \lambda_2)}{m_{s,00}^2} - \frac{2(\lambda_1 + \lambda_2)}{3m_{s,88}^2} - \frac{\sqrt{2}(17\lambda_1 + 5\lambda_2)}{3m_{s,08}^2} \right\} + y \left\{ \frac{\sqrt{2}(3\lambda_1 + \lambda_2)}{m_{s,00}^2} - \frac{2\sqrt{2}(\lambda_1 + \lambda_2)}{3m_{s,88}^2} - \frac{2(5\lambda_1 + 2\lambda_2)}{3m_{s,08}^2} \right\} \left. \right], \quad (\text{B9}) \end{aligned}$$

$$\begin{aligned} \Sigma_{s,88}^{\text{tad}} = & \frac{8N_c g m_u \mathcal{A}(m_u^2)}{3} \left[c \left(\frac{1}{6m_{s,00}^2} + \frac{7}{6\sqrt{2}m_{s,08}^2} + \frac{1}{2m_{s,88}^2} \right) + x \left\{ \frac{(2\lambda_1 + \lambda_2)}{3m_{s,00}^2} + \frac{4(5\lambda_1 + \lambda_2)}{3\sqrt{2}m_{s,08}^2} + \frac{(6\lambda_1 + \lambda_2)}{2m_{s,88}^2} \right\} \right. \\ & + y \left\{ \frac{\sqrt{2}(\lambda_1 + 2\lambda_2)}{3m_{s,00}^2} - \frac{\sqrt{2}}{m_{s,88}^2} (3\lambda_1 + 2\lambda_2) - \frac{(17\lambda_1 + 10\lambda_2)}{3m_{s,08}^2} \right\} \left. \right] + \frac{4N_c g m_s \mathcal{A}(m_s^2)}{3} \left[c \left(\frac{1}{6m_{s,00}^2} + \frac{\sqrt{2}}{3m_{s,08}^2} - \frac{1}{m_{s,88}^2} \right) \right. \\ & + x \left\{ \frac{(2\lambda_1 + \lambda_2)}{3m_{s,00}^2} + \frac{\sqrt{2}(14\lambda_1 + \lambda_2)}{6m_{s,08}^2} - \frac{(6\lambda_1 + \lambda_2)}{m_{s,88}^2} \right\} + y \left\{ \frac{\sqrt{2}(\lambda_1 + 2\lambda_2)}{3m_{s,00}^2} - \frac{4(5\lambda_1 + 4\lambda_2)}{3m_{s,08}^2} + \frac{2\sqrt{2}(3\lambda_1 + 2\lambda_2)}{m_{s,88}^2} \right\} \left. \right], \quad (\text{B10}) \end{aligned}$$

$$\begin{aligned} \Sigma_{s,08}^{\text{tad}} = & \frac{8N_c g m_u \mathcal{A}(m_u^2)}{9} \left[c \left(\frac{1}{2m_{s,08}^2} + \frac{1}{2\sqrt{2}m_{s,88}^2} \right) + x \left\{ \frac{\sqrt{2}(\lambda_1 + \lambda_2)}{m_{s,00}^2} + \frac{(3\lambda_1 + 2\lambda_2)}{m_{s,08}^2} + \frac{(2\lambda_1 + \lambda_2)}{\sqrt{2}m_{s,88}^2} \right\} \right. \\ & + y \left\{ \frac{-2(\lambda_1 + \lambda_2)}{m_{s,00}^2} + \frac{\sqrt{2}\lambda_2}{m_{s,08}^2} + \frac{(\lambda_1 + 2\lambda_2)}{m_{s,88}^2} \right\} \left. \right] + \frac{4N_c g m_s \mathcal{A}(m_s^2)}{9} \left[c \left(\frac{1}{2m_{s,08}^2} - \frac{1}{\sqrt{2}m_{s,88}^2} \right) \right. \\ & + x \left\{ \frac{\sqrt{2}(\lambda_1 + \lambda_2)}{m_{s,00}^2} - \frac{\lambda_2}{m_{s,08}^2} - \frac{\sqrt{2}(2\lambda_1 + \lambda_2)}{m_{s,88}^2} \right\} + y \left\{ \frac{-2(\lambda_1 + \lambda_2)}{m_{s,00}^2} + \frac{\sqrt{2}(3\lambda_1 + 4\lambda_2)}{m_{s,08}^2} - \frac{2(\lambda_1 + 2\lambda_2)}{m_{s,88}^2} \right\} \left. \right], \quad (\text{B11}) \end{aligned}$$

$$\begin{aligned} \Sigma_{p,00}^{\text{tad}} = & \frac{8N_c g m_u \mathcal{A}(m_u^2)}{3} \left[c \left(\frac{1}{m_{s,00}^2} + \frac{1}{\sqrt{2}m_{s,08}^2} \right) + x \left(\lambda_1 + \frac{\lambda_2}{3} \right) \left\{ \frac{2}{m_{s,00}^2} + \frac{2\sqrt{2}}{m_{s,08}^2} + \frac{1}{m_{s,88}^2} \right\} \right. \\ & + y \left(\lambda_1 + \frac{\lambda_2}{3} \right) \left\{ \frac{\sqrt{2}}{m_{s,00}^2} - \frac{1}{m_{s,08}^2} - \frac{\sqrt{2}}{m_{s,88}^2} \right\} \left. \right] + \frac{4N_c g m_s \mathcal{A}(m_s^2)}{3} \left[c \left(\frac{1}{m_{s,00}^2} - \frac{\sqrt{2}}{m_{s,08}^2} \right) \right. \\ & + x \left(\lambda_1 + \frac{\lambda_2}{3} \right) \left\{ \frac{2}{m_{s,00}^2} - \frac{\sqrt{2}}{m_{s,08}^2} - \frac{2}{m_{s,88}^2} \right\} + y \left(\lambda_1 + \frac{\lambda_2}{3} \right) \left\{ \frac{\sqrt{2}}{m_{s,00}^2} - \frac{4}{m_{s,08}^2} + \frac{2\sqrt{2}}{m_{s,88}^2} \right\} \left. \right], \quad (\text{B12}) \end{aligned}$$

$$\begin{aligned} \Sigma_{p,88}^{\text{tad}} = & \frac{8N_c g m_u \mathcal{A}(m_u^2)}{3} \left[-\frac{c}{2} \left(\frac{1}{m_{s,00}^2} + \frac{3}{\sqrt{2}m_{s,08}^2} + \frac{1}{m_{s,88}^2} \right) + x \left\{ \frac{(2\lambda_1 + \frac{\lambda_2}{3})}{m_{s,00}^2} + \frac{\sqrt{2}(2\lambda_1 + \frac{\lambda_2}{3})}{m_{s,08}^2} + \frac{(\lambda_1 + \frac{\lambda_2}{6})}{m_{s,88}^2} \right\} \right. \\ & + y \left\{ \frac{\sqrt{2}(\lambda_1 + \frac{2\lambda_2}{3})}{m_{s,00}^2} - \frac{1}{m_{s,08}^2} \left(\lambda_1 + \frac{2\lambda_2}{3} \right) - \frac{\sqrt{2}(\lambda_1 + \frac{\lambda_2}{3})}{m_{s,88}^2} \right\} \left. \right] + \frac{4N_c g m_s \mathcal{A}(m_s^2)}{3} \left[-c \left(\frac{1}{2m_{s,00}^2} - \frac{1}{m_{s,88}^2} \right) \right. \\ & + x \left\{ \frac{(2\lambda_1 + \frac{\lambda_2}{3})}{m_{s,00}^2} - \frac{\sqrt{2}(\lambda_1 - \frac{\lambda_2}{6})}{m_{s,08}^2} - \frac{2(\lambda_1 + \frac{\lambda_2}{6})}{m_{s,88}^2} \right\} + y \left\{ \frac{\sqrt{2}(\lambda_1 + \frac{2\lambda_2}{3})}{m_{s,00}^2} - \frac{4}{m_{s,08}^2} \left(\lambda_1 + \frac{2\lambda_2}{3} \right) + \frac{2\sqrt{2}(\lambda_1 + \frac{2\lambda_2}{3})}{m_{s,88}^2} \right\} \left. \right], \quad (\text{B13}) \end{aligned}$$

$$\begin{aligned} \Sigma_{p,08}^{\text{tad}} = & \frac{8N_c g m_u \mathcal{A}(m_u^2)}{3} \left[-\frac{c}{2} \left(\frac{1}{m_{s,08}^2} + \frac{\sqrt{2}}{m_{s,88}^2} \right) + x \left\{ \frac{\sqrt{2}(\lambda_1 + \frac{\lambda_2}{3})}{m_{s,00}^2} + \frac{(3\lambda_1 + \frac{2\lambda_2}{3})}{m_{s,08}^2} + \frac{\sqrt{2}(\lambda_1 + \frac{\lambda_2}{6})}{m_{s,88}^2} \right\} \right. \\ & + y \left\{ -2 \frac{(\lambda_1 + \frac{2\lambda_2}{3})}{m_{s,00}^2} + \frac{\sqrt{2}}{m_{s,08}^2} \left(\frac{\lambda_2}{3} \right) + \frac{(\lambda_1 + \frac{2\lambda_2}{3})}{m_{s,88}^2} \right\} \left. + \frac{4N_c g m_s \mathcal{A}(m_s^2)}{3} \left[-\frac{c}{2} \left(\frac{1}{m_{s,08}^2} - \frac{\sqrt{2}}{m_{s,88}^2} \right) \right. \right. \\ & \left. \left. + x \left\{ \frac{\sqrt{2}(\lambda_1 + \frac{\lambda_2}{3})}{m_{s,00}^2} - \frac{\lambda_2}{3m_{s,08}^2} + \frac{-2\sqrt{2}(\lambda_1 + \frac{\lambda_2}{6})}{m_{s,88}^2} \right\} + y \left\{ \frac{-2(\lambda_1 + \frac{\lambda_2}{3})}{m_{s,00}^2} + \frac{\sqrt{2}}{m_{s,08}^2} \left(3\lambda_1 + \frac{4\lambda_2}{3} \right) - \frac{2(\lambda_1 + \frac{2\lambda_2}{3})}{m_{s,88}^2} \right\} \right] \right], \quad (\text{B14}) \end{aligned}$$

$$\begin{aligned} \Sigma_{p,11}^{\text{tad}} = & \frac{8N_c g m_u \mathcal{A}(m_u^2)}{3} \left[\frac{c}{2} \left(\frac{-1}{m_{s,00}^2} + \frac{1}{\sqrt{2}m_{s,08}^2} + \frac{1}{m_{s,88}^2} \right) + x \left(\lambda_1 + \frac{\lambda_2}{2} \right) \left\{ \frac{2}{m_{s,00}^2} + \frac{2\sqrt{2}}{m_{s,08}^2} + \frac{1}{m_{s,88}^2} \right\} \right. \\ & \left. + y \lambda_1 \left\{ \frac{\sqrt{2}}{m_{s,00}^2} - \frac{1}{m_{s,08}^2} - \frac{\sqrt{2}}{m_{s,88}^2} \right\} \right] + \frac{4N_c g m_s \mathcal{A}(m_s^2)}{3} \left[\frac{c}{2} \left(\frac{-1}{m_{s,00}^2} + \frac{2\sqrt{2}}{m_{s,08}^2} - \frac{2}{m_{s,88}^2} \right) \right. \\ & \left. + x \left(\lambda_1 + \frac{\lambda_2}{2} \right) \left\{ \frac{2}{m_{s,00}^2} - \frac{\sqrt{2}}{m_{s,08}^2} - \frac{2}{m_{s,88}^2} \right\} + y \lambda_1 \left\{ \frac{\sqrt{2}}{m_{s,00}^2} - \frac{4}{m_{s,08}^2} + \frac{2\sqrt{2}}{m_{s,88}^2} \right\} \right], \quad (\text{B15}) \end{aligned}$$

$$\begin{aligned} \Sigma_{p,44}^{\text{tad}} = & \frac{8N_c g m_u \mathcal{A}(m_u^2)}{3} \left[-\frac{c}{4} \left(\frac{2}{m_{s,00}^2} + \frac{2\sqrt{2}}{m_{s,08}^2} + \frac{1}{m_{s,88}^2} \right) + x \left\{ \frac{2(\lambda_1 + \frac{\lambda_2}{4})}{m_{s,00}^2} + \frac{\sqrt{2}(2\lambda_1 + \frac{5\lambda_2}{4})}{m_{s,08}^2} + \frac{(\lambda_1 + \lambda_2)}{m_{s,88}^2} \right\} \right. \\ & \left. + y \left\{ \frac{\sqrt{2}(\lambda_1 + \frac{\lambda_2}{2})}{m_{s,00}^2} - \frac{1}{m_{s,08}^2} (\lambda_1 + 2\lambda_2) - \frac{\sqrt{2}(\lambda_1 + \frac{5\lambda_2}{4})}{m_{s,88}^2} \right\} \right] + \frac{4N_c g m_s \mathcal{A}(m_s^2)}{3} \left[-\frac{c}{4} \left(\frac{2}{m_{s,00}^2} - \frac{\sqrt{2}}{m_{s,08}^2} - \frac{2}{m_{s,88}^2} \right) \right. \\ & \left. + x \left\{ \frac{2(\lambda_1 + \frac{\lambda_2}{4})}{m_{s,00}^2} - \frac{\sqrt{2}(\lambda_1 - \frac{\lambda_2}{2})}{m_{s,08}^2} - \frac{2(\lambda_1 + \lambda_2)}{m_{s,88}^2} \right\} + y \left\{ \frac{\sqrt{2}(\lambda_1 + \frac{\lambda_2}{2})}{m_{s,00}^2} - \frac{2}{m_{s,08}^2} \left(2\lambda_1 + \frac{7\lambda_2}{4} \right) + \frac{2\sqrt{2}(\lambda_1 + \frac{5\lambda_2}{4})}{m_{s,88}^2} \right\} \right]. \quad (\text{B16}) \end{aligned}$$

APPENDIX C: INTEGRALS

The divergent loop integrals are regularized by incorporating dimensional regularization,

$$\int_p = \left(\frac{e^{\gamma_E} \Lambda^2}{4\pi} \right)^\epsilon \int \frac{d^d p}{(2\pi)^d}, \quad (\text{C1})$$

where $d = 4 - 2\epsilon$, γ_E is the Euler-Mascheroni constant, and Λ is the renormalization scale associated with the $\overline{\text{MS}}$:

$$\begin{aligned} \mathcal{A}(m_f^2) &= \int_p \frac{1}{p^2 - m_f^2} \\ &= \frac{im_f^2}{(4\pi)^2} \left[\frac{1}{\epsilon} + 1 + \ln(4\pi e^{-\gamma_E}) + \ln \left(\frac{\Lambda^2}{m_f^2} \right) \right]. \end{aligned}$$

We rewrite this after redefining $\Lambda^2 \rightarrow \Lambda^2 \frac{e^{\gamma_E}}{4\pi}$,

$$\mathcal{A}(m_f^2) = \frac{im_f^2}{(4\pi)^2} \left[\frac{1}{\epsilon} + 1 + \ln \left(\frac{\Lambda^2}{m_f^2} \right) \right], \quad (\text{C2})$$

$$\begin{aligned} \mathcal{B}(p^2, m_f) &= \int_k \frac{1}{(k^2 - m_f^2)[(k+p)^2 - m_f^2]} \\ &= \frac{i}{(4\pi)^2} \left[\frac{1}{\epsilon} + \ln \left(\frac{\Lambda^2}{m_f^2} \right) + \mathcal{C}(p^2, m_f) \right], \quad (\text{C3}) \end{aligned}$$

$$\mathcal{B}'(p^2, m_f) = \frac{i}{(4\pi)^2} \mathcal{C}'(p^2, m_f), \quad (\text{C4})$$

$$\mathcal{C}(p^2, m_f) = 2 - 2\sqrt{\frac{4m_f^2}{p^2} - 1} \arctan \left(\frac{1}{\sqrt{\frac{4m_f^2}{p^2} - 1}} \right);$$

$$\mathcal{C}'(p^2, m_f) = \frac{4m_f^2}{p^4 \sqrt{\frac{4m_f^2}{p^2} - 1}} \arctan \left(\frac{1}{\sqrt{\frac{4m_f^2}{p^2} - 1}} \right) - \frac{1}{p^2}, \quad (\text{C5})$$

$$\mathcal{C}(p^2, m_f) = 2 + \sqrt{1 - \frac{4m_f^2}{p^2}} \ln \left(\frac{1 - \sqrt{1 - \frac{4m_f^2}{p^2}}}{1 + \sqrt{1 - \frac{4m_f^2}{p^2}}} \right); \quad \mathcal{C}'(p^2, m_f) = \frac{2m_f^2}{p^4 \sqrt{\frac{4m_f^2}{p^2} - 1}} \ln \left(\frac{1 - \sqrt{1 - \frac{4m_f^2}{p^2}}}{1 + \sqrt{1 - \frac{4m_f^2}{p^2}}} \right) - \frac{1}{p^2}. \quad (\text{C6})$$

Equations (C5) and (C6) are valid with the constraints ($p^2 < 4m_f^2$) and ($p^2 > 4m_f^2$) respectively:

$$\mathcal{B}(p^2, m_u, m_s) = \int_k \frac{1}{(k^2 - m_s^2)[(k+p)^2 - m_u^2]} = \frac{i}{(4\pi)^2} \left[\frac{1}{\epsilon} + \ln \left(\frac{\Lambda^2}{m_u^2} \right) + \mathcal{C}(p^2, m_u, m_s) \right], \quad (\text{C7})$$

$$\mathcal{C}(p^2, m_u, m_s) = 2 - \frac{1}{2} \left[1 + \frac{m_s^2 - m_u^2}{p^2} \right] \ln \left(\frac{m_s^2}{m_u^2} \right) - \frac{\mathcal{G}(p^2)}{p^2} \left[\arctan \left(\frac{p^2 - m_s^2 + m_u^2}{\mathcal{G}(p^2)} \right) + \arctan \left(\frac{p^2 + m_s^2 - m_u^2}{\mathcal{G}(p^2)} \right) \right], \quad (\text{C8})$$

$$\mathcal{G}(p^2) = \sqrt{\{(m_s + m_u)^2 - p^2\} \{p^2 - (m_s - m_u)^2\}}, \quad (\text{C9})$$

$$\mathcal{C}'(p^2, m_u, m_s) = \frac{m_s^2 - m_u^2}{2p^4} \ln \left(\frac{m_s^2}{m_u^2} \right) + \frac{p^2(m_s^2 + m_u^2) - (m_s^2 - m_u^2)^2}{p^4 \mathcal{G}(p^2)} \left[\arctan \left(\frac{p^2 - m_s^2 + m_u^2}{\mathcal{G}(p^2)} \right) + \arctan \left(\frac{p^2 + m_s^2 - m_u^2}{\mathcal{G}(p^2)} \right) \right] - \frac{1}{p^2}. \quad (\text{C10})$$

-
- [1] N. Cabibbo and G. Parisi, *Phys. Lett. B* **59**, 67 (1975).
[2] L. D. McLerran and B. Svetitsky, *Phys. Rev. D* **24**, 450 (1981); B. Svetitsky, *Phys. Rep.* **132**, 1 (1986).
[3] B. Muller, *Rep. Prog. Phys.* **58**, 611 (1995).
[4] H. Meyer-Ortmanns, *Rev. Mod. Phys.* **68**, 473 (1996).
[5] D. H. Rischke, *Prog. Part. Nucl. Phys.* **52**, 197 (2004).
[6] A. AliKhan, A. Aoki, R. Burkhalter, S. Ejiri, M. Fukugita, S. Hashimoto *et al.*, *Phys. Rev. D* **64**, 074510 (2001).
[7] S. Digoal, E. Laermann, and H. Satz, *Eur. Phys. J. C* **18**, 583 (2001).
[8] F. Karsch, *Lect. Notes Phys.* **583**, 209 (2002).
[9] Z. Fodor, S. D. Katz, and K. K. Szabo, *Phys. Lett. B* **568**, 73 (2003).
[10] C. R. Allton, M. Doring, S. Ejiri, S. J. Hands, O. Kaczmarek, F. Karsch, E. Laermann, and K. Redlich, *Phys. Rev. D* **71**, 054508 (2005).
[11] F. Karsch, *J. Phys. G* **31**, S633 (2005).
[12] Y. Aoki, Z. Fodor, S. D. Katz, and K. K. Szabo, *Phys. Lett. B* **643**, 46 (2006).
[13] M. Cheng, N. H. Christ, S. Datta, J. van der Heide, C. Jung, F. Karsch *et al.*, *Phys. Rev. D* **74**, 054507 (2006).
[14] M. Cheng, N. H. Christ, S. Datta, J. van der Heide, C. Jung, F. Karsch *et al.*, *Phys. Rev. D* **77**, 014511 (2008).
[15] M. G. Alford, A. Schmitt, K. Rajagopal, and T. Schafer, *Rev. Mod. Phys.* **80**, 1455 (2008).
[16] K. Fukushima and T. Hatsuda, *Rep. Prog. Phys.* **74**, 014001 (2011).
[17] G. 't Hooft, *Phys. Rev. Lett.* **37**, 8 (1976); *Phys. Rev. D* **14**, 3432 (1976).
[18] J. T. Lenaghan, D. H. Rischke, and J. Schaffner-Bielich, *Phys. Rev. D* **62**, 085008 (2000); J. T. Lenaghan and D. H. Rischke, *J. Phys. G* **26**, 431 (2000).
[19] B. J. Schaefer and M. Wagner, *Phys. Rev. D* **79**, 014018 (2009).
[20] A. M. Polyakov, *Phys. Lett.* **72B**, 477 (1978).
[21] K. Fukushima, *Phys. Lett. B* **591**, 277 (2004).
[22] B. Svetitsky and L. G. Yaffe, *Nucl. Phys.* **B210**, 423 (1982).
[23] R. D. Pisarski, *Phys. Rev. D* **62**, 111501(R) (2000).
[24] B. Layek, A. P. Mishra, A. M. Srivastava, and V. K. Tiwari, *Phys. Rev. D* **73**, 103514 (2006).
[25] C. Ratti, M. A. Thaler, and W. Weise, *Phys. Rev. D* **73**, 014019 (2006).
[26] K. Fukushima, *Phys. Rev. D* **78**, 114019 (2008).
[27] O. Scavenius, A. Mocsy, I. N. Mishustin, and D. H. Rischke, *Phys. Rev. C* **64**, 045202 (2001).
[28] D. Roder, J. Ruppert, and D. H. Rischke, *Phys. Rev. D* **68**, 016003 (2003).
[29] K. Fukushima, K. Kamikado, and B. Klein, *Phys. Rev. D* **83**, 116005 (2011).
[30] M. Grahl and D. H. Rischke, *Phys. Rev. D* **88**, 056014 (2013).
[31] A. Jakovac, A. Patkos, Z. Szepe, and P. Szepfalusy, *Phys. Lett. B* **582**, 179 (2004).
[32] T. Herpay, A. Patkós, Zs. Szép, and P. Szepfalusy, *Phys. Rev. D* **71**, 125017 (2005).
[33] T. Herpay and Zs. Szép, *Phys. Rev. D* **74**, 025008 (2006).
[34] P. Kovács and Zs. Szép, *Phys. Rev. D* **75**, 025015 (2007).
[35] P. Kovacs and Zs. Szepe, *Phys. Rev. D* **75**, 025015 (2007).

- [36] T. Kahara and K. Tuominen, *Phys. Rev. D* **78**, 034015 (2008); **80**, 114022 (2009); **82**, 114026 (2010).
- [37] E. S. Bowman and J. I. Kapusta, *Phys. Rev. C* **79**, 015202 (2009); J. I. Kapusta and E. S. Bowman, *Nucl. Phys.* **A830**, 721C (2009).
- [38] G. Fejos and A. Patkos, *Phys. Rev. D* **82**, 045011 (2010).
- [39] A. Jakovac and Zs. Szep, *Phys. Rev. D* **82**, 125038 (2010).
- [40] L. Ferroni, V. Koch, and M. B. Pinto, *Phys. Rev. C* **82**, 055205 (2010).
- [41] G. Marko and Zs. Szep, *Phys. Rev. D* **82**, 065021 (2010).
- [42] A. Mocsy, I. N. Mishustin, and P. J. Ellis, *Phys. Rev. C* **70**, 015204 (2004).
- [43] B.-J. Schaefer and J. Wambach, *Nucl. Phys.* **A757**, 479 (2005).
- [44] B.-J. Schaefer and J. Wambach, *Phys. Rev. D* **75**, 085015 (2007).
- [45] B. J. Schaefer, J. M. Pawlowski, and J. Wambach, *Phys. Rev. D* **76**, 074023 (2007).
- [46] B. J. Schaefer, M. Wagner, and J. Wambach, *Phys. Rev. D* **81**, 074013 (2010).
- [47] H. Mao, J. Jin, and M. Huang, *J. Phys. G* **37**, 035001.
- [48] U. S. Gupta and V. K. Tiwari, *Phys. Rev. D* **81**, 054019 (2010).
- [49] R. D. Pisarski and F. Wilczek, *Phys. Rev. D* **29**, 338 (1984).
- [50] M. A. Halasz, A. D. Jackson, R. E. Shrock, M. A. Stephanov, and J. J. M. Verbaarschot, *Phys. Rev. D* **58**, 096007 (1998).
- [51] V. Skokov, B. Friman, E. Nakano, K. Redlich, and B.-J. Schaefer, *Phys. Rev. D* **82**, 034029 (2010).
- [52] R. Khan and L. T. Kyllingstad, *AIP Conf. Proc.* **1343**, 504 (2011).
- [53] U. S. Gupta and V. K. Tiwari, *Phys. Rev. D* **85**, 014010 (2012).
- [54] B.-J. Schaefer and M. Wagner, *Phys. Rev. D* **85**, 034027 (2012).
- [55] S. Chatterjee and K. A. Mohan, *Phys. Rev. D* **85**, 074018 (2012).
- [56] J. O. Andersen and A. Tranberg, *J. High Energy Phys.* **08** (2012) 002.
- [57] V. K. Tiwari, *Phys. Rev. D* **86**, 094032 (2012).
- [58] S. Chatterjee and K. A. Mohan, *Phys. Rev. D* **86**, 114021 (2012).
- [59] V. K. Tiwari, *Phys. Rev. D* **88**, 074017 (2013).
- [60] T. K. Herbst, J. M. Pawlowski, and B.-J. Schaefer, *Phys. Rev. D* **88**, 014007 (2013).
- [61] J. Weyrich, N. Strodthoff, and L. von Smekal, *Phys. Rev. C* **92**, 015214 (2015).
- [62] P. Kovacs, Zs Szep, and Gy Wolf, *Phys. Rev. D* **93**, 114014 (2016).
- [63] Andreas Zacchi and Jürgen Schaffner-Bielich, *Phys. Rev. D* **97**, 074011 (2018).
- [64] Andreas Zacchi and Jürgen Schaffner-Bielich, *Phys. Rev. D* **100**, 123024 (2019).
- [65] S. K. Rai and V. K. Tiwari, *Eur. Phys. J. Plus* **135**, 844 (2020).
- [66] K. Kajantie, M. Laine, K. Rummukainen, and M. E. Shaposhnikov, *Nucl. Phys.* **B458**, 90 (1996).
- [67] P. Adhikari, J. O. Andersen, and P. Kneschke, *Phys. Rev. D* **95**, 036017 (2017).
- [68] S. Carignano, M. Buballa, and B.-J. Schaefer, *Phys. Rev. D* **90**, 014033 (2014).
- [69] J. O. Andersen, W. R. Naylor, and A. Tranberg, *Rev. Mod. Phys.* **88**, 025001 (2016).
- [70] S. Carignano, M. Buballa, and W. El-Kamhawy, *Phys. Rev. D* **94**, 034023 (2016).
- [71] P. Adhikari, J. O. Andersen, and P. Kneschke, *Phys. Rev. D* **96**, 016013 (2017).
- [72] P. Adhikari, J. O. Andersen, and P. Kneschke, *Phys. Rev. D* **98**, 074016 (2018).
- [73] A. Folkestad and J. O. Andersen, *Phys. Rev. D* **99**, 054006 (2019).
- [74] S. K. Rai and V. K. Tiwari, *Phys. Rev. D* **105**, 094010 (2022).
- [75] G. Fejos, *Phys. Rev. D* **92**, 036011 (2015).
- [76] G. Fejos and A. Hosaka, *Phys. Rev. D* **94**, 036005 (2016).
- [77] Fabian Rennecke and Bernd-Jochen Schaefer, *Phys. Rev. D* **96**, 016009 (2017).
- [78] G. Fejos and A. Hosaka, *Phys. Rev. D* **98**, 036009 (2018).
- [79] G. Fejos and A. Patkos, *Phys. Rev. D* **105**, 096007 (2022).
- [80] J. I. Kapusta and C. Gale, *Finite Temperature Field Theory Principles and Applications* (Cambridge University Press, Cambridge, England, 2006).
- [81] R. Kobes, G. Kunstatter, and A. Rebhan, *Phys. Rev. Lett.* **64**, 2992 (1990); *Nucl. Phys.* **B355**, 1 (1991).
- [82] A. K. Rebhan, *Phys. Rev. D* **48**, R3967 (1993).
- [83] Jianing Li, Jin Gui, and Pengfei Zhuang, *Chin. Phys. C* **47**, 104102 (2023).